UNIVERSITE JOSEPH KI-ZERBO

ECOLE DOCTORALE INFORMATIQUE ET CHANGEMENT CLIMATIQUE (EDICC)

BURKINA FASO

La Patrie ou la Mort, nous Vaincrons

Order N° : .....

MASTER RESEARCH PROGRAM

SPECIALITY: INFORMATICS FOR CLIMATE CHANGE (ICC)

MASTER THESIS

Subject:

ASSESSING THE DYNAMICS OF HEATWAVES OVER THE SAHEL REGION OF WEST AFRICA: CHARACTERIZATION AND PROJECTIONS

Presented (21/07/2025), by:

OYERIBHOR, Susan Osaremeh

Examination Jury

President: Pr. Alfa Oumar DISSA, Professor at Université Joseph KI-ZERBO

Members :

Dr Sidiki ZONGO, Associate Professor at Université Joseph KI-ZERBO (external examiner) ;

Pr. Sié KAM title, Professor at Université Joseph KI-ZERBO **(**supervisor) ;

Prof Vincent AJAYI, Professor at Federal University of Technology, Akure, Nigeria (co-supervisor)

Academic year 2024-2025

DEDICATION

I dedicate this thesis to the Almighty, who has blessed me with the wisdom to pursue this path; to my late parent and my family, who sacrificed so much to see me succeed; and to my friends, who reminded me that life is about more than just academic achievements

ACKNOWLEDGEMENTS

I extend my heartfelt gratitude to the funders, Federal Ministry of Research, Technology and Space (BMFTR), Germany and WASCAL for providing the scholarship that made this research possible; Prof. Amadé Ouédraogo, Director of the École Doctorale Informatique et Changement Climatique (ED-ICC), for his leadership and vision;

Dr. Ousamane Coulibaly, Deputy Director of ED-ICC, for his continuous support;

Dr. Benewindé Zoungrana, Scientific Coordinator, for his guidance throughout this program; My supervisor, Prof. Kam Sié, whose mentorship and dedication have shaped this work; my co-supervisor, Prof. Vincent Ajayi, for his invaluable insights, support, and collaboration; and the distinguished jury members who honored this work with their time and expertise. Dr. Emmanuel Poan, my industrial supervisor at The Red Cross Climate Centre, for providing an exceptional internship experience ;

Finally, to my family (Mr and Mrs. Osemwegie, Benita Oyeribhor, Charles Chilaka) and friends (Triumph Orowale, Faith Adeyemi, Matthew Taiwo, Victor Arowolo), and Batch 4 students, whose encouragement and support sustained me throughout this academic journey.

ABSTRACT

This study investigates the historical trends and future projections of heatwaves over the Sahel region of West Africa, a climate-sensitive and socioeconomically vulnerable area. Utilizing ERA5 reanalysis data (1984–2014) and statistically downscaled outputs from 11 CMIP6 models under SSP2-4.5 and SSP5-8.5 scenarios, the study examines five heatwave metrics (frequency, number, duration, amplitude, and magnitude) across three heatwave definitions (TX90, TN90, EHF). The results confirm that the Sahel is experiencing intensifying heatwave events. Historically, daytime heatwaves (TX90) show higher frequencies (1.0–1.9 events/year), while nighttime heatwaves (TN90) reveal significant positive trends in frequency and duration, especially in the northern zones. The Excess Heat Factor (EHF) underscores the growing intensity and compound impact of heat extremes. Model validation using Taylor diagrams and Mann-Kendall trend tests confirms the robustness of projections despite biases among models. Future projections reveal alarming trends. By 2091, under SSP5-8.5, HWF could exceed 25 days/year, with amplitude values surpassing 50°C in parts of the central Sahel. These findings suggest a severe escalation in heat-related health risks, especially due to rising nighttime temperatures that limit physiological recovery. The study confirms the hypothesis that heatwaves in the Sahel are intensifying and are expected to worsen under future climate scenarios. This research provides vital input for developing region-specific early warning systems and adaptation plans. It highlights the urgency of strengthening climate resilience in the Sahel through enhanced forecasting, infrastructure planning, and health interventions.

Keywords: Sahel, heatwave, Climate Change, CMIP6, ERA5, EHF, SSP5-8.5, , Mann-Kendall, thermal extremes.

RESUMÉ

Cette étude examine les tendances historiques et les projections futures des vagues de chaleur dans la région sahélienne de l'Afrique de l'Ouest, une zone particulièrement vulnérable aux changements climatiques. À l'aide des données de réanalyse ERA5 (1984–2014) et des projections issues de 11 modèles CMIP6, statistiquement réduits selon les scénarios SSP2-4.5 et SSP5-8.5, l'analyse porte sur cinq indices de vague de chaleur (fréquence, nombre, durée, amplitude, et magnitude) pour trois définitions (TX90, TN90, EHF). Les résultats confirment une intensification des vagues de chaleur dans la région. Historiquement, les vagues diurnes (TX90) sont plus fréquentes (1,0 à 1,9 événements/an), tandis que les vagues nocturnes (TN90) présentent des tendances fortement positives, notamment au nord du Sahel. Le facteur de chaleur excessive (EHF) souligne l'aggravation de l'intensité des événements extrêmes. La validation des modèles à l'aide de diagrammes de Taylor et du test de Mann-Kendall confirme la robustesse des tendances malgré certaines divergences entre modèles. Les projections futures révèlent des perspectives préoccupantes. D'ici 2091, sous SSP5-8.5, la fréquence des vagues de chaleur (HWF) pourrait dépasser 25 jours/an, avec des amplitudes supérieures à 50°C dans certaines zones. Ces conditions accentueraient les risques pour la santé, notamment en raison des températures nocturnes élevées qui empêchent la récupération thermique.

Cette étude apporte des données cruciales pour la mise en place de systèmes d'alerte précoce et de stratégies d'adaptation spécifiques à la région.

Mots-clés : Sahel, vague de chaleur, changement climatique, CMIP6, ERA5, EHF, SSP5-8.5, Mann-Kendall, extrêmes thermiques.

ACRONYM AND ABBREVIATION

ACCESS-CM2	Australian Community Climate and Earth System Simulator – Climate Model version 2
ACCESS-ESM1-5	Australian Community Climate and Earth System Simulator – Earth System Model version 1.5
CDO	Climate Data Operators
CMCC-ESM2	Centro Euro-Mediterraneo sui Cambiamenti Climatici – Earth System Model version 2
CMIP6	Coupled Model Intercomparison Project Phase 6
CRMSE	Centered Root Mean Square Error
EC-EARTH3	European Community Earth-System Model version 3
EC-EARTH3-Veg-LR	EC-Earth3 with dynamic vegetation module at Low Resolution
ECMWF	European Centre for Medium-Range Weather Forecasts
ED-ICC	École Doctorale Informatique et Changement Climatique
EHF	Excess Heat Factor
ERA5	Fifth Generation ECMWF Reanalysis
GCM	General Circulation Model
HWA	Heatwave Amplitude
HWD	Heatwave Duration
HWF	Heatwave Frequency
HWM	Heatwave Magnitude
HWN	Heatwave Number
IPSL-CM6A-LR	Institut Pierre-Simon Laplace – Climate Model version 6A, Low Resolution
ITCZ	Inter-Tropical Convergence Zone
ITD	Inter-Tropical Discontinuity
KIOST-ESM	Korea Institute of Ocean Science and Technology – Earth System Model
MAE	Mean Absolute Error
MBE	Mean Bias Error
MIROC6	Model for Interdisciplinary Research on Climate version 6
MJO	Madden-Julian Oscillation

MK	Mann-Kendall
MME	Multi-Model Ensemble
MPI-ESM1-2-HR	Max Planck Institute – Earth System Model version 1.2, High Resolution
MPI-ESM1-2-LR	Max Planck Institute – Earth System Model version 1.2, Low Resolution
MRI-ESM2-0	Meteorological Research Institute – Earth System Model version 2.0
NEX-GDDP	NASA Earth Exchange - Global Daily Downscaled Projections
RCP	Representative Concentration Pathway
SSP	Shared Socioeconomic Pathways
TN90	90th Percentile of Minimum Temperature
TX90	90th Percentile of Maximum Temperature

TABLE OF CONTENTS

LIST OF TABLES

LIST OF FIGURES

INTRODUCTION

Contextual Background

Climate change has significantly altered global weather patterns, resulting in more frequent and intense climate extremes worldwide. The Sahel region of West Africa, a semi-arid area stretching across the continent, has experienced pronounced warming over recent decades, making it particularly vulnerable to extreme heat events (Guigma, 2021).

Heatwaves, one of the most dangerous natural hazards, are defined as prolonged periods of abnormally high temperatures that can cause significant adverse effects on human health and comfort (Guigma, Todd and Wang., 2020). In the Sahel, they are characterized by relatively short-lasting events with a mean duration between three and five days, but with extreme magnitude given the already hot climate. Most locations in the Sahel experience one to two heatwave events annually, with the eastern and central Sahel being more susceptible compared to western regions (Guigma, Todd and Wang., 2020).

Heatwaves in West Africa originate from shifts in the Intertropical Convergence Zone (ITCZ), which modulate monsoon dynamics and sea surface temperatures (SSTs). The ITCZ's northward migration during boreal summer (June–July) alters atmospheric circulation, enhancing heatwave frequency over the Sahel due to reduced convection and rainfall suppression (Guigma *et al*., 2021). These shifts are tightly linked to Atlantic SST anomalies (Adeniyi, 2017), which also influence the strength and height of moist southerly winds. The so-called "inter-Tupelian" intrusion reflects Atlantic wind surges, which, at mid-altitudes, disrupt ITCZ positioning, driving episodic rain and heat extremes (Wane *et al*.,2024). Also, complex thermodynamic processes drive the occurrence of Sahelian heatwaves. Heat advection and the greenhouse effect of water vapor have been identified as the main underlying causes (Guigma *et al*., 2021; Sambou *et al*., 2021). Low-level atmospheric circulation disturbances drive these mechanisms by enabling the movement of warmer and more moisture-laden air toward the Sahel region. On a broader scale, large-scale tropical climate patterns such as the Madden-Julian Oscillation (MJO), along with equatorial Rossby and Kelvin wave systems, influence both the likelihood and strength of heat extremes in this area (Guigma, 2021).

Forecasting capabilities for Sahelian heat extremes extend effectively up to two to three weeks in advance, with nocturnal temperature events showing greater predictive accuracy compared to daytime episodes. Heat events during the pre-monsoon period (April through June) exhibit enhanced forecast reliability relative to those in the latter part of winter (Guigma *et al*., 2021).

Prediction accuracy improves notably when tropical climate modes are in their active states, indicating their utility as key indicators for anticipating extreme temperature occurrences.

Future projections indicate a concerning trend. Under global warming scenarios of 1.5°C and 2°C, heat wave is expected to increase significantly across West Africa, with substantial proportions of the population at risk of heat-related illnesses (Sylla *et al*., 2018). The frequency, intensity, and duration of heatwaves are projected to increase, particularly in the drier regions of the central and eastern Sahel (Diedhiou *et al.,* 2018).

This has important implications for early warning systems and adaptation planning. Notably, daytime and nighttime heatwaves show low synchronicity in the Sahel, providing some relief to populations as continuous heat exposure is more detrimental to health (Guigma, Todd and Wang., 2020). Improving the representation of tropical modes in climate models could enhance heatwave predictability, allowing for more effective early warning systems (Guigma *et al*., 2021). This becomes increasingly important as forestation activities may influence future heatwave characteristics, potentially increasing events in forested zones while decreasing them in the Sahel and along the Guinea coast (Odoulami *et al*., 2017). As climate change progresses, addressing the increasing threat of heatwaves in the Sahel becomes increasingly urgent. Effective mitigation and adaptation strategies, informed by an improved understanding of the dynamics of these extreme events, will be essential for protecting vulnerable populations in this already hot and climatically challenging region.

Problem Statement and Rationale of the Study

Problem Statement

The Sahel region of West Africa faces an escalating threat from heatwave events that are becoming more frequent, intense, and prolonged due to climate change. Despite the severity of this issue, there remains a significant knowledge gap in understanding the comprehensive dynamics of these extreme heat events across the region. Africans must collect data to analyze it over a long period, and by doing so, adaptation plans will be mastered. Current research has established the basic characteristics of Sahelian heatwaves (Guigma, Todd and Wang, 2020), but lacks detailed analysis of their spatiotemporal patterns, the complex interaction between local and regional drivers, and reliable future projections specific to the Sahel. This knowledge deficit hampers the development of effective early warning systems and adaptation strategies for a region where populations are highly vulnerable due to limited adaptive capacity, outdoor-

dependent livelihoods, and inadequate infrastructure. Furthermore, the dearth of locally calibrated thermal indices appropriate for the Sahelian context complicates accurate heat risk assessment. Given the anticipated rise in extreme heat events across different climate warming projections (Sylla *et al*., 2018), it becomes critically important to fill these knowledge gaps to safeguard public health, food security, and economic resilience throughout the Sahel..

Rationale

This study is critically needed for several compelling reasons. First, the Sahel is experiencing warming at a rate 1.5 times faster than the global average (Guigma, 2021), making it a hotspot for extreme heat events. Despite this alarming trend, heatwaves in the region remain understudied compared to those in developed regions, creating a significant equity gap in climate research.

Second, the populations of the Sahel are among the most vulnerable to heat impacts globally due to their heavy reliance on outdoor labor in agriculture and the informal sector, limited access to cooling infrastructure, and constrained economic resources for adaptation (Sylla *et al*., 2018). Accurate characterization of heat risks is therefore essential for protecting human lives and livelihoods. Third, the distinctive characteristics of Sahelian heatwaves where nighttime and daytime events show low synchronicity require specialized understanding beyond what can be extrapolated from studies in other regions, (Guigma, Todd and Wang, 2020).

Finally, robust projections of future heat extremes are essential for long-term adaptation planning in the region. Current climate projections indicate a significant increase in heatwaves under various warming scenarios (Diedhiou *et al*., 2018), but these lack the spatial and temporal specificity needed for effective regional planning.

By addressing these knowledge gaps, this study will provide crucial information for developing targeted early warning systems, informing evidence-based adaptation policies, and helping to build resilience among vulnerable Sahelian communities facing an increasingly hot future. The findings will also contribute to addressing global inequities in climate research and adaptation support.

Research Question, Hypotheses, and Objectives

Main Research Question

- How are the historical and projected dynamics of heatwaves manifested in the Sahel region?

Specific Research Questions

1. What are the climatological characteristics and trends of historical heatwaves in the Sahel region?
2. What are the projected changes and trends in heatwave characteristics under SSP2-4.5 and SSP5-8.5 for near- and far-future scenarios in the Sahel region?

Main Research Hypothesis

- Heatwaves in the Sahel are intensifying in frequency, duration, and magnitude, and are expected to accelerate under future climate scenarios.

Specific Research Hypotheses

1. Historical heatwave patterns show significant spatial variability with increasing trends in frequency and intensity across the Sahel region.
2. Future climate scenarios project more frequent, intense, and longer-lasting heatwaves for the Sahel region under SSP2-4.5 and especially under SSP5-8.5.

Main Research Objective

- To investigate historical trends and future projections of heatwaves in the Sahel region.

Specific Research Objectives

1. Analyze the climatology patterns and trends of heatwave characteristics across the Sahel region.
2. Evaluate future projections of heatwaves and trends under SSP2-4.5 and SSP5-8.5 for the near and far future across the Sahel region.

CHAPTER 1: LITERATURE REVIEW

1.1 Introduction

This chapter critically examines the current understanding of heatwave dynamics in the Sahel region, focusing on historical characterization and future projections. The review addresses spatial characteristics of historical heatwave events, projected changes under future climate scenarios, and implications for human thermal comfort and adaptation planning.

1.2 Concept of Heatwaves

As noted by Aderotoye, Zaitchik and Asare (2024), "the definitions and measurements of heatwaves are often unclear and inconsistent, and they tend to vary depending on the specific group affected or the study context". Heatwaves are generally understood as prolonged periods of abnormally high temperatures that exceed certain thresholds relative to the local climate. Figure 1 shows that even a small increase in average temperatures makes a big difference to heat extremes. As the range of daily temperatures shifts to warmer levels, hotter days become more likely and more intense (Poynting and Stallard, 2024).

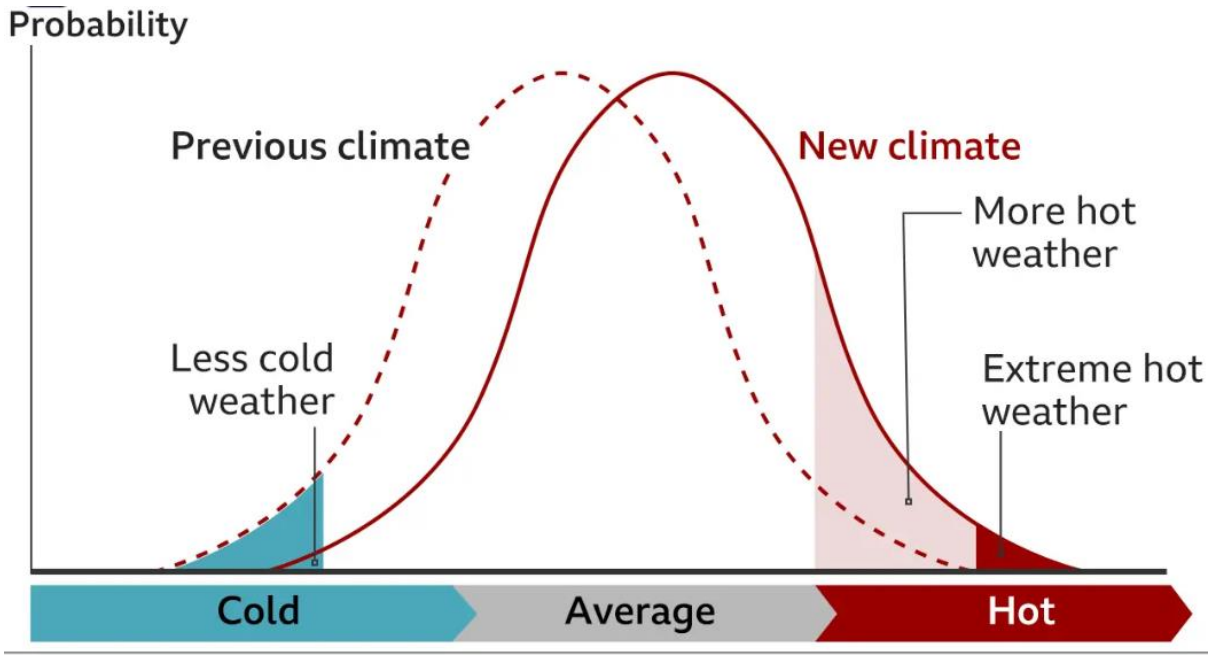

Figure 1 : Hotter, Longer Heatwave

Source: *Poynting and Stallard (2024)*

The conceptual understanding of both heatwaves has evolved significantly over time, shifting from purely meteorological definitions to more impact-based approaches that consider human health outcomes and vulnerability factors. This evolution reflects growing recognition that the health impacts of extreme heat depend not only on absolute temperatures but also on factors such as humidity, exposure duration, acclimatization, and socioeconomic conditions.

1.3 Understanding Heatwave Formation and Contributing Factors

Heatwaves are caused by several interconnected mechanisms. Figure 2 shows how the systems of high pressure keep warm air from evaporating by trapping it in a specific location. By pushing air to sink and compress, these high-pressure systems—also referred to as anticyclones—create a dome of heat that raises surface temperatures. Under these high-pressure systems, there are fewer clouds, which increases solar radiation and warms the land and air above it. Several days to weeks may pass during extended periods of abnormally high temperatures as a result of this confluence of circumstances (Copernicus, 2024).

Global warming significantly amplifies these phenomena by raising baseline atmospheric temperatures. Enhanced greenhouse gas concentrations create warmer starting conditions, making heat episodes more severe when they occur. Modified atmospheric circulation patterns associated with climate shifts may also promote longer-lasting high-pressure zones that sustain extreme temperatures (Copernicus, 2024).

Urban environments compound these effects through heat island phenomena, where concrete infrastructure and reduced vegetation create localized temperature increases compared to rural surroundings. Cities, therefore, experience intensified heat during extreme weather events. Modified land surfaces from human activities like forest clearing and agricultural development further influence regional temperature patterns by changing how energy is absorbed and released (Copernicus, 2024).

The convergence of natural atmospheric processes with human-induced environmental changes creates increasingly frequent and severe heat episodes. Understanding these multiple contributing factors helps explain why extreme heat events have become more common and intense in recent decades, particularly in densely populated areas where infrastructure magnifies the underlying meteorological conditions (Copernicus, 2024).

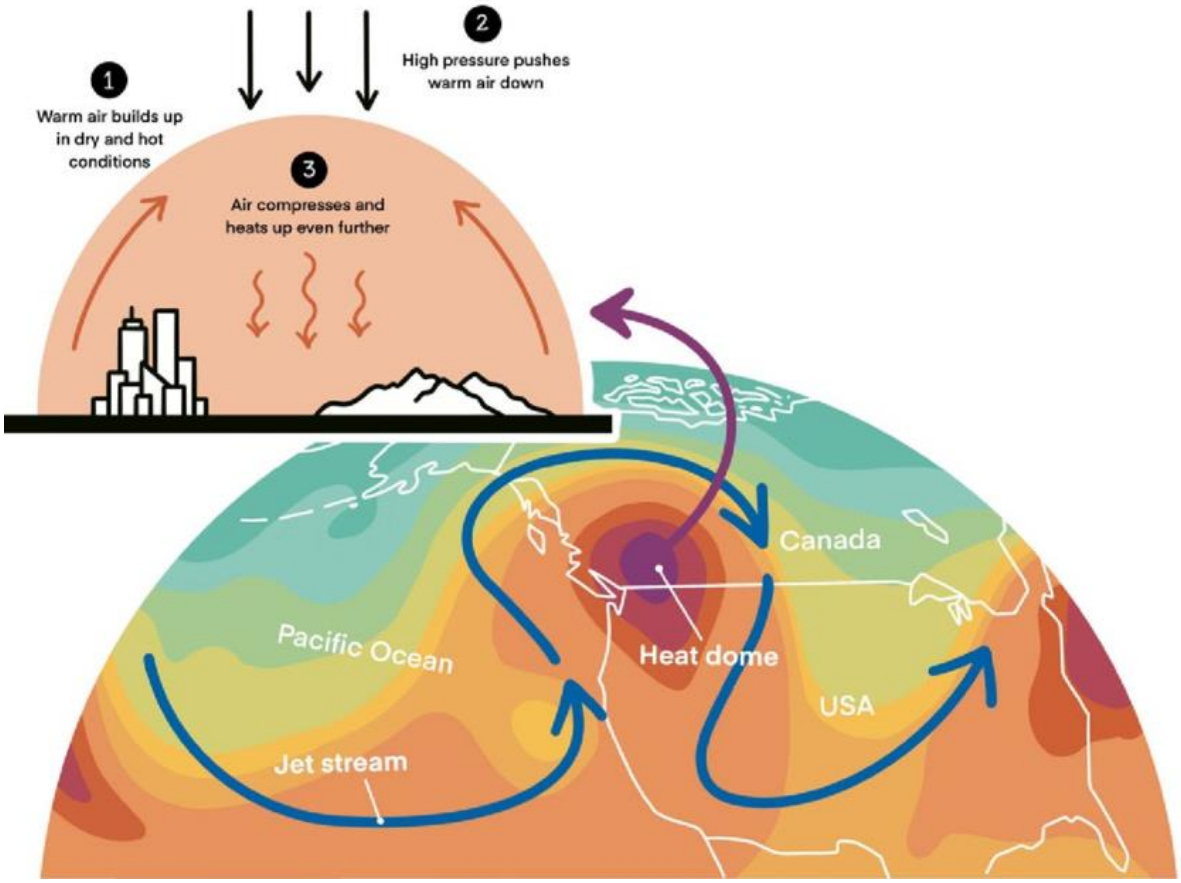

Figure 2 : How a heat dome is formed

Source: Eberle, Higuera Roa and Sparkes (2022)

Humans are susceptible to heat stress due to a number of important risk factors. By reducing perspiration evaporation, the body's primary cooling mechanism, environmental factors like high temperatures and humidity levels significantly increase the risk. Higher humidity levels prevent sweat from evaporating from our skin, which cools our bodies.

The diagram in Figure 3 shows heat sources (sun, reflected radiation, ground conduction) overwhelming the body's cooling mechanisms (sweat evaporation, respiration, infrared radiation release) (Havenith, 2001). When heat gain exceeds heat loss through these pathways, core body temperature rises dangerously, potentially causing heat-related illness or death.

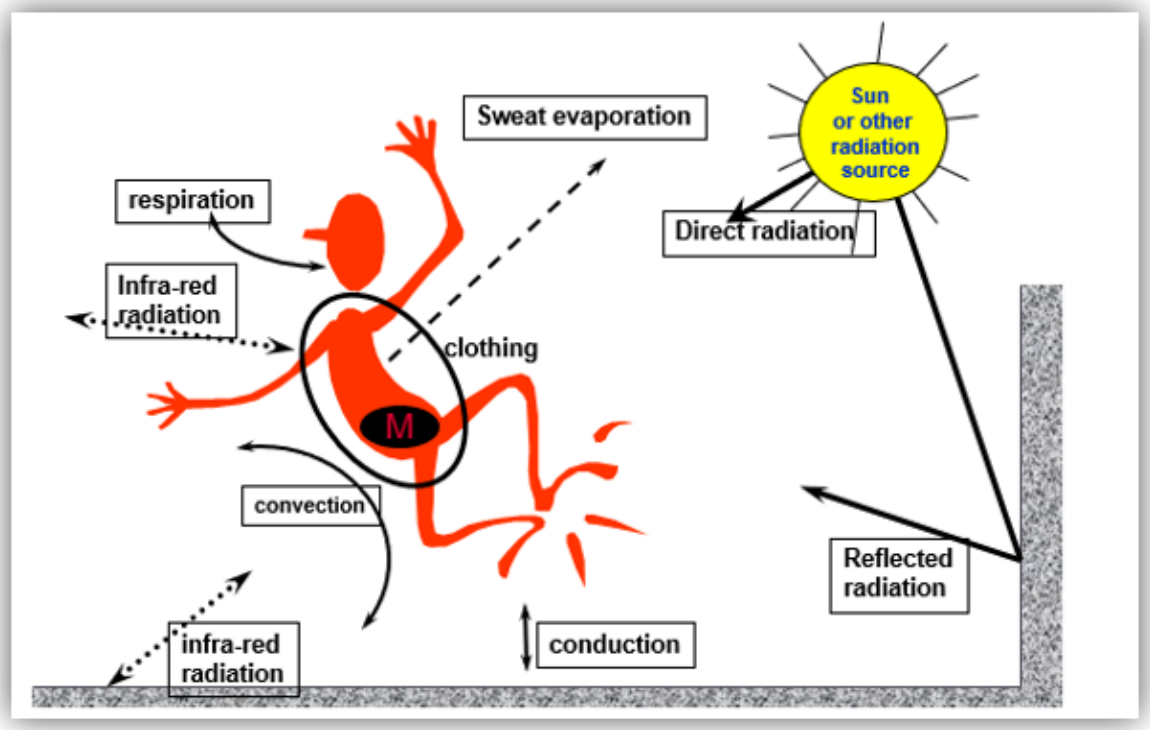

Figure 3 : The human heat budget

Source: Havenith (2001)

1.4 Types of Heatwave

Heatwaves are categorized into two main types: dry heatwaves and wet heatwaves. Dry heatwaves are characterized by high temperatures and low humidity, while wet heatwaves are influenced by high temperatures combined with elevated humidity levels (Ngoungue Langue *et al.*, 2023). The interplay of humidity and temperature is crucial; concomitant heatwaves, those occurring both day and night, pose a greater health risk as they do not allow the body adequate time to recover from the heat experienced during the day (Ngoungue Langue *et al.*, 2023). The dynamics of daytime and nighttime heatwaves in the Sahel are driven by distinct atmospheric conditions intensified by climate change. Daytime events correlate with low humidity, clear skies, and high solar radiation, amplifying surface temperatures (Oueslati *et al*, 2017). Conversely, nighttime heatwaves are linked to increased atmospheric moisture and cloud cover, trapping outgoing longwave radiation and elevating nocturnal temperatures (Oueslati *et al.*, 2017; Nangombe *et al.*, 2019). Understanding these temporal variations is crucial for targeted adaptation strategies in a region projected to warm 1.5 times faster than the global

average (USAID, 2024). Figure 4 summarizes the physical processes associated with the daytime and nighttime heatwaves. The blue downward arrow indicates a decrease, and the red upward arrow indicates an increase.

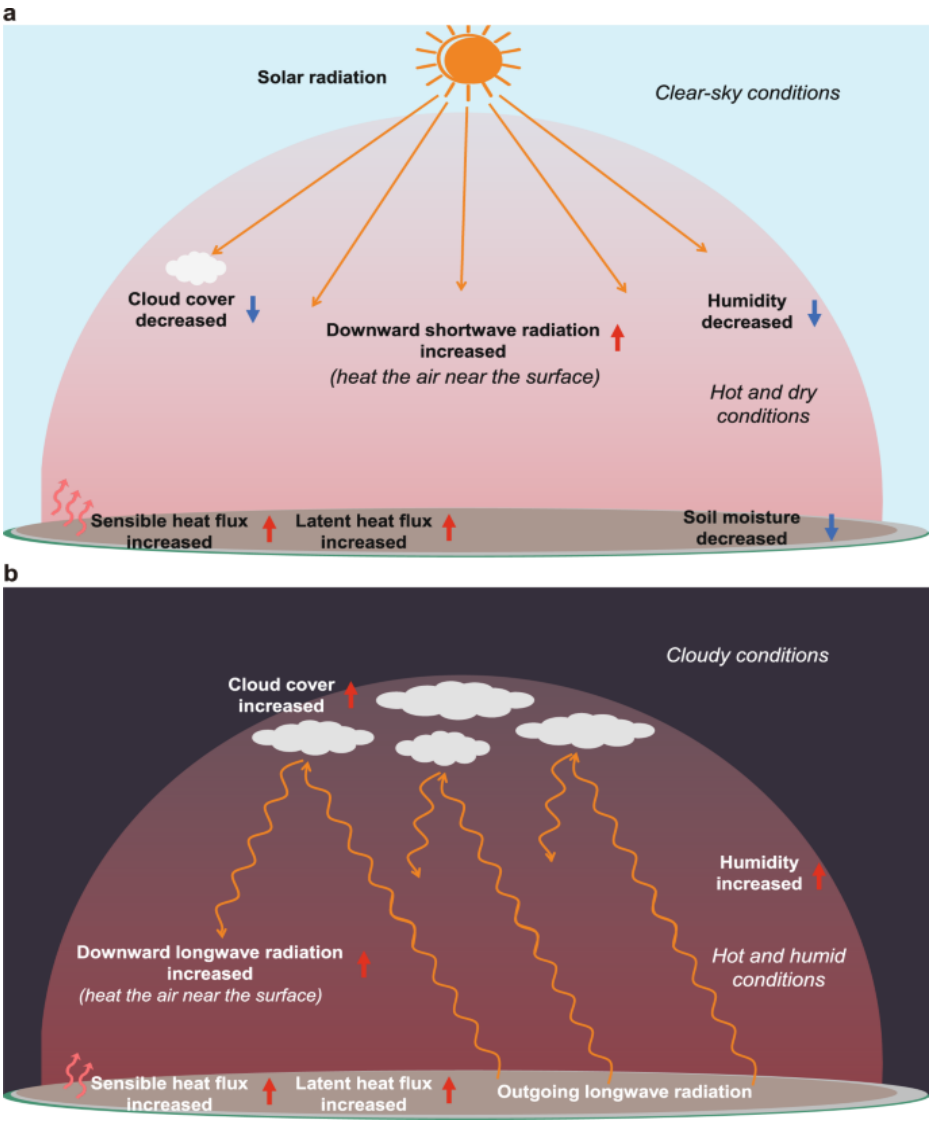

Figure 4 **a** schematic diagram of daytime heatwave, **b** schematic diagram of nighttime heatwave

Source: Wu et al. (2023)

1.5 Measurement and Indices

Various indices have been developed to quantify heatwaves, each with different applications and limitations. Heatwaves are measured using indices like Excess Heat Factor (EHF), TX90, and TN90, which assess temperature anomalies. EHF combines the intensity and

acclimatization of heat by evaluating 3-day average temperatures relative to recent and long-term climatology (Nairn and Fawcett, 2015). TX90 and TN90 represent days when maximum and minimum temperatures exceed the 90th percentile of a reference period, respectively, indicating extreme daytime and nighttime heat (Perkins and Alexander, 2013).. Research in the region has demonstrated that "the greenhouse effect of water vapor is the main driver of heatwaves in the western Sahel, increasing minimum temperatures by enhanced downward longwave radiation" (Oueslati *et al.*, 2017), underscoring the importance of considering humidity in heat stress evaluations.

1.6 Historical Characterization of Heatwaves in the Sahel

1.6.1 Spatial Patterns

Recent research indicates that the Sahel region endures some of the most severe heatwave conditions globally. According to Ragatoa *et al.* (2024), the Sahel experiences particularly high heatwave levels, with evidence of increasing heatwave intensity over time. This trend is concerning as the region is already characterized by extreme temperatures, with maximum temperatures in the Sahel frequently exceeding 45°C and minimum temperatures remaining high even at night (World Wealth Attribution, 2024). The seasonal cycle of heatwaves in the Sahel shows distinct patterns, with heat stress peaking in spring (March-May) before the monsoon season (Guigma, Todd, and Wang, 2020). This timing is significant as it coincides with pre-monsoon conditions when humidity begins to rise but before the cooling effects of monsoon rains.

1.7 Future Projections of Heatwaves

1.7.1 Climate Change Scenarios

The literature consistently projects worsening heat conditions across the Sahel under future climate scenarios. The region is expected to experience temperature rises approximately 1.5 times faster than the global average (USAID, 2024), making it a hotspot for climate change impacts. Under high-emission scenarios, parts of the Sahel could experience persistent and increased heating of up to ~6.5°C, significantly exceeding the estimated mean global temperature increase (Kwawuvi *et al.*, 2023).

Projections for the long-term evolution of springtime heat waves (March-May) in West Africa under different climate scenarios suggest significant intensification. Analysis of observed and projected changes from 1950 to 2100 indicates a clear trend toward more frequent, longer-lasting, and more intense heat events (Sambou *et al.*, 2021). This trend is particularly pronounced in the Sahel region, where heatwave is projected to be most severe. Projections of future heatwaves in the Sahel region indicate a significant increase in both frequency and intensity due to ongoing climate change. The most optimistic scenario, based on Representative Concentration Pathway (RCP) 2.6, predicts that heatwaves lasting 15 days will become the norm by the end of the century (Muzenda, 2025). This alarming trend is supported by climate models that suggest extreme heat events are becoming more probable, with recent studies indicating that climate change has already made certain extreme heatwaves ten times more likely (Ngoungue Langue, Lavaysse and Flamant, 2025). Subseasonal forecasting models have shown promise for predicting the onset of heatwaves in West African cities up to two weeks in advance, thereby allowing for better preparedness and response measures (Ngoungue Langue *et al.*, 2023). This is particularly crucial as the region faces an upward trend in the duration, intensity, and frequency of heatwaves, with the last decade (2012-2020) contributing significantly to the overall increase in heatwave characteristics compared to the earlier decade (Kunda, Gosling and Foody, 2024). Some researchers project more frequent droughts, driven by declining vegetation cover across the continent, which could exacerbate the effects of heatwaves (Slayi, Zhou and Jaja, 2024).

- **Physiological Limits and Adaptation Boundaries**

A particularly concerning aspect of future projections is the potential breach of physiological limits to adaptation. When wet-bulb temperatures exceed certain thresholds (approximately 35°C), even healthy individuals cannot physiologically cool themselves through perspiration, potentially leading to fatal heat stress without artificial cooling. Studies indicate that under high-emission scenarios, parts of the Sahel could approach or exceed these critical thresholds during extreme heat events, creating conditions that are physiologically intolerable for extended periods. This raises fundamental questions about habitability and necessary adaptation measures in the region.

- **Population Exposure**

The projected increase in extreme heat events across the Sahel poses serious challenges for population exposure, particularly in the absence of effective climate mitigation strategies. Without intervention, this densely inhabited region could face conditions of heat stress for nearly six months annually, intensifying vulnerability to climate-related health risks (Parkes, Buzan and Huber, 2022). The interplay of rapid population growth, expanding urban centers, and rising temperatures will significantly heighten the number of individuals at risk. According to Ceccherini *et al*. (2017), analyses comparing observational and reanalysis data indicate that exposure to extreme heat is expected to surge across West Africa, particularly in regions like the Sahel. Recent projections also underscore the intergenerational burden of climate change, with children born in 2020 likely to experience four to six times more heatwave events than those born in the 1960s (Tesfaye, 2022). This raises urgent concerns about equity and justice, as future generations in vulnerable regions face increasingly severe climate impacts.. The health implications of these projected heatwaves are profound. As heatwaves grow more intense, the risks to vulnerable communities increase, with detrimental impacts on health infrastructure and public services (Alliance Sahel, 2024). Capacity-building efforts and robust climate risk management strategies are essential to prepare local authorities and communities for these anticipated changes (Deglon *et al.,* 2025)

1.8 Adaptation and Early Warning Systems

In response to these challenges, there is growing emphasis on developing health early warning systems to reduce extreme temperature-related mortality in the Sahel. A heat health early warning system for the region aims to provide timely alerts and enable preventive measures during extreme heat events (USAID, 2024). However, the effectiveness of such systems depends on accurate forecasting, communication infrastructure, and community response capacity—all of which remain challenging in resource-constrained settings. Research on subseasonal forecasts of heat waves in West African cities suggests that there is potential for predictability that could inform early warning systems (Ngoungue Langue, Lavaysse and Flamant, 2025). However, the literature also reveals inconsistencies in heatwave definitions and measurements, which "tend to vary depending on the specific group affected or the study context" (Aderotoye, Zaitchik and Asare, 2024). Standardizing these definitions while accounting for local context is essential for effective monitoring and response.

CHAPTER 2: MATERIALS AND METHODS

2.1 Introduction

This chapter presents the methodology employed to carry out the objectives of the study.

2.2 Study Area

The West African Sahel extends longitudinally from Senegal in the west to northern Nigeria in the east as shown in Figure 5, forming a semi-arid transitional belt between the arid Sahara Desert to the north and the wetter Sudanian savannas to the south. Geographically, this zone lies approximately between 12°N and 18°N latitude and 15°W to 20°E longitude as defined by Omotosho and Abiodun (2007).

The focus for this research cuts across the following **five (5) countries** with the following unique physiographic features:

- **Senegal** includes the Ferlo region with sandy soils and sparse vegetation.
- **Mali** features the Niger River Inner Delta, an essential seasonal wetland.
- **Burkina Faso** is defined by plateaus and lowland plains with lateritic soils.
- **Niger** contains expansive dune fields and rocky outcrops in the southern Sahel.
- **Northern Nigeria** showcases savanna grasslands, punctuated by plateaus and inselbergs.

The entire Sahelian band is characterized by flat to gently undulating terrain and sparse vegetation cover dominated by grasses, acacia trees, and drought-resistant shrubs (Sultan and Gaetani, 2016). This landscape creates a unique environmental context where climatic extremes are amplified by the region's physical geography and limited vegetation buffer.

The Sahel experiences a semi-arid climate with pronounced seasonal contrasts. The climate is characterized by a short unimodal rainy season from June to September, driven by the northward movement of the Intertropical Discontinuity (ITD), and a long dry season from October to May, dominated by the dry and dusty Harmattan winds from the desert. Annual precipitation exhibits strong spatial gradients, ranging from approximately 150 mm in northern areas close to the Sahara to 600 mm in the southern fringe of the region. Temperature extremes

are common, with average daytime highs reaching over 40°C during the pre-monsoon months and significant diurnal temperature ranges (Sylla *et al.,* 2018).

Historically, the Sahel has experienced major climatic upheavals, with prolonged droughts in the 1970s–80s resulting in widespread famine, desertification, and displacement. Though precipitation patterns have shown some recovery, rainfall remains highly variable, and temperatures have steadily increased by 1–2°C over the last century. This warming trend has led to more frequent heat waves and unpredictable rainfall patterns (Giannini *et al*., 2008; Sultan and Gaetani, 2016).

The Sahelian region is home to over 100 million people, primarily in rural communities relying on rain-fed agriculture and pastoralism. These climate-sensitive livelihoods are increasingly threatened by rainfall variability, soil degradation, and rising heat stress, which collectively compromise food security and incomes. The region's adaptive capacity is constrained by limited access to irrigation, weak infrastructure, inadequate weather information systems, and sociopolitical instability in several areas. Consequently, seasonal migration, livelihood diversification, and traditional ecological knowledge have become core resilience strategies among Sahelian communities (Morton, 2007; Ouédraogo, Dembélé and Somé, 2010).

The West African Sahel represents a critical region for studying heatwaves due to its acute vulnerability to climate change and extreme weather conditions. The region's semi-arid conditions, low adaptive capacity, and high climate variability make it increasingly susceptible to intense and prolonged heatwaves linked to both natural climate variability and anthropogenic influences (Guigma, 2021). Climate models project that heatwave frequency and intensity in the Sahel will significantly increase under global warming scenarios, exacerbating socio-economic vulnerabilities in a region already grappling with environmental stressors (Sambou *et al.,* 2021).

The Sahel functions as both an ecologically fragile and socially sensitive region, where climate-induced heat stress intersects with food insecurity, migration, and conflict (Busby *et al.,* 2014). Recent reviews emphasize that climate change impacts, including heatwaves, are more pronounced in the Sahel due to compounded effects such as droughts, biodiversity loss, and deforestation (N'gobi *et al.,* 2022). This convergence of factors establishes the region as a "climate hotspot," making it both a relevant and urgent study area for heatwave research.

Moreover, localized studies have illustrated the unique vulnerability of Sahelian populations to heat-related hazards, emphasizing the need for targeted adaptation strategies (Sow and Gaye, 2024). Given its climatic exposure, socio-economic fragility, and the projected escalation of heat extremes, the West African Sahel represents a vital geographic focus for understanding the multifaceted impacts of heatwaves under global climate change scenarios.

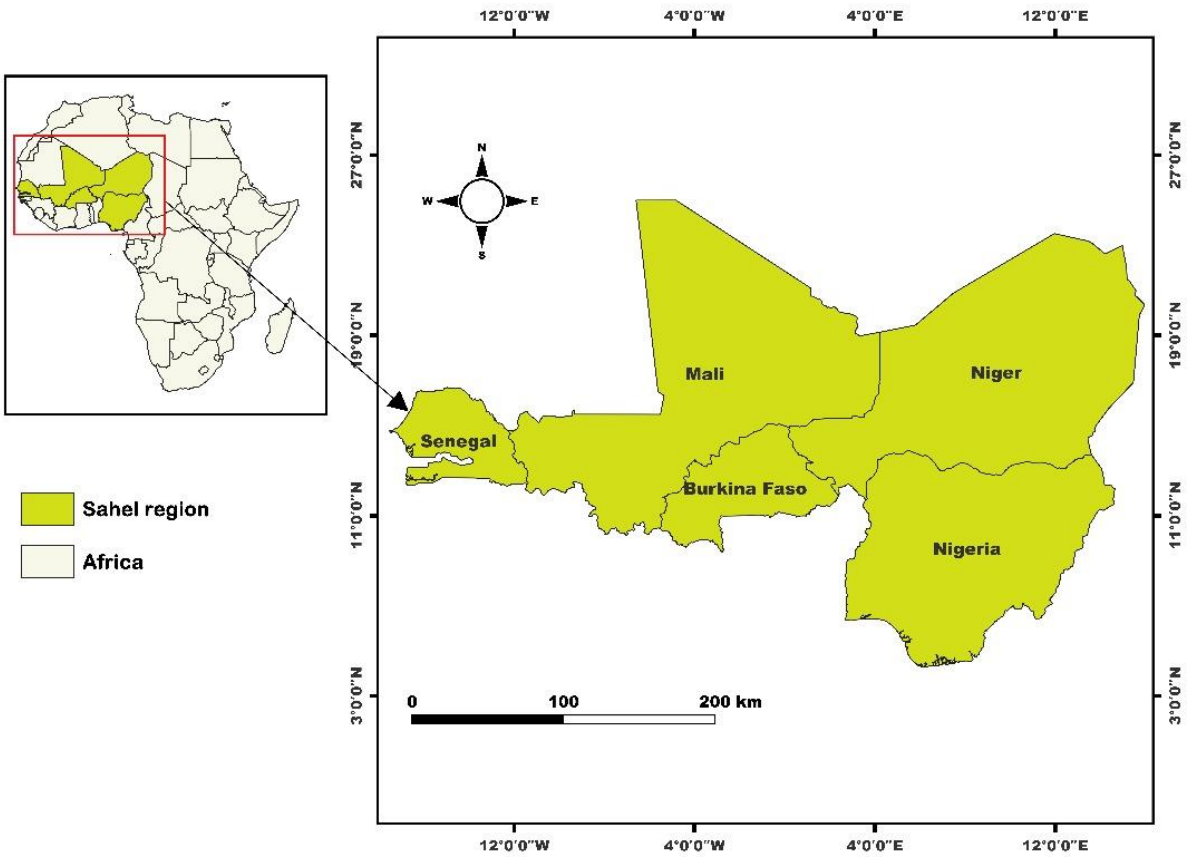

Figure 5 The map of the West African Sahel region

Source: Tambol, Vodounou and Moussa (2023)

2.3 Data Description

2.3.1 ERA5 Reanalysis

Reanalysis datasets are frequently employed as substitutes for direct observational climate and weather data, especially in regions with limited observational coverage such as Africa, due to issues of availability and accessibility (Gleixner, Demissie and Diro, 2020). To obtain consistent climate information over large areas with uniform spatial resolution, this study

utilizes the ERA5 reanalysis—developed by the European Centre for Medium-Range Weather Forecasts (ECMWF)—which represents the fifth generation of ECMWF global atmospheric reanalyses (Hersbach *et al.,* 2020). ERA5 offers hourly outputs of a wide array of atmospheric variables, provided at a spatial resolution of 0.25° × 0.25° and 137 vertical levels, extending from the surface up to 0.01 hPa. This high-resolution, bias-adjusted dataset enables detailed analysis of climate change effects at localized scales (Wu *et al*., 2020).

For this study, ERA5 data covering the period from 1984 to 2014 were employed, specifically focusing on variables such as 2-meter air temperature and both daytime and nighttime extremes. ERA5 has been extensively applied in climate studies across Africa, including those by Barbier *et al*. (2018), Ngoungue Langue *et al.* (2023), and Engdaw et al. (2022), validating its utility for regional climate assessments.

2.3.2 NASA NEX-GDDP

To analyze both historical climate trends and future projections, this study employs the NASA Earth Exchange Global Daily Downscaled Projections (NEX-GDDP) dataset. This dataset offers statistically downscaled outputs from eleven General Circulation Models (GCMs) that are part of the Coupled Model Intercomparison Project Phase 6 (CMIP6), providing data at a high spatial resolution of 0.25° (approximately 25 km) (see Table 1). The dataset is publicly available via NASA's data portal at (NEX-GDDP includes daily maximum and minimum temperature data for three distinct periods: the historical baseline (1984–2014), the near future (2030–2060), and the far future (2061–2091). These projections are provided under two Shared Socioeconomic Pathways: SSP2-4.5, representing a moderate-emissions scenario, and SSP5-8.5, reflecting a high-emissions future (Jones and O'Neill, 2016).

Table 1 : GCM Models from CMIP6 Used in This Study and Their References

Model number	Model name	Modeling center (country)	Resolution (lon × lat)	References	Resolution
1	ACCESS-CM2	Commonwealth Scientific and Industrial Research Organization (Australia)	0.25 ×0.25	Bi et al. (2020)	Daily
2	ACCESS-ESM1-5	Commonwealth Scientific and Industrial Research Organization (Australia)	0.25 ×0.25	Ziehn et al. (2020)	Daily
3	CMCC-ESM2	Euro-Mediterranean Center on Climate Change Foundation (Italy)	0.25 ×0.25	Lovato et al. (2022)	Daily
4	EC-EARTH3	EC-EARTH consortium, Rossby Center, Swedish Meteorological and Hydrological Institute/SMHI (Sweden)	0.25 ×0.25	Döscher et al. (2022)	Daily
5	EC-EARTH3-Veg-LR	EC-EARTH consortium, Rossby Center, Swedish Meteorological and Hydrological Institute/SMHI (Sweden)	0.25 ×0.25	EC-Earth (2020)	Daily
6	IPSL-CM6A-LR	Institut Pierre-Simon Laplace (France)	0.25 ×0.25	Boucher et al. (2020)	Daily
7	KIOST-ESM	Korea Institute of Ocean Science and Technology, Korea Meteorological Administration (Republic of Korea)	0.25 ×0.25	Lee, Wang, et al. (2020)	Daily
8	MIROC6	Japan Agency for Marine-Earth Science and Technology (Japan)	0.25 ×0.25	Tatebe et al. (2019)	Daily
9	MPI-ESM1-2-HR	Max Planck Institute for Meteorology (Germany)	0.25 ×0.25	Müller et al. (2018)	Daily
10	MPI-ESM1-2-LR	Max Planck Institute for Meteorology (Germany)	0.25 ×0.25	Mauritsen et al. (2019)	Daily
11	MRI-ESM2-0	Meteorological Research Institute (Japan)	0.25 ×0.25	Yukimoto et al. (2019)	Daily

2.4 Method of Analysis

2.4.1 Model Evaluation

This research employs Taylor diagrams, following the methodology established by Taylor (2001) and Yan et al. (2022), to assess the performance of eleven (11) climate models sourced from the NASA NEX-GDDP CMIP6 dataset. The Taylor diagram provides an intuitive framework for comparing the spatial patterns of model outputs, both in their original form and after post-processing, emphasizing their agreement with observational data. These diagrams simultaneously incorporate several assessment metrics: standard deviation, centered root mean square error (CRMSE), correlation coefficient, mean bias error (MBE), and mean absolute error (MAE) to quantify how well each model reproduces the observed data.

Standard deviation of observations:

$$\sigma_{obs} = \sqrt{\frac{1}{N}\sum_{n=1}^{N}(X_{obsn} - \bar{X}_{obs})^2}$$

(Equation 1)

Equation 1 calculates the variability in the observed data around its mean. It measures how spread out the observational values are from the average observed value.

Standard deviation of the model:

$$\sigma_{model} = \sqrt{\frac{1}{N}\sum_{n=1}^{N}(X_n - \bar{X})^2}$$

(Equation 2)

Equation 2 measures the variability in the model-simulated data around its mean, indicating how much the model predictions vary from their average value.

Centered root mean square error (CRMSE) is defined as:

$$CRMSE = \sqrt{\frac{1}{N}\sum_{n=1}^{N}[(X_n - \bar{X}) - (X_{obsn} - \bar{X}_{obs})]^2}$$

(Equation 3)

Equation 3 quantifies the magnitude of errors between the model and observed data after removing their respective means. It focuses on pattern differences rather than bias, making it particularly useful for evaluating how well models capture spatial or temporal variability.

Correlation coefficient (r) of the observed data and the model data

$$r = \frac{[\frac{1}{N}\sum_{n=1}^{N}(X_n - \bar{X}) - (X_{obsn} - \bar{X}_{obs})]}{(\sigma_{model}\,\sigma_{obs})}$$

(Equation 4)

Equation 4 measures the linear relationship between the model and observed data, ranging from -1 to 1. Values close to 1 indicate a strong positive correlation, while values near 0 suggest no linear relationship.

Mean Bias Error (MBE):

$$MBE = 1/N\sum(X_n - X_{obsn}) \qquad (Equation\ 5)$$

Equation 5 measures the average difference between model predictions and observations. Positive values indicate the model overestimates, while negative values indicate underestimation. This metric reveals systematic bias in the model.

Mean Absolute Error (MAE):

$$MAE = 1/N\sum|X_n - X_{obsn}| \qquad (Equation\ 6)$$

Equation 6 calculates the average magnitude of errors without considering their direction. It provides a measure of overall prediction accuracy, where lower values indicate better model performance.

Taylor's Diagram Relationship

The central root mean square error, correlation coefficient, and standard deviation of the simulated and observed data follow the relationships in Equation 7, which constitute the fundamental component of the Taylor diagram:

$$\mathrm{CRMSE}^2 = \sigma_{obs}^2 + \sigma_{model}^2 - 2 \cdot \sigma_{obs} \cdot \sigma_{model} \cdot r$$

(Equation 7)

This framework provides a concise summary of how well each model reproduces the observed climate variability.

2.4.2 Trend Analysis and Significance Testing

The Mann–Kendall test (Mk) represents a non-parametric statistical technique for detecting monotonic trends within time series datasets (Mann, 1945; Kendall, 1975; Wang *et al.*, 2021). This approach was applied to detect discontinuities arising from non-homogeneous temporal sequences. Its distinctive feature is the lack of assumptions about data distribution, which has made it broadly adopted for trend analysis (Mondal *et al.*, 2012). These characteristics have led to its extensive application in trend studies (Ilori and Ajayi, 2020; Arowolo and Oluleye, 2022; Arowolo *et al.*, 2025). Its advantages include the elimination of normality requirements for the time series, the ability to handle datasets with missing values, and its resistance to the effects of outliers.

The Mk statistics in Equation 8 are formulated as follows:

$$K = \sum_{i=1}^{n} \sum_{j=1}^{i-1} sign(x_i - x_j)$$

(Equation 8)

Where: xi and xj = values of the sequential generic data,

n = data total length.

Sign Test

sign (xi-xj) can be defined as;

$$sign(x_i - x_j) = \begin{cases} 1, & if \ \ x_i - x_j > 0 \\ 0, & if \ \ x_i - x_j = 0 \\ -1, & if \ \ x_i - x_j < 0 \end{cases}$$

(Equation 9)

Equation 9 function assigns +1 for increasing trends, 0 for no change, and -1 for decreasing trends between data pairs.

Variance Calculation:

The variance Var (S) in Equation 10 was calculated as follows when S statistic is approximately distributed with the E(S) mean

$$Var(S) = \ (n(n-1)(2n+5) - \sum_t t\,(t-1)(2t+5))$$

(Equation 10)

Where t = $any\ given\ tie\ extent$

$\sum t = summation\ of\ all\ values\ of\ the\ tie\ number$

n = Length of series

The Z **standardized test statistic** Z is computed in Equation 11:

$$Z = \begin{cases} 1, & if\ K < 0 \\ 0, & if\ K = 0 \\ \dfrac{S+1}{\sqrt{Var(S)}}, & if\ K > 0 \end{cases}$$

(Equation 11)

When a dataset containing n variables exhibits random distribution with independence, absence of trend, and equal likelihood of ordering, the null hypothesis (H0) is accepted. The absolute value of the Z statistic (test statistic) is subsequently compared against the critical value $Z(1 - p/2)$ at the p significance level to determine whether to reject or accept the H_0 hypothesis.

2.4.3 Ensemble Mean of Multi-Model

To reduce individual model biases and uncertainties, the Multi-Model Ensemble Mean (MME) was computed by averaging across the selected models (Gleckler, Taylor and Doutriaux 2008; Knutti *et al*., 2010), as shown in Equation 12

$$MME = \frac{1}{N}\sum_{i=1}^{N} X_i$$

(Equation 12)

Where:

X_i is the output from the i^{th} model

N is the total Number of models

The MME technique capitalizes on the advantages of individual climate models while minimizing the impact of their limitations. Through the process of combining multiple model outputs, the ensemble average delivers a more stable and dependable depiction of climatic parameters (Arowolo *et al*., 2025). The effectiveness of MME methods in climate forecasting has been extensively demonstrated.

2.4.4 Heat Wave Indices and Definition

This study employed three distinct heat wave definitions following the methodology developed by Perkins and Alexander (2013) to characterize heat wave events across the West African Sahel region.

The original model datasets for daily maximum temperature (TX) and daily minimum temperature (TN) underwent comprehensive pre-processing using Climate Data Operators (CDO) software. This pre-processing workflow was designed to ensure full compatibility with ClimPACT2 software requirements and followed the standardized procedures outlined by Perkins and Alexander (2013). The ClimPACT2 is an R software package that calculates the ET-SCI indices as well as additional climate extremes indices from data stored in text or netCDF files (Alexander and Herold, 2016). The output was then visualized using Python.

The following three heat wave definitions were applied:

(1) CTX90pct: A heat wave is identified when the daily maximum temperature (Tmax) exceeds the calendar day 90th percentile threshold for at least three consecutive days. The threshold is calculated based on a 15-day window centered on each calendar day using the 1981-2010 base period. (Perkins and Alexander, 2013)

(2) CTN90pct: A heat wave is identified when the daily minimum temperature (Tmin) exceeds the calendar day 90th percentile threshold for at least three consecutive days. Similar to CTX90pct, thresholds are calculated using a 15-day running window centered on each day.

(3) EHF (Excess Heat Factor): A heat wave is identified when the EHF is positive for at least three consecutive days. The EHF combines two indices:

$$\mathrm{EHIaccl} = [(\mathrm{TMi} + \mathrm{TMi}-1 + \mathrm{TMi}-2)/3] - [\mathrm{TMi}-3 + \ldots + \mathrm{TMi}-32)/30]$$

(Equation 13)

Equation 13 compares the 3-day average temperature with the preceding 30-day average, representing short-term acclimatization.

$$\mathrm{EHIsig} = [(\mathrm{TMi} + \mathrm{TMi}-1 + \mathrm{TMi}-2)/3] - \mathrm{TM90i}$$

(Equation 14)

Equation 14 component compares the 3-day average with the 90th percentile threshold, representing the climatological significance.

$$\mathrm{EHF} = \mathrm{EHIsig} \times \max(1, \quad \mathrm{EHIaccl})$$

(Equation 15)

where TMi represents the daily mean temperature (average of Tmax and Tmin) for day i, and TM90, i is the 90th percentile of the mean daily temperature in Equation 15. The use of calendar day percentiles with a running window allows these definitions to account for the seasonal cycle and climate variability specific to the West African Sahel region.

2.4.5 Heat Wave Aspects

For each heat wave definition, five aspects were calculated to comprehensively characterize heat wave events during the extended summer season

(1) Heatwave Number (HWN): The count of distinct heat wave events occurring in each summer season.

(2) Heatwave Frequency (HWF): The total number of days participating in heat wave events per season.

(3) Heatwave Duration (HWD): The length (in days) of the longest heat wave event in each season.

(4) Heatwave Cumulative Magnitude (HWM): The cumulative temperature departure above the applicable threshold during heat wave events within a season.

(5) Heatwave Amplitude (HWA): The peak temperature (or temperature anomaly) of the hottest day during the hottest heat wave of each season.

CHAPTER 3: RESULTS AND DISCUSSION

3.1 Introduction

This chapter presents the spatial heatwave characterization analysis for both historical and projected data and discusses their implications for understanding extreme temperature events in the study region.

3.2 Model Evaluation

The Taylor diagrams in Appendix A and summary of model performance statistics is presented in Table 2. Table 2 presents Taylor diagrams comparing observed and model-simulated data for **maximum temperature (TX)** and **minimum temperature**, respectively. These diagrams evaluate model performance using three statistical indicators: standard deviation (SD), correlation coefficient (R), and root mean square error (RMSE). The black star symbol on each diagram represents the reference observational dataset (ERA5), while the curved dashed line represents RMSE contours. The concentric green arcs indicate standard deviation, and the radial blue lines show correlation values.

Table 2 reveals most models clustered around a correlation range of **0.76 to 0.85**, with standard deviation values between **2.1 and 2.5**. The **MPI-ESM1-2-HR** model performed best, showing a correlation of approximately **0.85**, a standard deviation of **2.2**, and RMSE of **0.9**, closely mirroring the observed data. MRI-ESM2-0 and ACCESS-ESM1-5 also performed well, with correlation coefficients of **0.76–0.83** and moderate error metrics.

Table 2 shows slightly improved correlation for most models, ranging between **0.78 and 0.87**, with standard deviations generally close to the observed reference (2.4). **MPI-ESM1-2-HR** again had the best performance with a high correlation of **0.87**, low standard deviation (**2.1**), and the lowest RMSE (**0.8**), suggesting strong agreement with ERA5. ACCESS-ESM1-5 and EC-Earth3 also demonstrated reasonably good performance.

Table 2 : Standard Deviation, Correlation Coefficient and Root Mean Square Error of Minimum and Maximum Temperatures from Taylor's Diagram.

Model	Max Temp R^2	Max Temp SD	Max Temp RMSE	Min Temp R^2	Min Temp SD	Min Temp RMSE
ACCESS-ESM1-5	0.83	2.2	1.0	0.84	2.2	1.0
EC-Earth3	0.82	2.5	1.2	0.82	2.5	1.2
MPI-ESM1-2-HR	0.85	2.2	0.9	0.87	2.1	0.8
MRI-ESM2-0	0.76	2.3	1.3	0.78	2.3	1.2

3.3 Analysis of Heatwave Characteristics over the Sahel Region of West Africa

a. Heatwave Number

The spatial distribution of Heat Wave Number (HWN) across the study area reveals distinct patterns across the three thermal indices examined. For TX90 (Figure 6), observed values range from 1.0-1.9 events per year, with higher frequencies concentrated in the northern Sahel regions (Guigma *et al.,* 2020). The ENSMEAN and individual climate models generally capture this spatial pattern, though ACCESS-ESM1-5 and EC-Earth3 show notable overestimation in the eastern regions, consistent with documented model biases in reproducing West African heat extremes (Sylla *et al.,* 2018).

TN90 analysis (Figure 7) demonstrates lower HWN values (0.50-1.58 events/year) compared to TX90 (Figure 21), indicating that consecutive warm nights are less frequent than consecutive hot days across the region. This pattern aligns with findings from similar arid climates where nighttime cooling allows heat dissipation despite extreme daytime temperatures (Oueslati *et al.,* 2017). The MPI-ESM1-2-HR model shows better agreement with observations for TN90 (Figure 7), while other models tend to underestimate nighttime heat wave frequency.

The Excess Heat Factor (EHF) results (Figure 8) show intermediate values between TX90 and TN90, with the observed pattern ranging from 1.0-1.9 events annually. The models

demonstrate varying skill in reproducing EHF patterns, with EC-Earth3 showing substantial overestimation in eastern regions (Nairn and Fawcett, 2015). These model discrepancies highlight ongoing challenges in accurately simulating complex heat wave dynamics across the climatically diverse West African region (Sambou *et al.*, 2021).

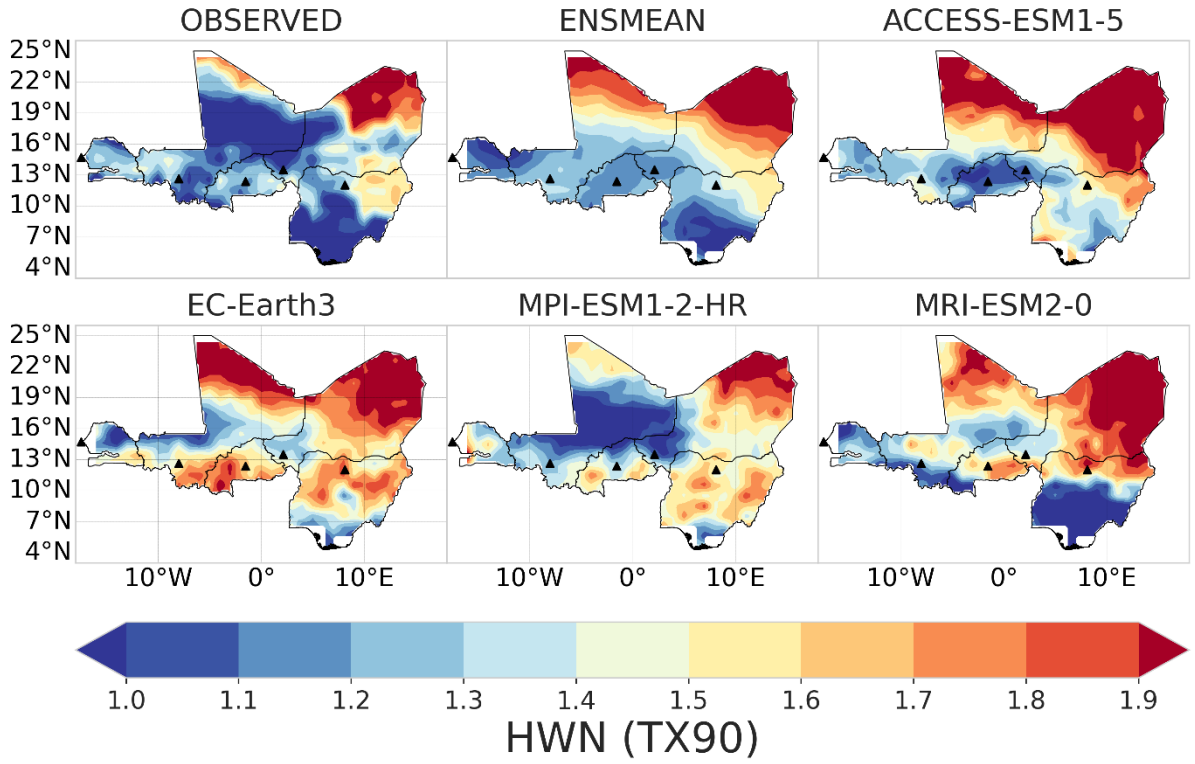

Figure 6 : Characterization of heatwaves in the Sahel Region using HWN (Heat Wave Number) °C for daytime (TX90th percentile) from 1984 - 2014.

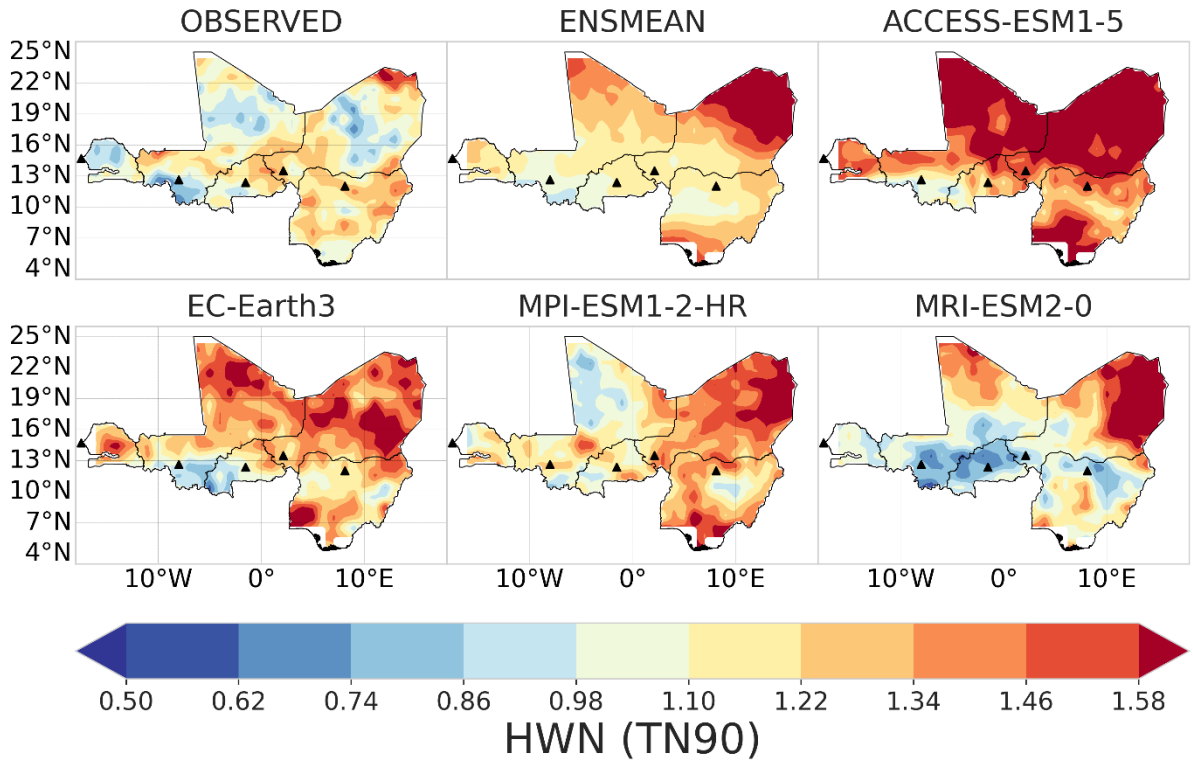

Figure 7 : Characterization of heatwaves in the Sahel Region using HWN (Heat Wave Number) °C for nighttime (TN90th percentile) from 1984 – 2014.

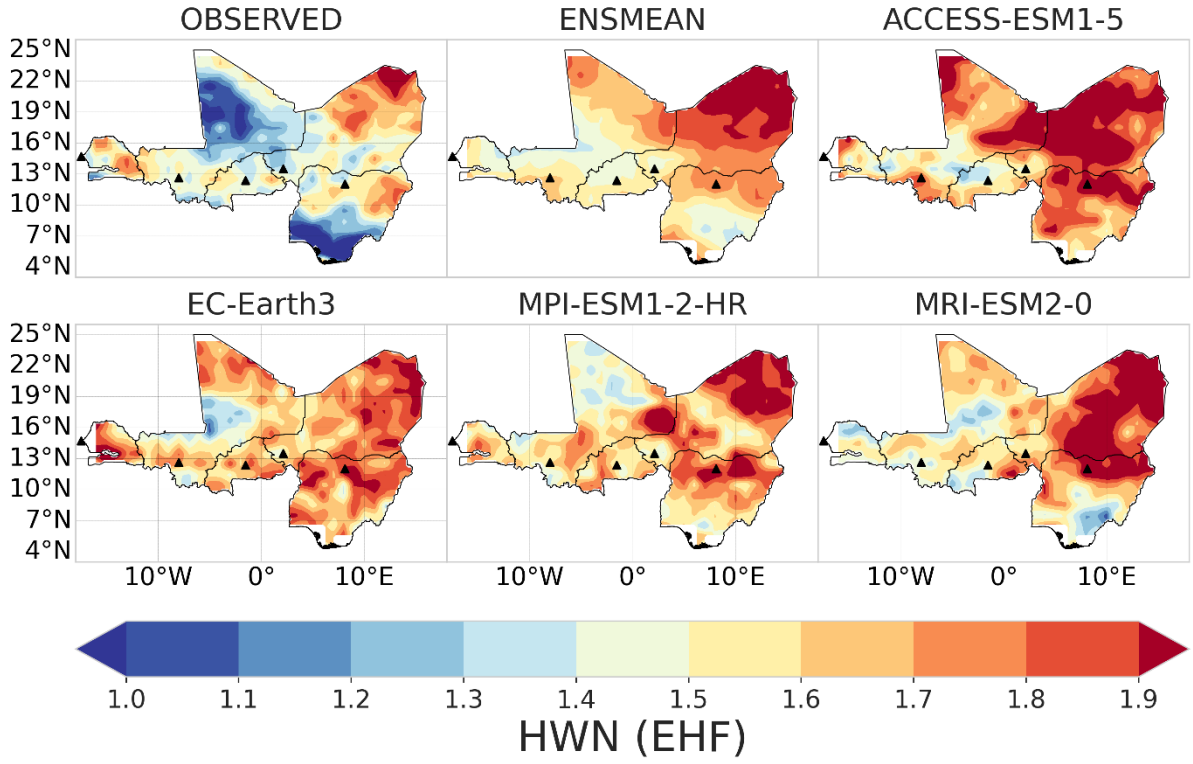

Figure 8 : Characterization of heatwaves in the Sahel Region using HWN (Heat Wave Number) °C for excess heat factor (EHF) from 1984 - 2014.

b. Heatwave Frequency

The heatwave frequency analysis across the Sahel region reveals distinct spatial and temporal patterns under different characterization methods. The TX90 analysis (Figure 9) reveals daytime heatwave frequencies between 0-9, with observed data indicating moderate frequencies of 2-5 across most regions. Model performance varies significantly, with some models underestimating frequencies in southern areas while overestimating in northern zones, highlighting the challenges in accurately representing heatwave characteristics across the climatically diverse Sahel region. Under the TN90 threshold (Figure 10), nighttime heatwave frequencies range from 3.0 to 6.6, with observed data displaying lower frequencies in central areas and higher values in peripheral regions. The model ensemble shows considerable variation, with ACCESS-ESM1-5 demonstrating pronounced overestimation in northern areas. EC-Earth3 presents contrasting spatial patterns compared to observations, while MPI-ESM1-2-HR and MRI-ESM2-0 show mixed performance across the domain.

For the EHF metric (Figure 11), heatwave frequency values range from 1 to 10, with observed data showing moderate frequencies of 3-6 across most areas, while climate models demonstrate varying performance. The ENSMEAN and ACCESS-ESM1-5 models show higher frequencies in the northern Sahelian zones, consistent with the region's arid characteristics. EC-Earth3 and MPI-ESM1-2-HR exhibit similar patterns with elevated frequencies in northeastern areas, reflecting the climatic gradient from humid southern regions to dry northern zones.

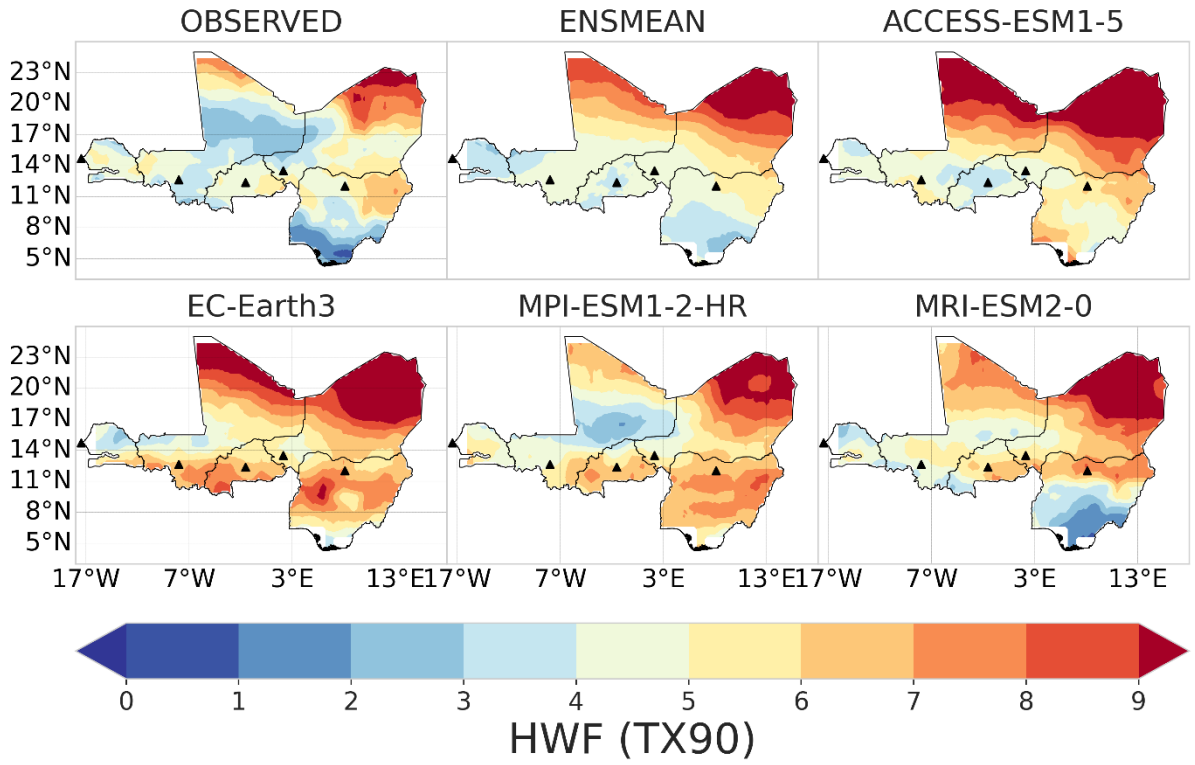

Figure 9 : Characterization of heatwaves in the Sahel Region using HWF (Heat Wave Frequency) °C for daytime (TX90th percentile) from 1984 - 2014.

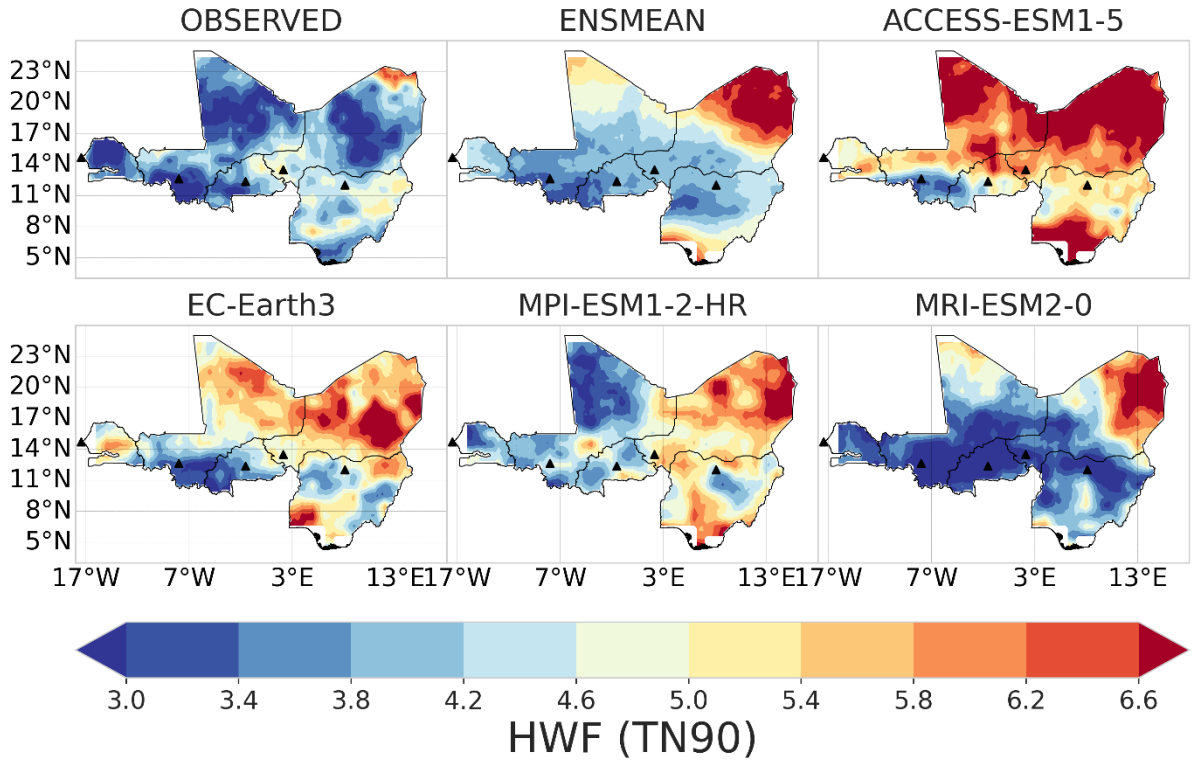

Figure 10 Characterization of heatwaves in the Sahel Region using HWF (Heat Wave Frequency) °C for nighttime (TN90th percentile) from 1984 - 2014.

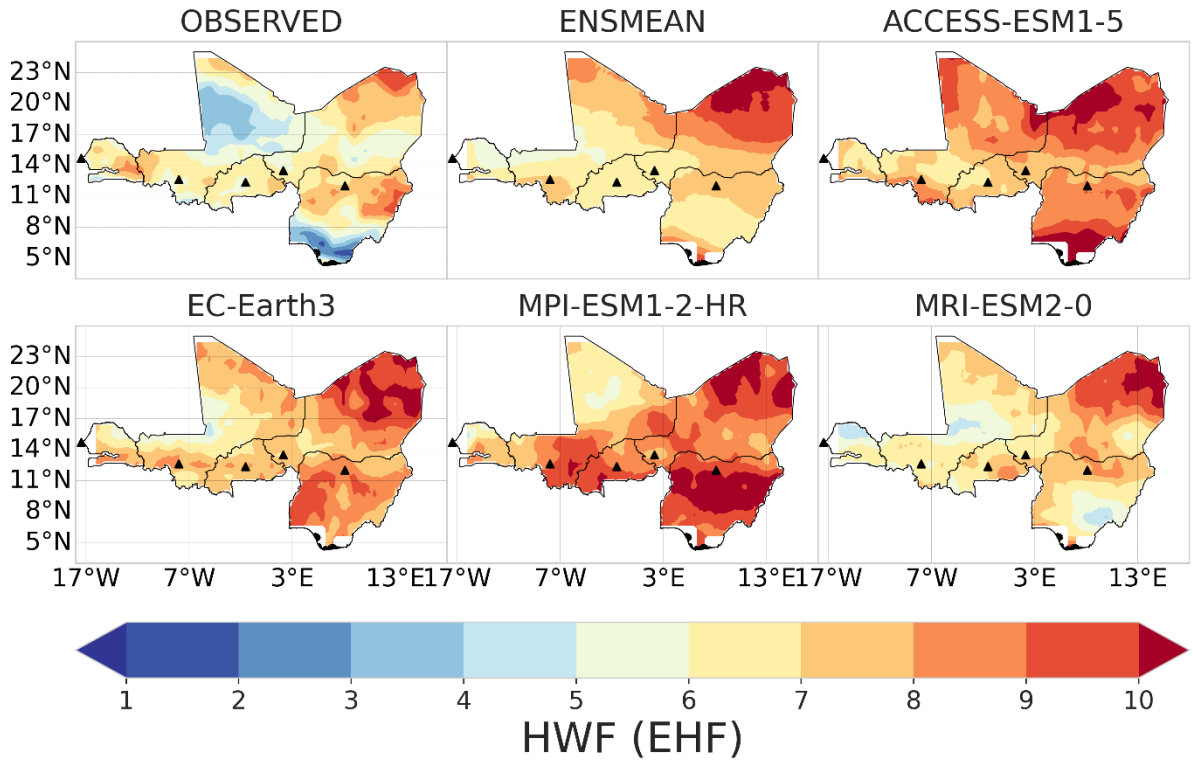

Figure 11 Characterization of heatwaves in the Sahel Region using HWF (Heat Wave Frequency) °C for excess heat factor (EHF) from 1984 - 2014.

c. Heatwave Amplitude

The three figures reveal distinct heatwave patterns across the Sahel region, with varying model performances in capturing observed climate dynamics. The observed data consistently demonstrate a pronounced north-south gradient, where northern Sahelian areas experience the most severe heatwave conditions while southern regions show relatively moderate intensities.

For daytime heatwaves (Figure 12), the observed data display HWA values ranging from 30-48°C, with northern regions reaching extreme temperatures above 46°C. The ENSMEAN effectively captures this spatial pattern, though with slightly enhanced amplitude across the central belt. Among individual models, ACCESS-ESM1-5 and MRI-ESM2-0 closely replicate the observed gradient, while EC-Earth3 and MPI-ESM1-2-HR show reasonable agreement but with some overestimation in northern areas.

Nighttime heatwaves (Figure 13) exhibit a more compressed range of 24-33°C, with the observed data showing moderate intensities across most of the region. The ENSMEAN maintains good correspondence with observations, particularly in the central Sahel. ACCESS-ESM1-5 demonstrates exceptional accuracy in reproducing the observed nighttime patterns, while EC-Earth3 shows notable warming bias in northern regions.

The Excess heat factor (EHF) Figure 14 reveals minimal threat levels in observed data, with values predominantly below 3°C across the region. However, ACCESS-ESM1-5 and MRI-ESM2-0 significantly overestimate EHF values, suggesting potential model limitations in representing combined intensity-duration effects. These discrepancies highlight the importance of model selection for regional climate impact assessments and adaptation planning strategies.

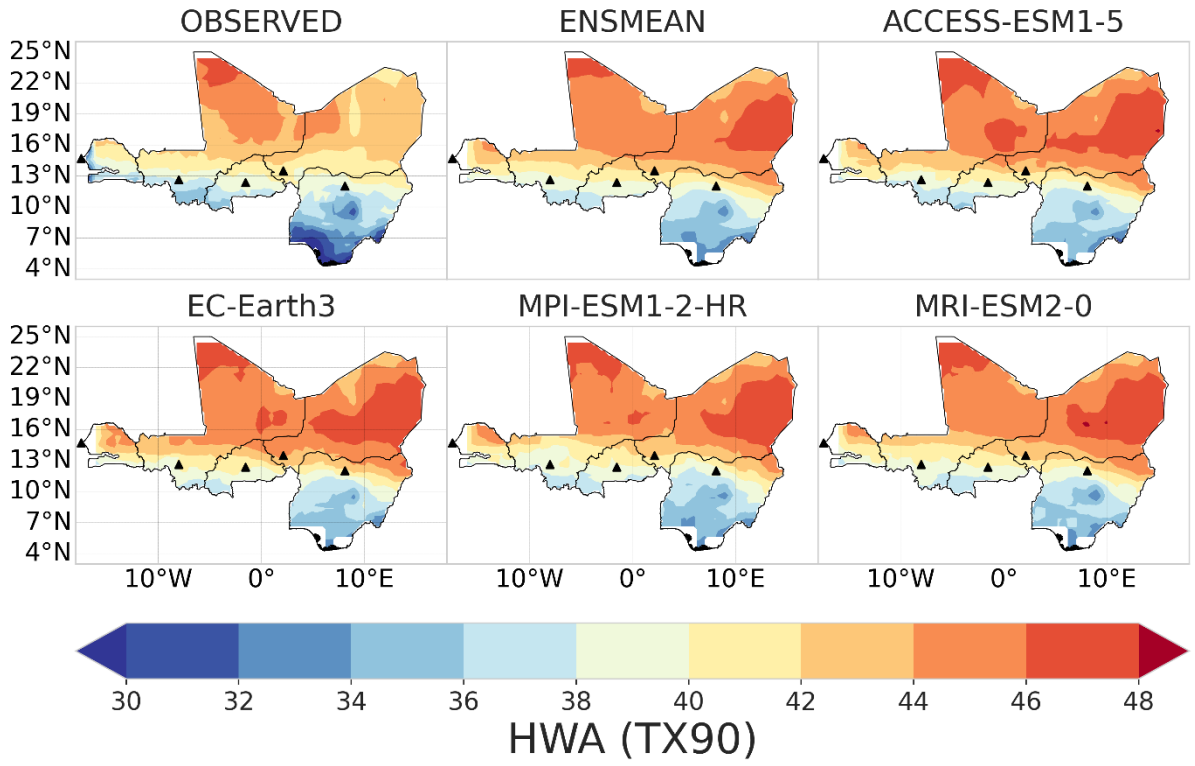

Figure 12 Characterization of heatwaves in the Sahel Region using HWA (Heat Wave Amplitude) °C for daytime (TX90th percentile) from 1984 - 2014.

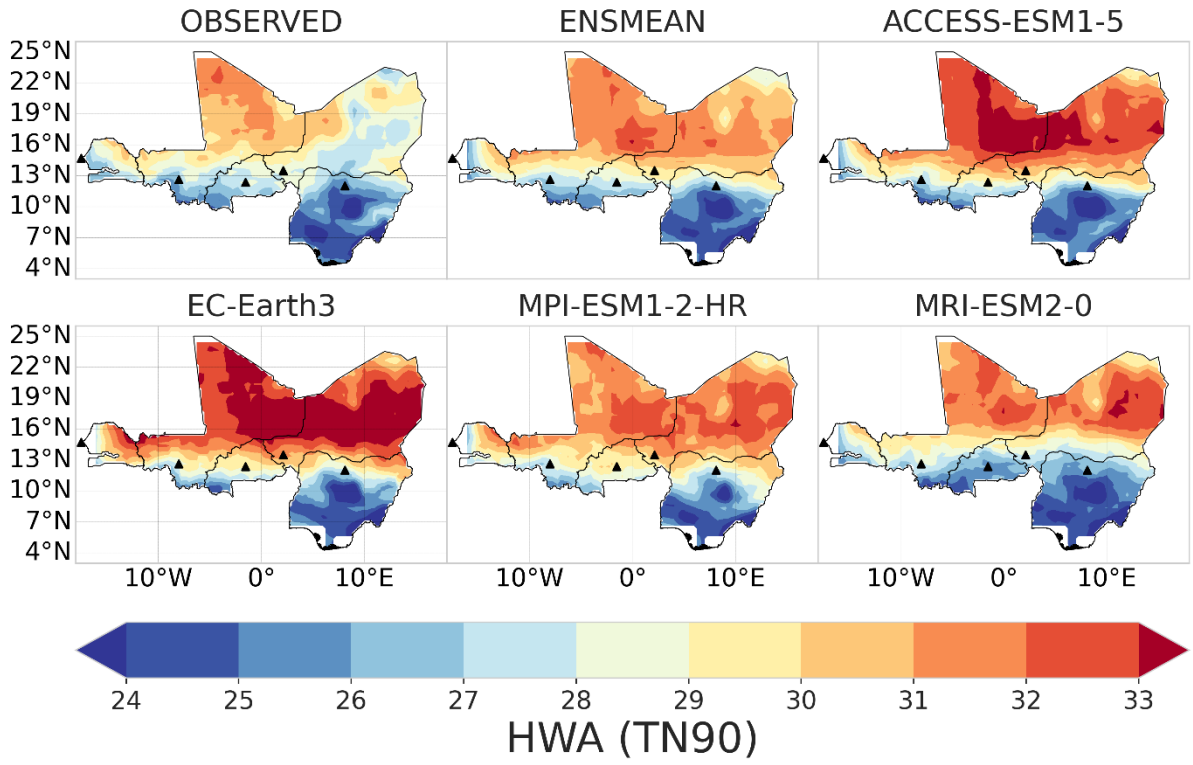

Figure 13 : Characterization of heatwaves in the Sahel Region using HWA (Heat Wave Amplitude) °C for nighttime (TN90th) from 1984 - 2014.

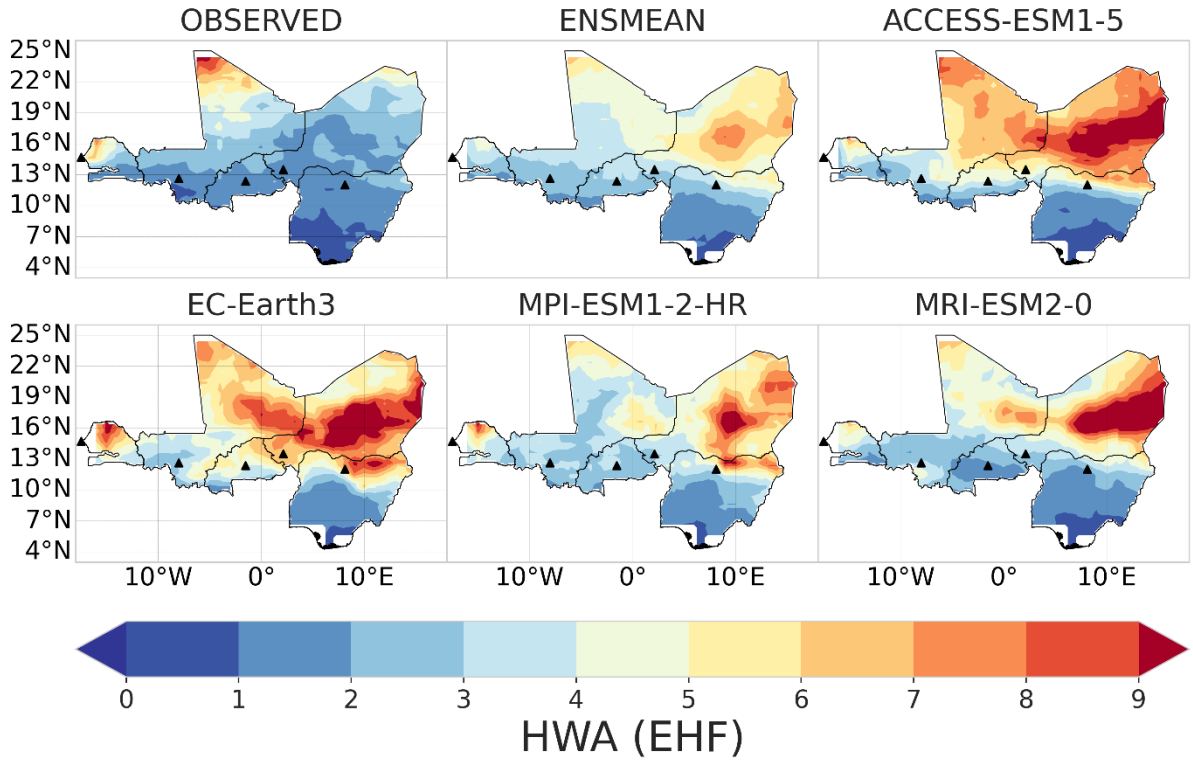

Figure 14 : Characterization of heatwaves in the Sahel Region using HWA (Heat Wave Amplitude) °C for excess heat factor (EHF) from 1984 - 2014.

d. Heatwave Duration

For Heatwave Duration (HWD) analysis across the Sahel region (Figures 15-17), the observed data reveals distinct spatial patterns for nighttime (TN90), daytime (TX90), and excess heatwave factor (EHF) metrics. For daytime heatwave duration (TX90) (Figure 15), the observed pattern demonstrates more pronounced spatial variability, with northern regions experiencing 4-6 days of continuous heatwave conditions, while southern areas record shorter durations of 3-4 days. This distribution highlights the vulnerability of northern Sahel populations to extended daytime heat exposure, potentially impacting agricultural productivity and human health. Under nighttime conditions (TN90), (Figure 16) the observed data shows predominantly 3-4 days of heatwave duration across most of the region, with slightly elevated values (4-5 days) in specific northern areas. The central and southern portions generally experience shorter durations, indicating less severe nighttime heat stress compared to northern territories.

Regarding model performance, ACCESS-ESM1-5 shows reasonable agreement with observed patterns for both nighttime and daytime analyses, though it tends to slightly overestimate durations in certain regions. EC-Earth3 demonstrates significant overestimation, particularly in the northern areas, where it projects 5-6 days compared to the observed 3-4 days. MPI-ESM1-2-HR exhibits mixed performance, showing good correlation in some areas but overestimating in others. MRI-ESM2-0 consistently underestimates heatwave durations across the region.

The excess heatwave factor (Figure 17) analysis reveals that observed conditions range between 4-6 days across most areas, with EC-Earth3 and MPI-ESM1-2-HR showing notable overestimation, while MRI-ESM2-0 significantly underestimates the intensity of extreme heat events throughout the Sahel region.

.

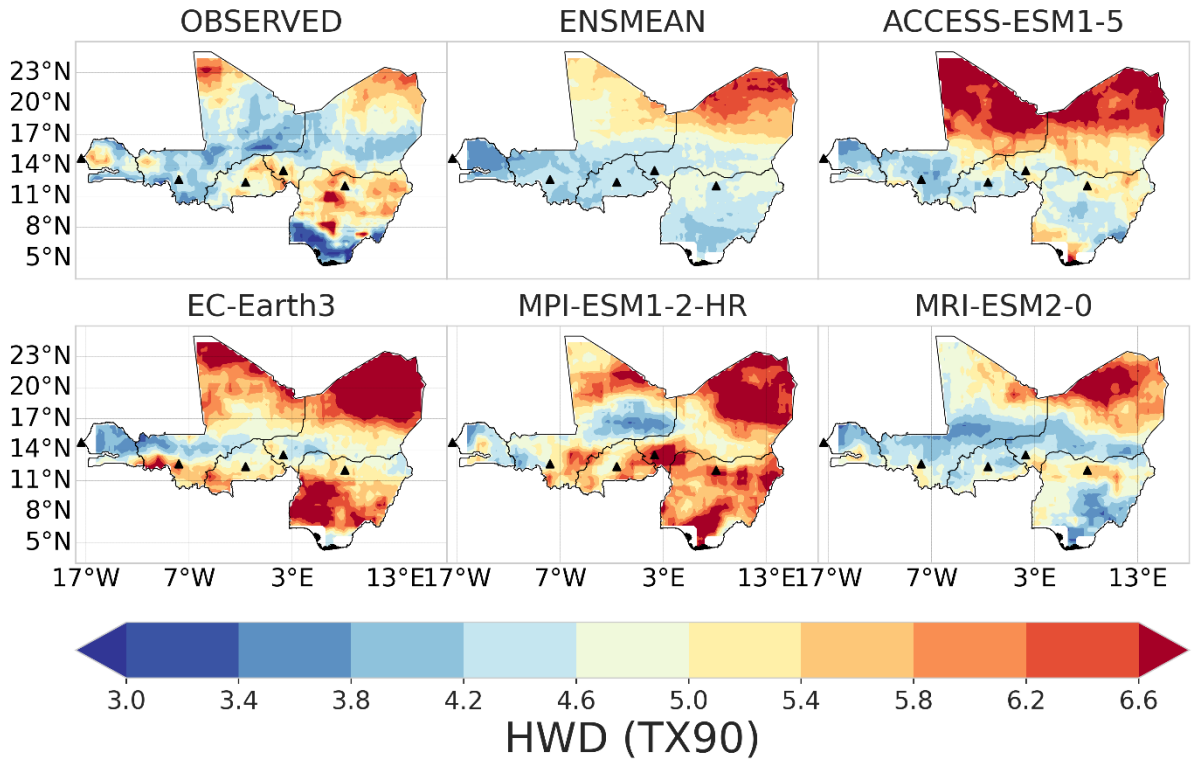

Figure 15 : Characterization of heatwaves in the Sahel Region using HWD (Heatwave Duration) °C for daytime (TX90) from 1984 - 2014.

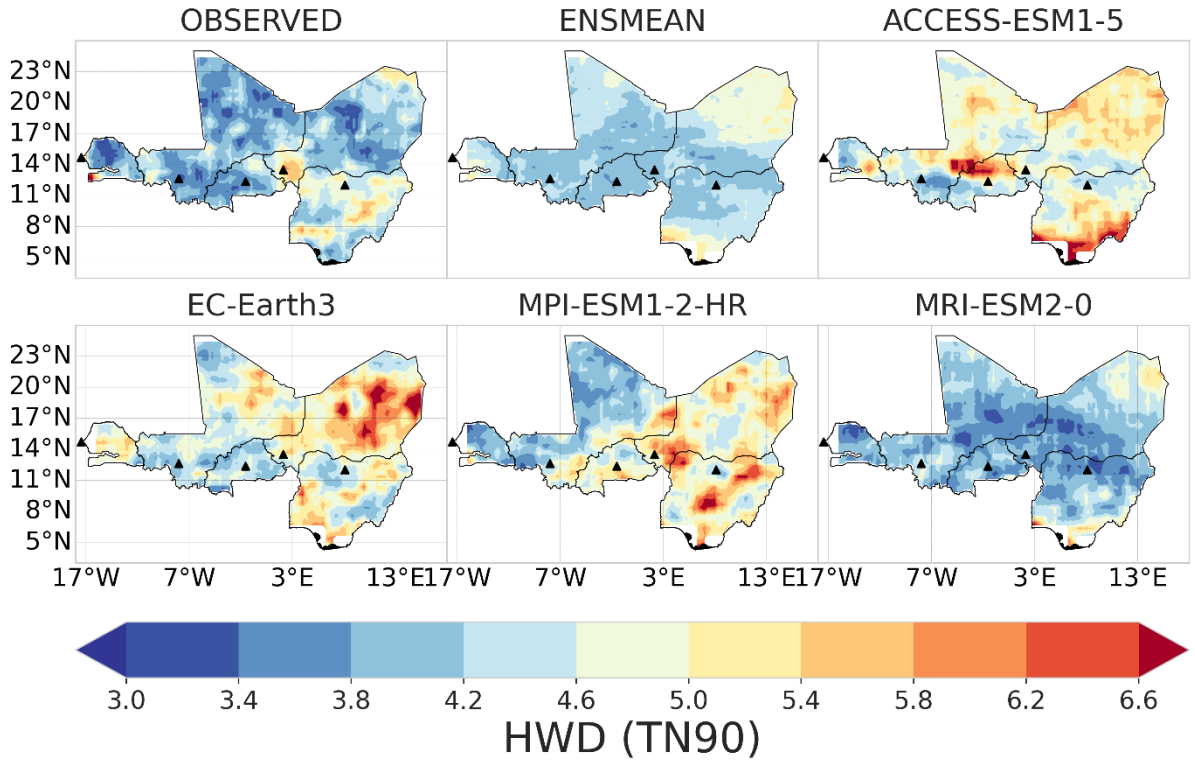

Figure 16: Characterization of heatwaves in the Sahel Region using HWD (Heatwave Duration)

°C for nighttime (TN90) from 1984 - 2014.

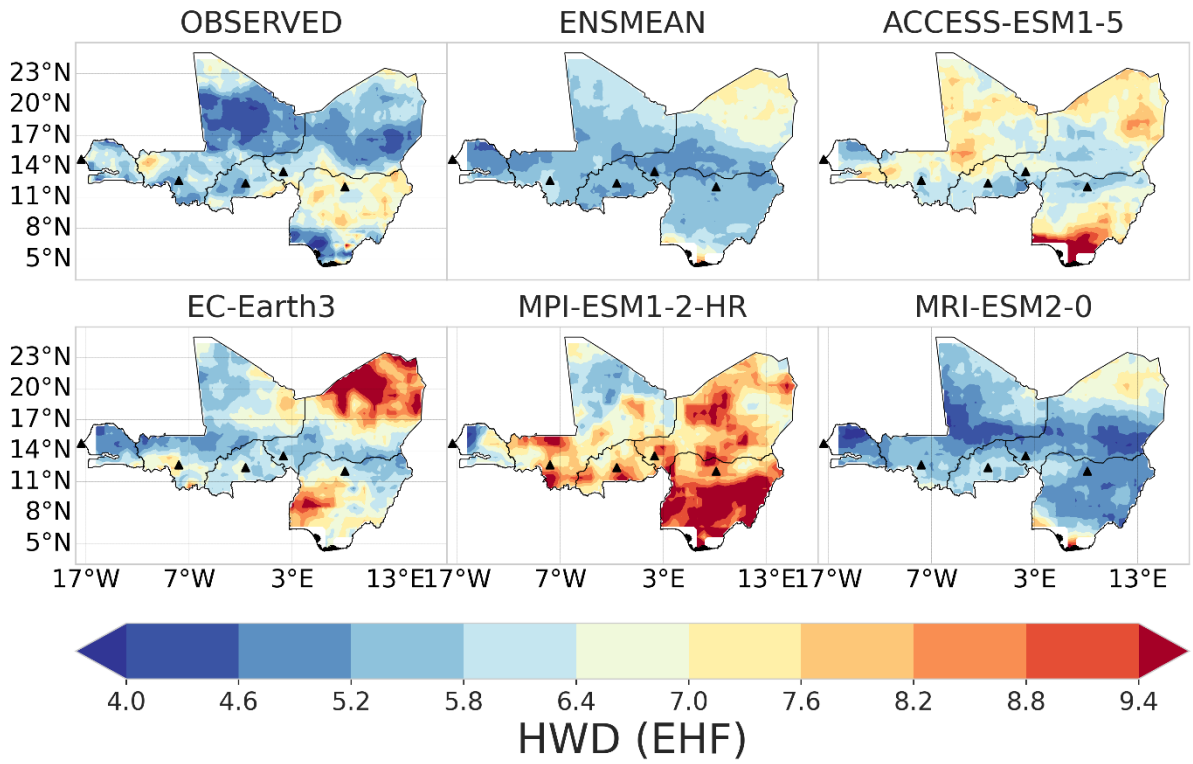

Figure 17 : Characterization of heatwaves in the Sahel Region using HWD (Heatwave Duration) °C for Excess Heat Factor (EHF) from 1984 - 2014.

e. **Heatwave Magnitude**

Looking at the heatwave magnitude (HWM) analysis across the Sahel region, three distinct patterns emerge from the model comparisons with observed data. Daytime heatwave conditions (Figure 18) exhibit significantly higher magnitudes, with observed values ranging from 27°C to 45°C. The models show remarkable consistency in replicating both the spatial distribution and intensity patterns, suggesting robust representation of daytime extreme temperature processes. All models capture the pronounced north-south gradient and the localized hotspots effectively.

For nighttime conditions (Figure 19), the observed HWM values range from approximately 23°C in the southern portions to 28°C in the northern Sahel, following the expected latitudinal temperature gradient. This spatial distribution reflects the region's position between the more humid Sudanian zone and the arid Saharan influences. The ensemble mean and individual

models (ACCESS-ESM1-5, EC-Earth3, MPI-ESM1-2-HR, and MRI-ESM2-0) demonstrate reasonable agreement with observations, maintaining similar spatial patterns while showing slightly elevated intensities across the domain.

However, the Excess Heat Factor (Figure 20) analysis reveals notable discrepancies between models and observations. The observed EHF values remain below 1.0 across most of the Sahel, indicating relatively moderate heatwave impact factors. While MPI-ESM1-2-HR and MRI-ESM2-0 approximate the observed low-impact scenario, other models, including ACCESS-ESM1-5 and EC-Earth3, significantly overestimate EHF values, reaching above 2.0-3.0 in some regions, potentially indicating systematic biases in their representation of heatwave persistence and cumulative effects.

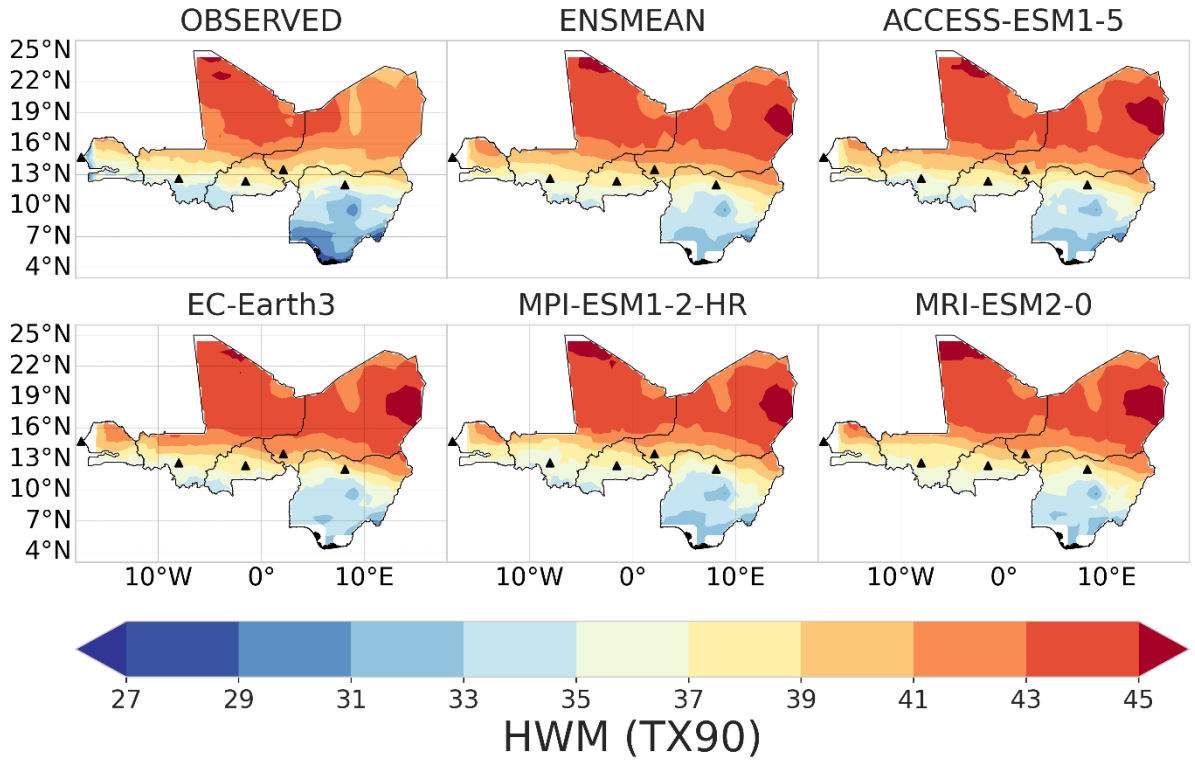

Figure 18 : Characterization of heatwaves in the Sahel Region using HWM (Heat Wave Magnitude) °C for daytime heatwave (TX90) from 1984 - 2014.

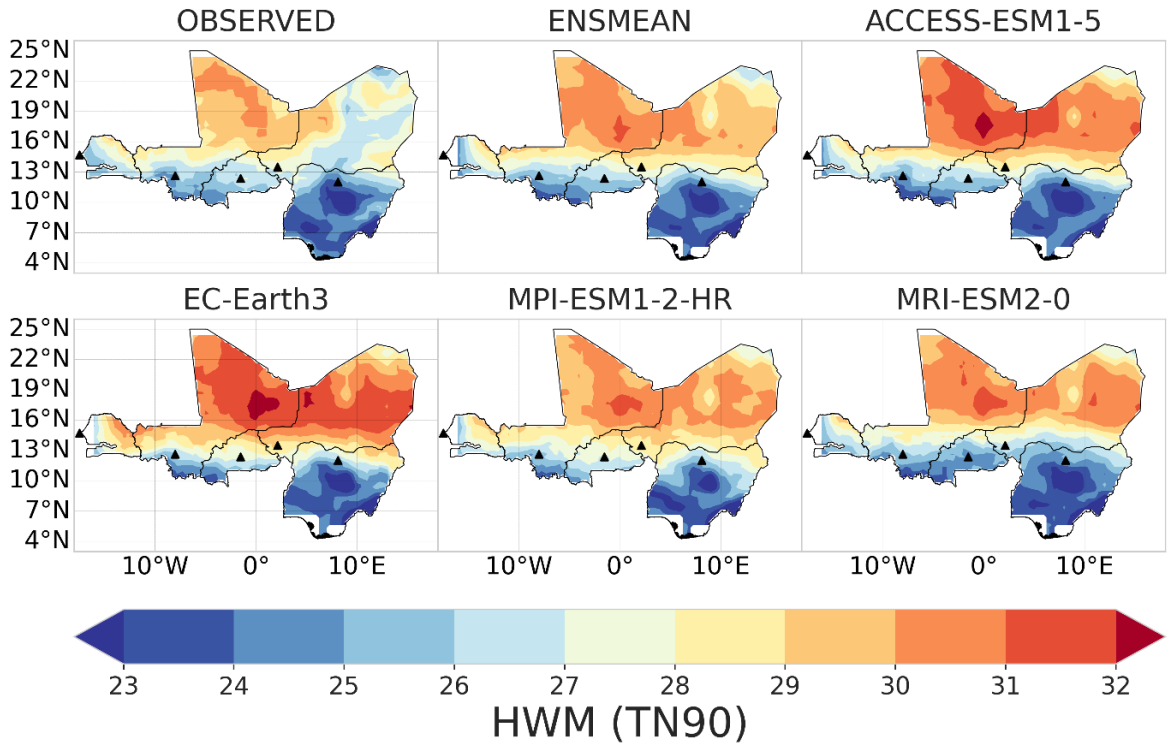

Figure 19 : Characterization of heatwaves in the Sahel Region using HWM (Heat Wave Magnitude) °C for nighttime heatwave (TN90) from 1984 - 2014.

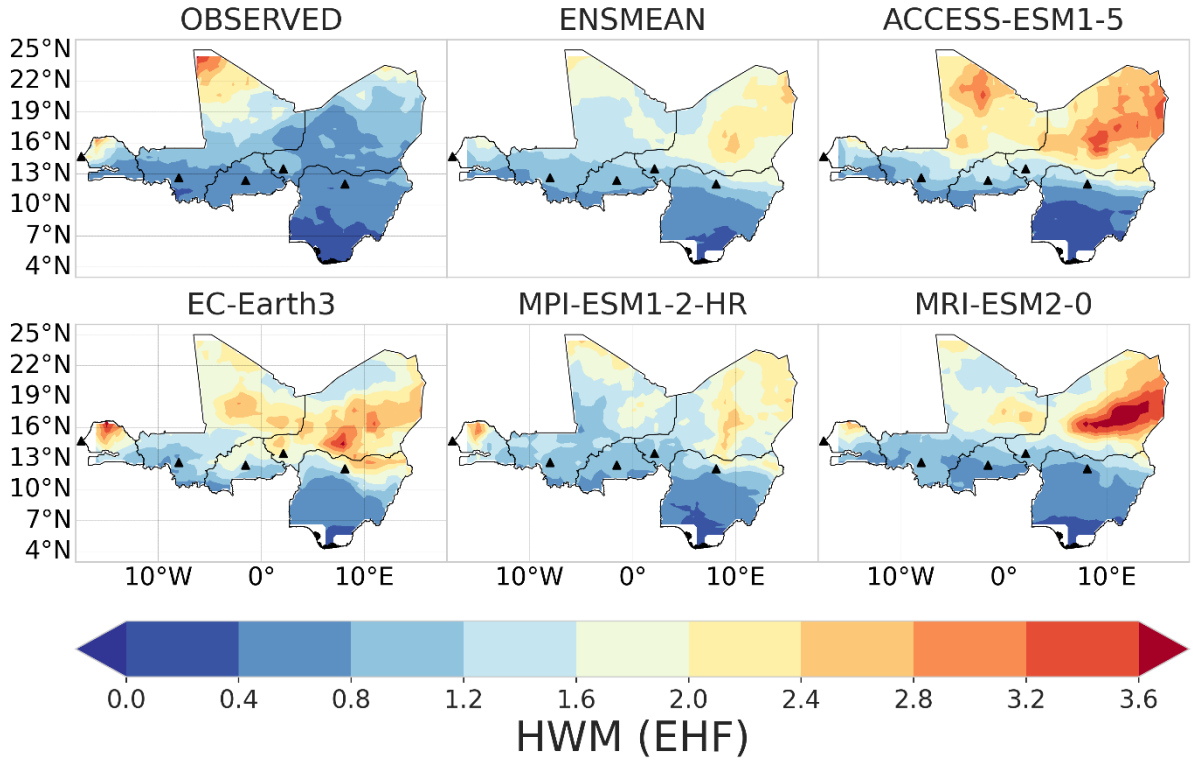

Figure 20 : Characterization of heatwaves in the Sahel Region using HWM (Heat Wave Magnitude) °C for nighttime heatwave (EHF) from 1984 - 2014.

3.4 Trend Analysis of Heatwave Characteristics

a. Heatwave Number Trend

A mixed pattern of positive and negative trends was observed for HWN_TX90 (Figure 21) across different regions of the country. The results obtained with models ACCESS-ESM1-5 and EC-Earth3 showed strong positive trends primarily in the northern regions, while model MPI-ESM1-2-HR displayed negative trends in the southern areas, indicating significant model disagreement for maximum temperature-based heatwave events. This discrepancy suggests potential model biases in simulating daytime heat extremes over the Sahel, consistent with findings by Oueslati et al. (2017), who identified challenges in capturing Sahelian heat wave mechanisms. The HWN_TN90 (Figure 22) exhibited a strong positive significant trend over the northern area, and moderate trends in the central regions. Most models overestimated the results by showing increased trends across the country, particularly ACCESS-ESM1-5 and EC-Earth3, while the model MPI-ESM1-2-HR showed contrasting patterns with negative trends in the southern areas.

A statistically significant positive trend was observed over the northern area for HWN_EHF (Figure 23). The ensemble mean showed moderate positive trends, while models such as ACCESS-ESM1-5 and EC-Earth3 overestimated the results by displaying strong positive trends across most regions, and the model MPI-ESM1-2-HR underestimated the results with weaker positive trends in the northern areas and negative trends in the southern regions. The trend in HWN varies significantly across different temperature indices, with nighttime minimum temperatures (TN90) showing the strongest positive trends, followed by the Excess Heat Factor (EHF), while daytime maximum temperatures (TX90) exhibit more spatially heterogeneous patterns. This indicated that the number of heatwave events is more pronounced during nighttime conditions, causing greater impacts on human health and comfort. This aligns with the dry climate characteristics of the Sahel, where nocturnal cooling typically prevents consecutive warm nights despite extreme daytime conditions (Guigma *et al.,* 2020).

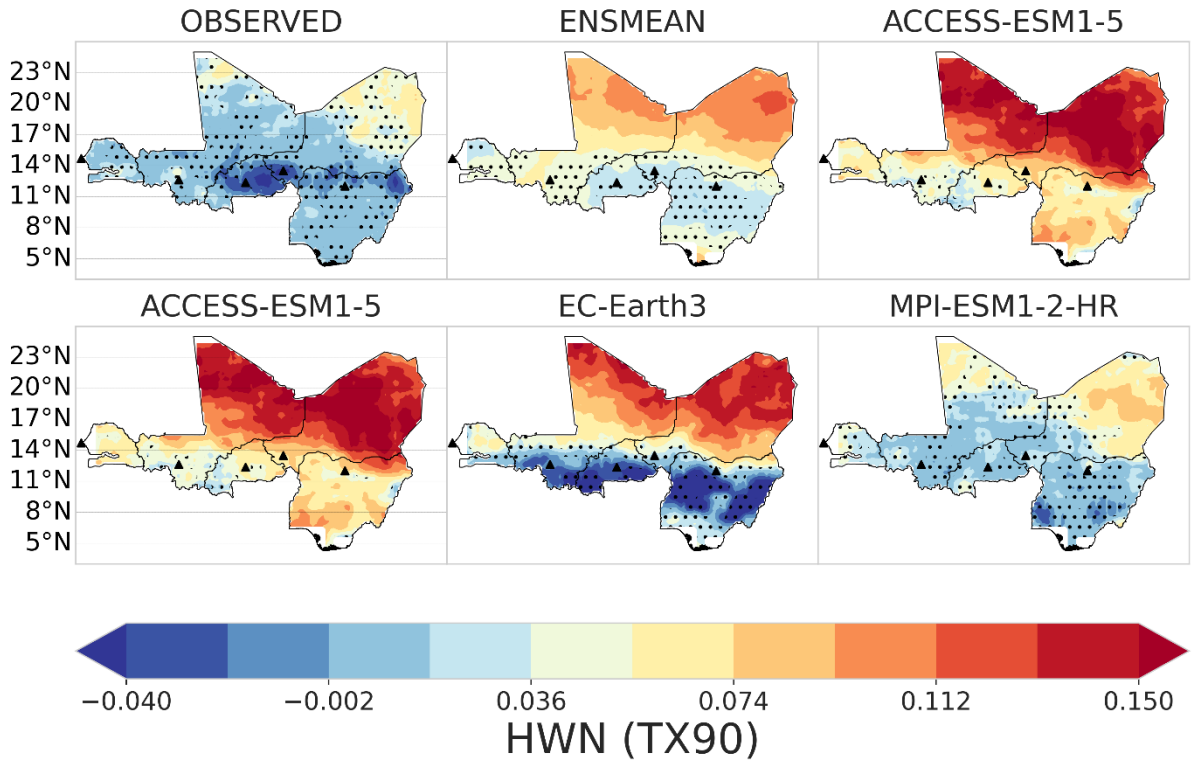

Figure 21 : Trend analysis of heatwaves for HWA (Heat Wave Number) °C for daytime (TX90) from 1984 - 2014. Black indicates statistical significance of trends at the 5%.

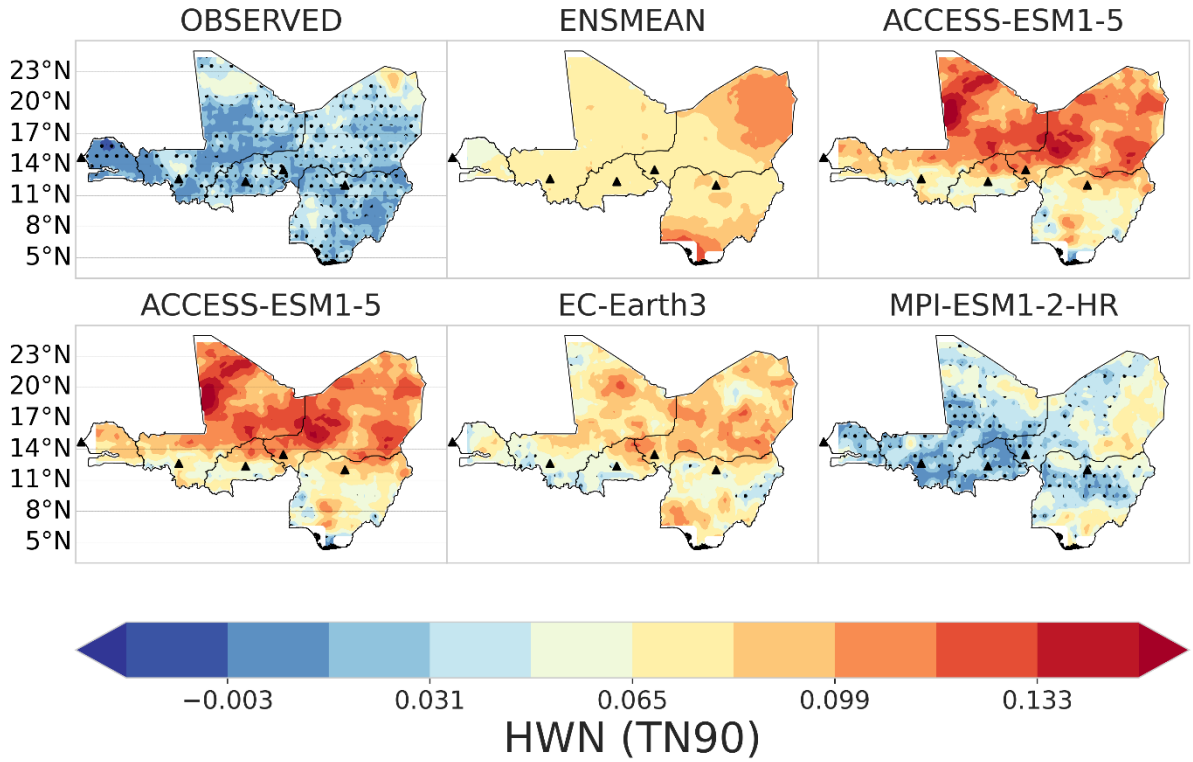

Figure 22 : Trend analysis of heatwaves for HWA (Heat Wave Number) °C for nighttime (TN90) from 1984 - 2014. Black indicates statistical significance of trends at the 5%.

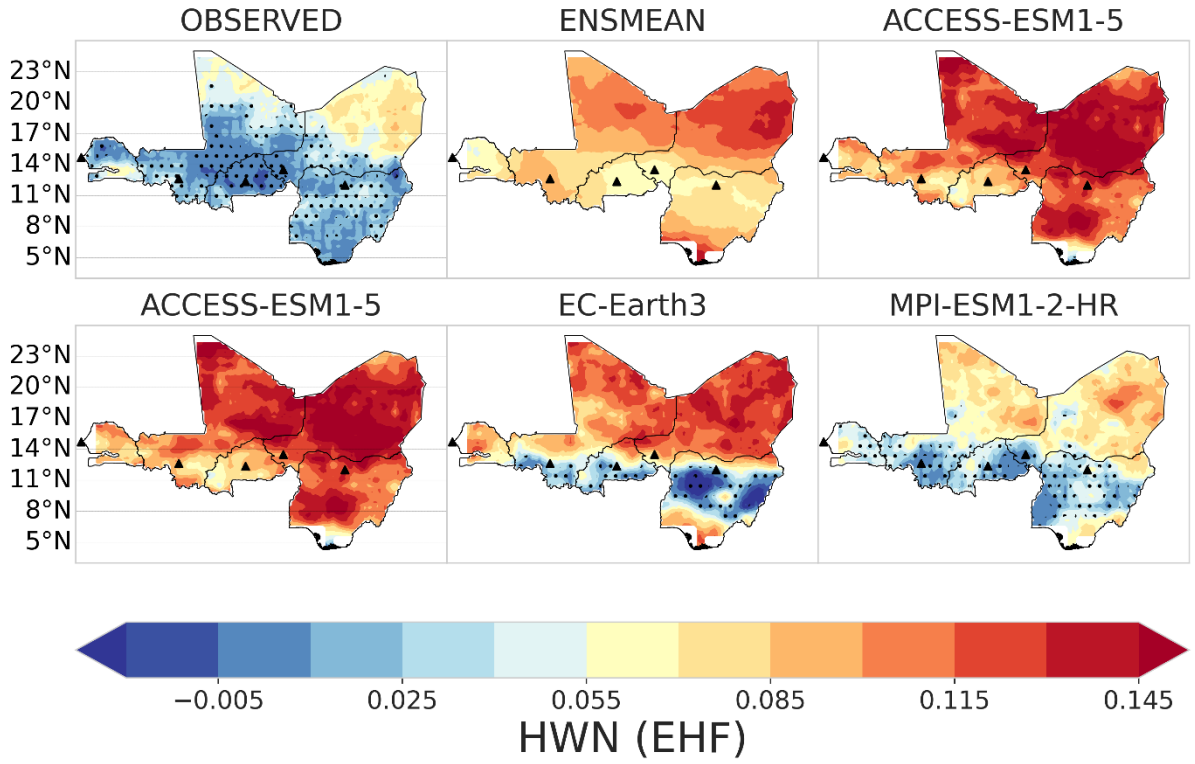

Figure 23 Trend analysis of heatwaves for HWA (Heat Wave Number) °C for excess heat factor (EHF) from 1984 - 2014. Black indicates statistical significance of trends at the 5%.

b. Heatwave Duration

The HWD_TX90 analysis (Figure 24) presents a markedly different pattern compared to nighttime temperatures in the historical record. The observed data shows significant negative trends across the central and southern Sahel, with dotted areas indicating statistical significance. The ensemble mean maintains relatively neutral conditions across most of the region. Among the individual historical model simulations, ACCESS-ESM1-5 shows strong positive trends in the northern sections while displaying negative trends in parts of the south. EC-Earth3 demonstrates predominantly negative trends across the central regions, contrasting with the more uniform positive trends exhibited by MPI-ESM1-2-HR across the northern and central areas.

The spatial distribution of HWD_TN90 trends (Figure 25) reveals a complex pattern of

historical temperature extremes across the Sahel region. The observed data demonstrate predominantly negative trends (blue coloration) across central and southern portions of the study area, with some positive trends evident in the northern and eastern sections. The ensemble mean (ENSMEAN) shows a relatively neutral to slightly positive trend across most of the region. However, the historical climate model simulations exhibit considerable variation in their representation of past trends. ACCESS-ESM1-5 displays strong positive trends (red coloration) particularly in the southern and eastern areas, while EC-Earth3 shows mixed patterns with both positive and negative trends across different sub-regions. The MPI-ESM1-2-HR model presents more moderate positive trends with spatial heterogeneity.

The HWD_EHF metric (Figure 26) reveals the most pronounced discrepancies between observed and simulated historical trends across the Sahel region. The observed data indicates significant negative trends in the central regions, with statistical significance marked by dotted patterns. However, the ensemble mean shows predominantly positive trends across the majority of the study area. All three individual historical climate model simulations (ACCESS-ESM1-5, EC-Earth3, and MPI-ESM1-2-HR) reproduce strong positive trends with high statistical significance across most of the region, as evidenced by the extensive red coloration and dotted patterns indicating significance.

The comparative analysis across the three HWD metrics reveals important discrepancies between observed historical trends and model simulations across the Sahel region. While observed data generally indicates decreasing heat wave durations in the historical period, particularly for nighttime and daytime temperature extremes, the climate models consistently simulate increasing trends, especially pronounced in the EHF metric. This divergence highlights the challenges climate models face in accurately reproducing historical temperature extreme patterns in semi-arid regions and suggests systematic biases in model representation of Sahel climate dynamics (Sanogo et al., 2015). The more pronounced model-observation discrepancies in the EHF metric, which combines both daytime and nighttime temperatures, suggest that the compound effects of temperature extremes are particularly challenging for models to simulate accurately in this region's historical climate record (Hulme, 2001).

These findings underscore the importance of model evaluation and bias correction in the Sahel region, where climate model accuracy is crucial for understanding past climate variability and informing future climate projections.

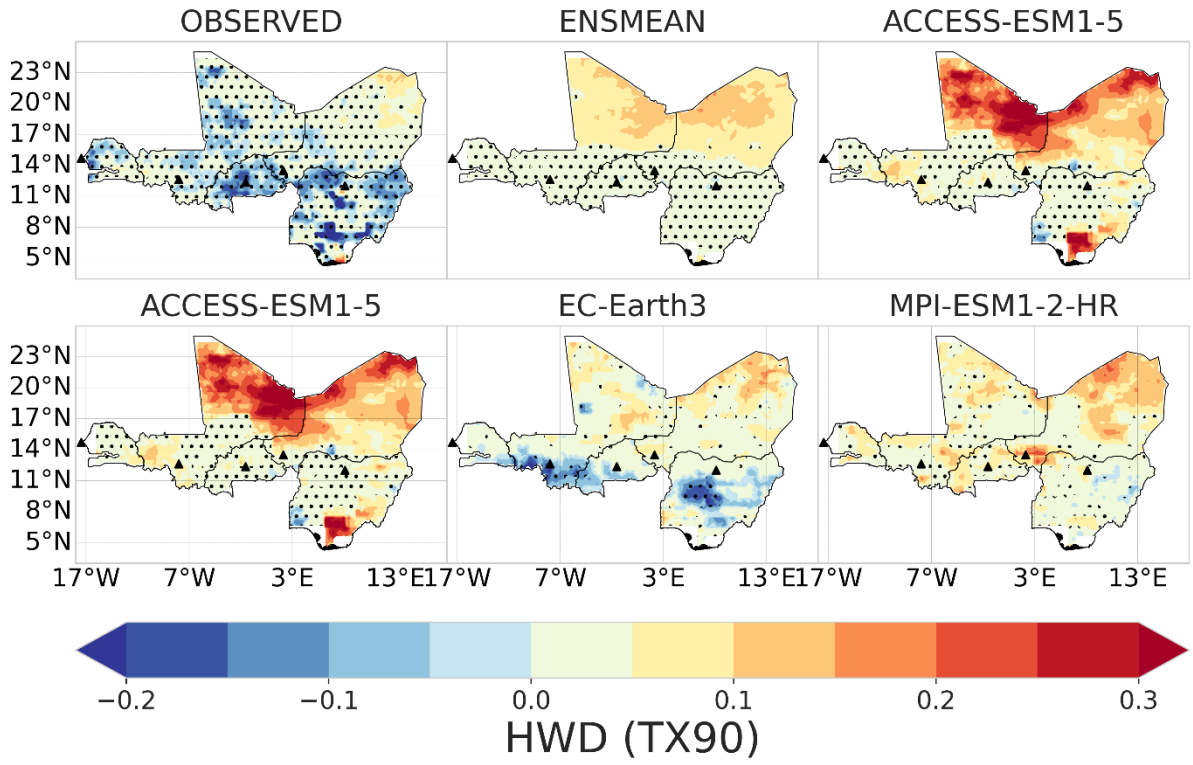

Figure 24 : Trend analysis of heatwaves for HWD (Heatwave Duration) for daytime (TX90) from 1984 – 2014, days/decade. Black indicates statistical significance of trends at the 5%.

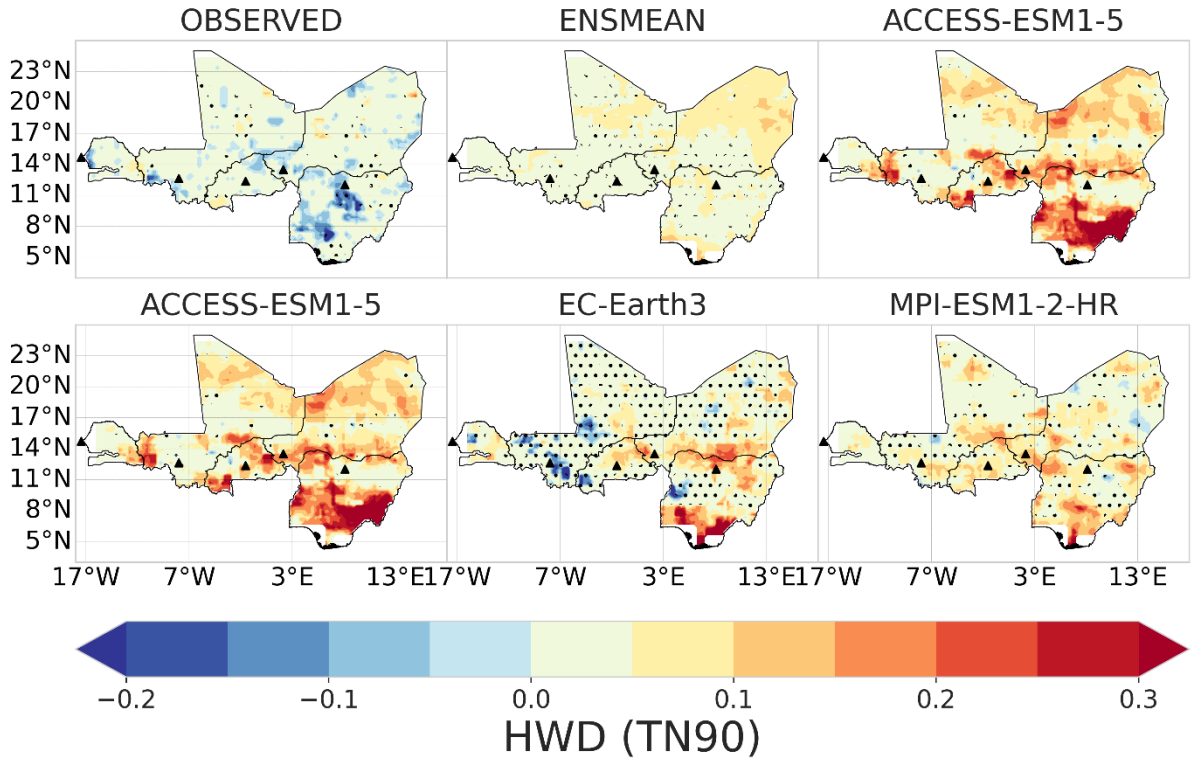

Figure 25 : Trend analysis of heatwaves for HWD (Heatwave Duration) for nighttime (TN90) from 1984 – 2014, days/decade. Black indicates statistical significance of trends at the 5%.

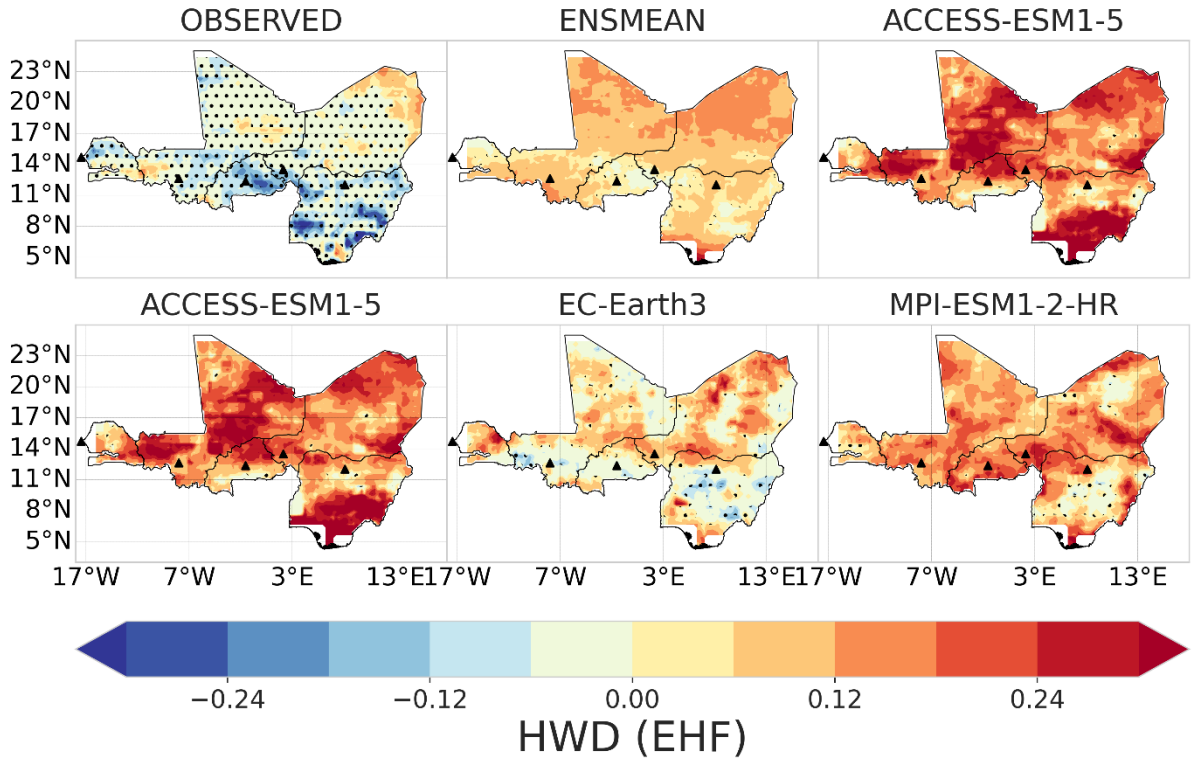

Figure 26 : Trend analysis of heatwaves for HWD (Heatwave Duration) for excess heat factor (EHF) from 1984 – 2014, days/decade. Black indicates statistical significance of trends at the 5%.

c. Heatwave Frequency

The heat wave frequency analysis based on different temperature metrics reveals distinct spatial patterns across the study region. The HWF (TX90) analysis (Figure 27) demonstrates a predominantly negative trend in observed data across much of the western and central portions of the study area, with some positive trends evident in the southeastern regions. The ensemble mean (ENSMEAN) exhibits contrasting patterns, with positive trends prevailing in the northern areas and negative trends in the southern regions. Among the climate models, ACCESS-ESM1-5 exhibits strong positive trends throughout most of the domain, while EC-Earth3 displays a more complex pattern with both positive and negative trends distributed across different zones. The MPI-ESM1-2-HR model shows predominantly negative trends in the central and southern areas with some positive trends in the northern regions.

The HWF (TN90) results (Figure 28) present a markedly different pattern compared to the maximum temperature-based analysis. Observed data indicate widespread negative trends across the majority of the study area, with the ensemble mean showing positive trends concentrated in the eastern and central regions. ACCESS-ESM1-5 consistently projects strong positive trends across the entire domain, demonstrating the model's tendency toward increased nighttime heat wave frequency. EC-Earth3 exhibits a mixed pattern with positive trends in the northern areas and negative trends in the southern regions, while MPI-ESM1-2-HR shows predominantly negative trends with some localized positive areas in the western portions.

The excess heat factor analysis (HWF EHF) (Figure 29) reveals yet another distinct spatial distribution pattern. The observed data shows negative trends dominating the western and central areas, with positive trends more prominent in the eastern regions. The ensemble mean indicates strong positive trends across the northern half of the domain, transitioning to more moderate values in the southern areas. ACCESS-ESM1-5 maintains its pattern of widespread positive trends, while EC-Earth3 shows a gradient from positive trends in the north to negative trends in the south. MPI-ESM1-2-HR demonstrates predominantly negative trends in the central and southern regions, with some positive trends in the northern areas.

The comparison between these three heat wave frequency metrics reveals important differences in how various temperature thresholds respond to climate change across the region. The nighttime temperature-based analysis (TN90) generally shows more pronounced positive trends in the model projections compared to the daytime maximum temperature metric (TX90), suggesting that nighttime warming may be more significant than daytime warming in this region. This finding aligns with previous research indicating that nighttime heat waves pose particular risks to human health and agricultural systems, as they prevent the natural cooling that typically occurs during evening hours.

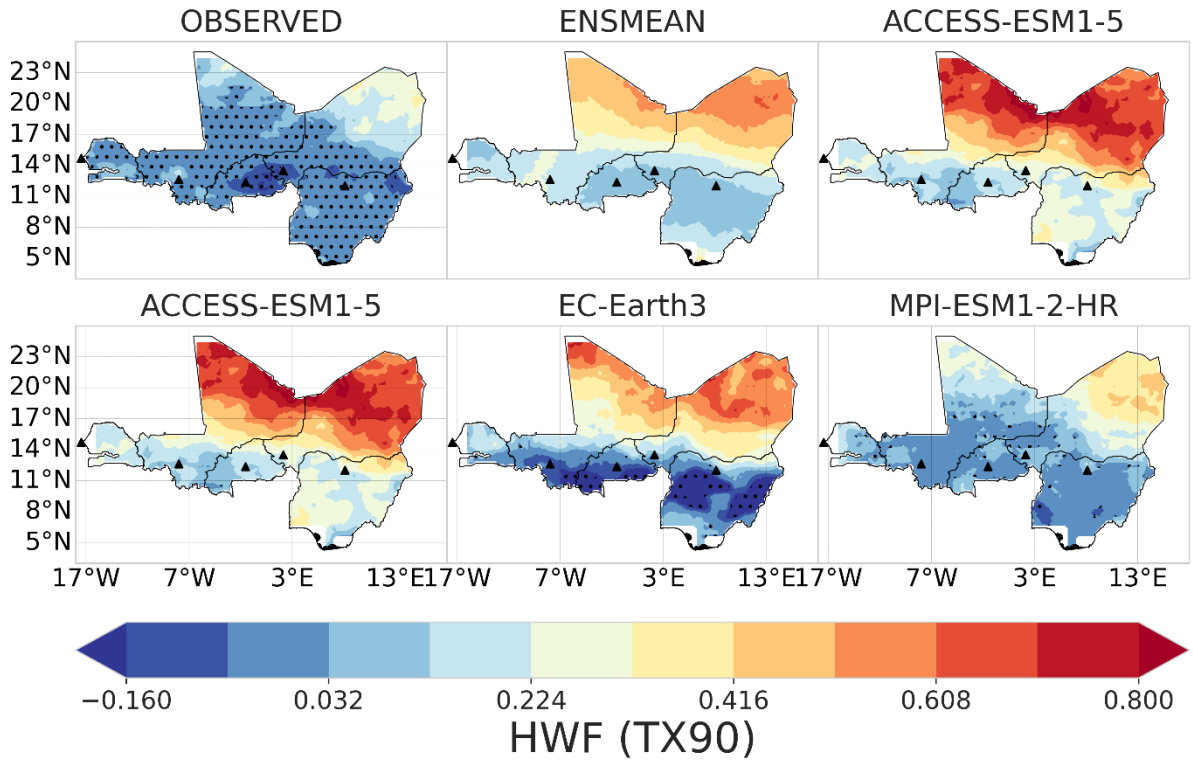

Figure 27 : Trend analysis of heatwaves for HWF (Heatwave Frequency) for daytime (TX90) from 1984 – 2014, days/decade. Black indicates statistical significance of trends at the 5%.

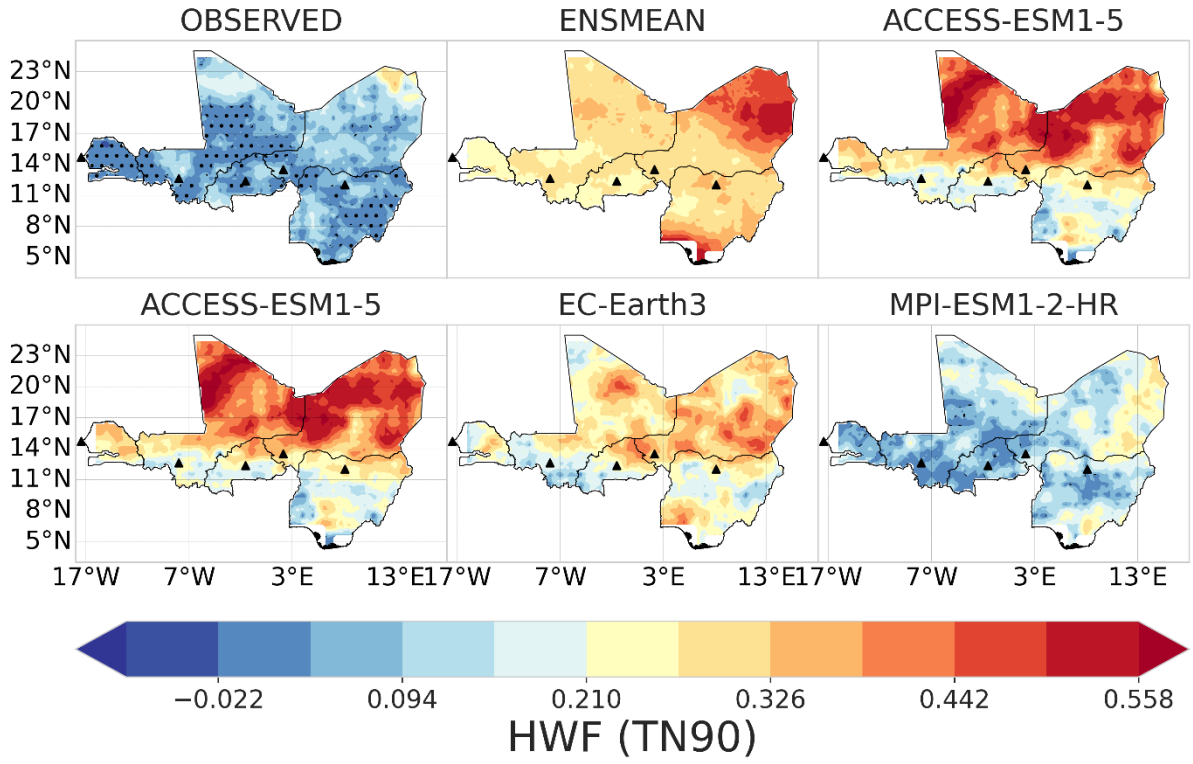

Figure 28 : Trend analysis of heatwaves for HWF (Heatwave Frequency) for nighttime (TN90) from 1984 – 2014, days/decade. Black indicates statistical significance of trends at the 5%.

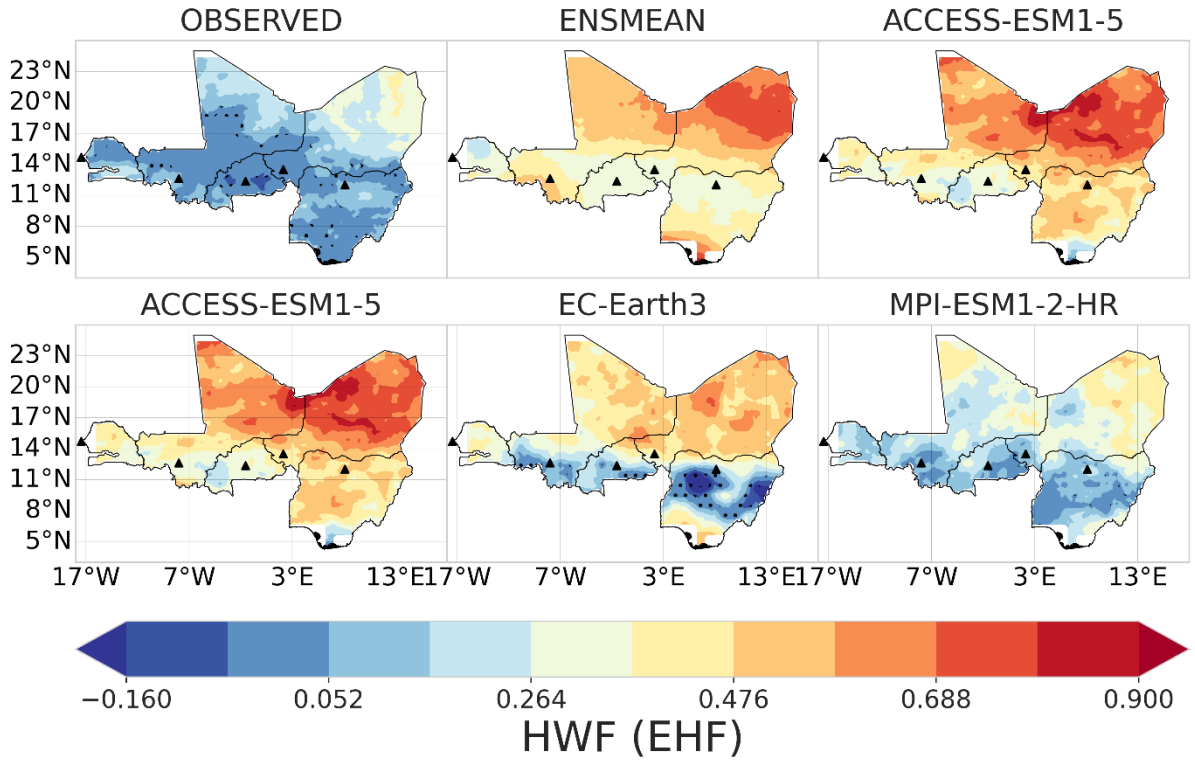

Figure 29 : Trend analysis of heatwaves for HWF (Heatwave Frequency) for excess heat factor (EHF) from 1984 – 2014, days/decade. Black indicates statistical significance of trends at the 5%.

d. Heatwave Amplitude

Based on the statistical analysis using the Mann-Kendall test with a significance level of 0.05, the spatial distribution maps reveal distinct patterns in heatwave area (HWA) trends across the study region. The dotted areas in the figures indicate locations where trends are statistically significant.

For HWA_TX90 (Figure 30), observed data demonstrates a predominantly negative trend across most of the study area, with statistically significant cooling patterns evident in the central and southern regions. The ENSMEAN model shows modest positive trends, while individual climate models exhibit varying responses. ACCESS-ESM1-5 displays strong positive trends with significant warming in the southern portions, contrasting with EC-Earth3 and MPI-ESM1-

2-HR models, which show more moderate positive trends with scattered significance patterns across the domain.

The HWA_TN90 analysis (Figure 31) reveals a different spatial pattern, with observed data showing mixed trends that are generally less pronounced than the TX90 results. The ENSMEAN exhibits slight positive tendencies, while ACCESS-ESM1-5 demonstrates notable positive trends with statistical significance concentrated in the central and southern areas. EC-Earth3 shows a more heterogeneous pattern with both positive and negative trends, and MPI-ESM1-2-HR displays moderate positive trends with limited statistical significance.

HWA_EHF (Figure 32) presents the most complex spatial distribution among the three metrics. Observed data indicate predominantly negative trends in the northern regions, with some positive trends in the south. The ENSMEAN shows consistent positive trends across most of the domain. ACCESS-ESM1-5 exhibits strong positive trends with widespread statistical significance, particularly in the northern and central regions. EC-Earth3 demonstrates mixed patterns with both positive and negative trends, while MPI-ESM1-2-HR shows moderate positive trends with scattered significance.

The comparison across these three heatwave definitions reveals that historical models generally suggest increasing heatwave areas, contrasting with observed negative trends in some metrics. The spatial coherence of trends varies considerably between the different heatwave definitions, with EHF-based trends showing the most spatial variability. These findings highlight the importance of considering multiple heatwave metrics when assessing regional climate change impacts, as different definitions capture distinct aspects of extreme.

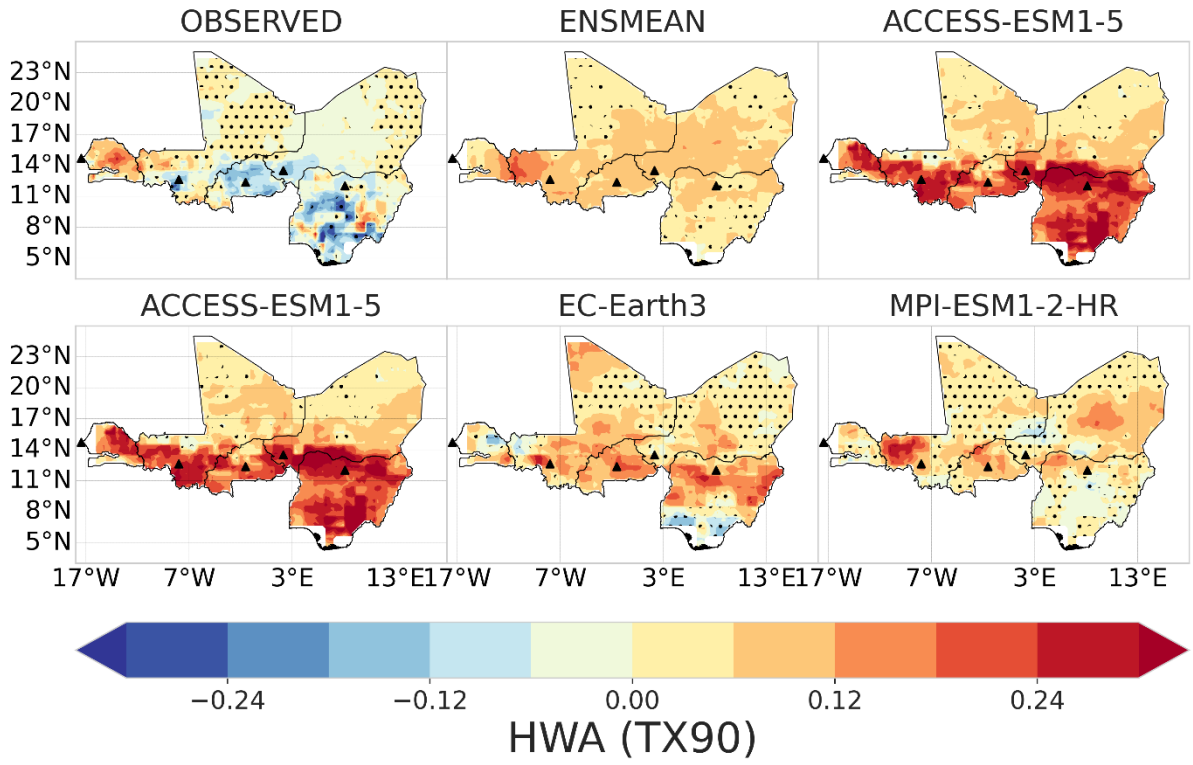

Figure 30 : Trend analysis of heatwaves for HWA (Heatwave Amplitude) for daytime (TX90th) from 1984 – 2014, days/decade. Black indicates statistical significance of trends at the 5%.

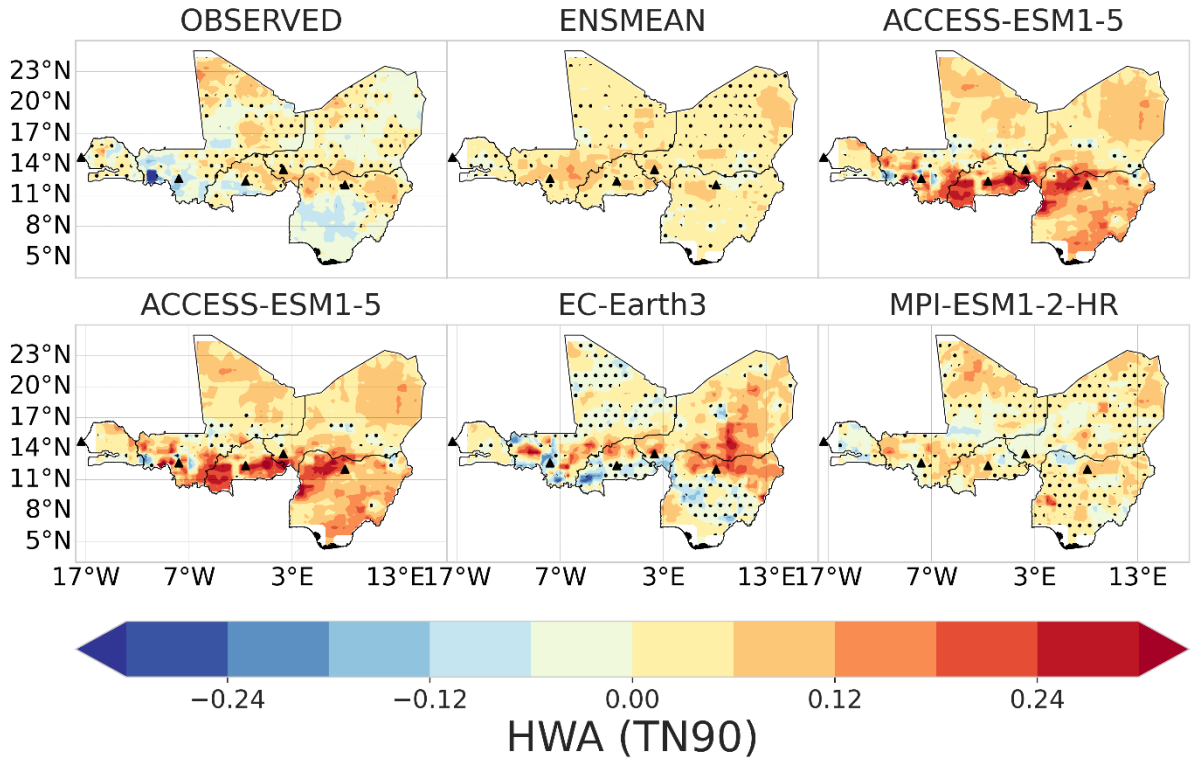

Figure 31 : Trend analysis of heatwaves for HWA (Heatwave Amplitude) for nighttime (TN90th) from 1984 – 2014, days/decade. Black indicates statistical significance of trends at the 5%.

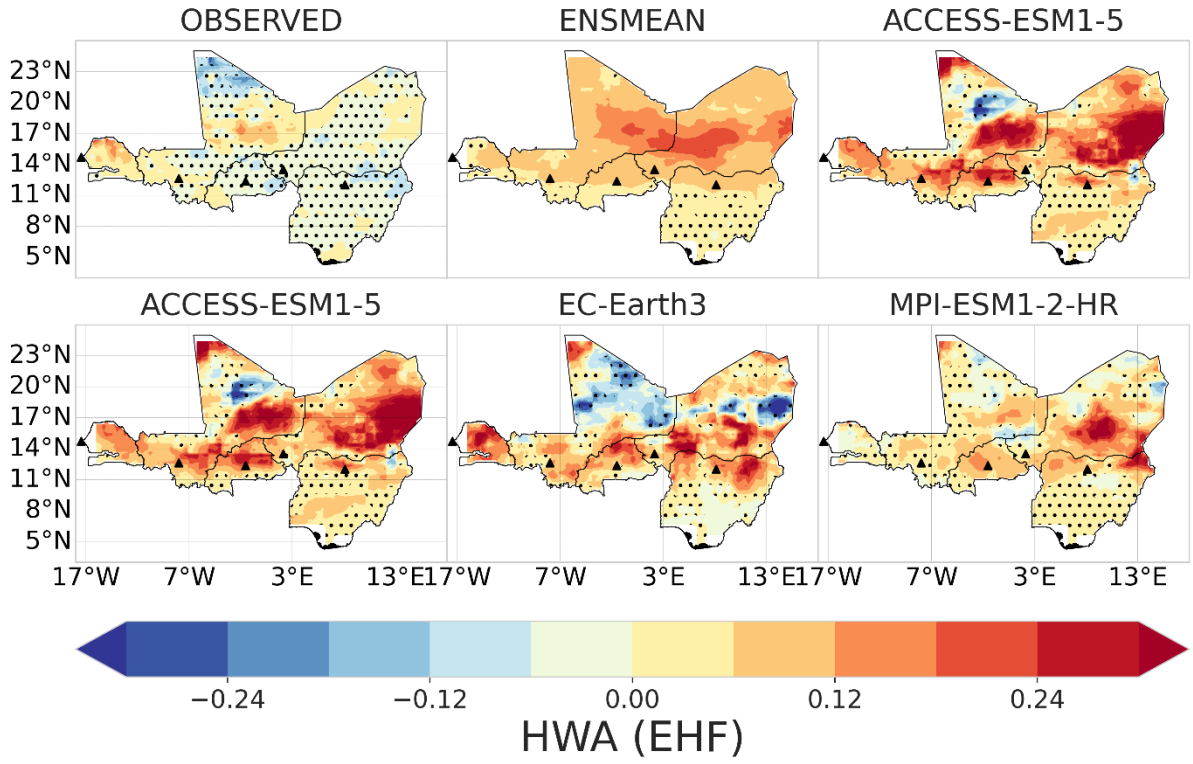

Figure 32 :Trend analysis of heatwaves for HWA (Heatwave Amplitude) for Excess Heat Factor (EHF) from 1984 – 2014, days/decade. Black indicates statistical significance of trends at the 5%.

e. Heatwave Magnitude

The HWM_TX90 (Figure 33) revealed a statistically significant downward trend predominantly across the southwestern and central regions of the study area, with notable positive trends observed in the northern sections. The ensemble mean (ENSMEAN) demonstrated mixed spatial patterns, while individual models showed varying responses. ACCESS-ESM1-5 exhibited strong negative trends in the southern regions with positive anomalies in the north, EC-Earth3 displayed predominantly negative trends with localized positive areas, and MPI-ESM1-2-HR showed more spatially heterogeneous patterns with both positive and negative trends distributed across the domain.

The HWM_TN90 (Figure 34) displayed contrasting spatial patterns with statistically

significant positive trends dominating the northern and eastern portions of the study region, while negative trends were concentrated in the southwestern areas. The observed data showed clear latitudinal gradients, with the ensemble mean capturing similar spatial distributions. Among the models, ACCESS-ESM1-5 demonstrated strong agreement with observations in the northern regions, while EC-Earth3 and MPI-ESM1-2-HR showed varying degrees of spatial coherence with mixed positive and negative trends across different geographical zones. The HWM_EHF (Figure 35) exhibited predominantly negative trends across most of the study domain, with statistically significant cooling patterns observed in the central and southern regions. Positive trends were limited to specific northern and eastern locations. The ensemble mean reflected these spatial patterns, while individual models showed considerable variability. ACCESS-ESM1-5 displayed strong negative trends in the southern areas with some positive anomalies in the northeast, EC-Earth3 showed mixed spatial patterns with both warming and cooling trends, and MPI-ESM1-2-HR demonstrated more uniform negative trends across the majority of the study region.

The heatwave magnitude results indicate complex regional variations in extreme temperature patterns, with differences between minimum and maximum temperature indices suggesting varying underlying mechanisms driving heat extremes. These findings align with regional climate studies that highlight the importance of understanding local-scale variations in extreme temperature events for effective climate adaptation planning and risk assessment strategies (Guigma *et al.*, 2021)

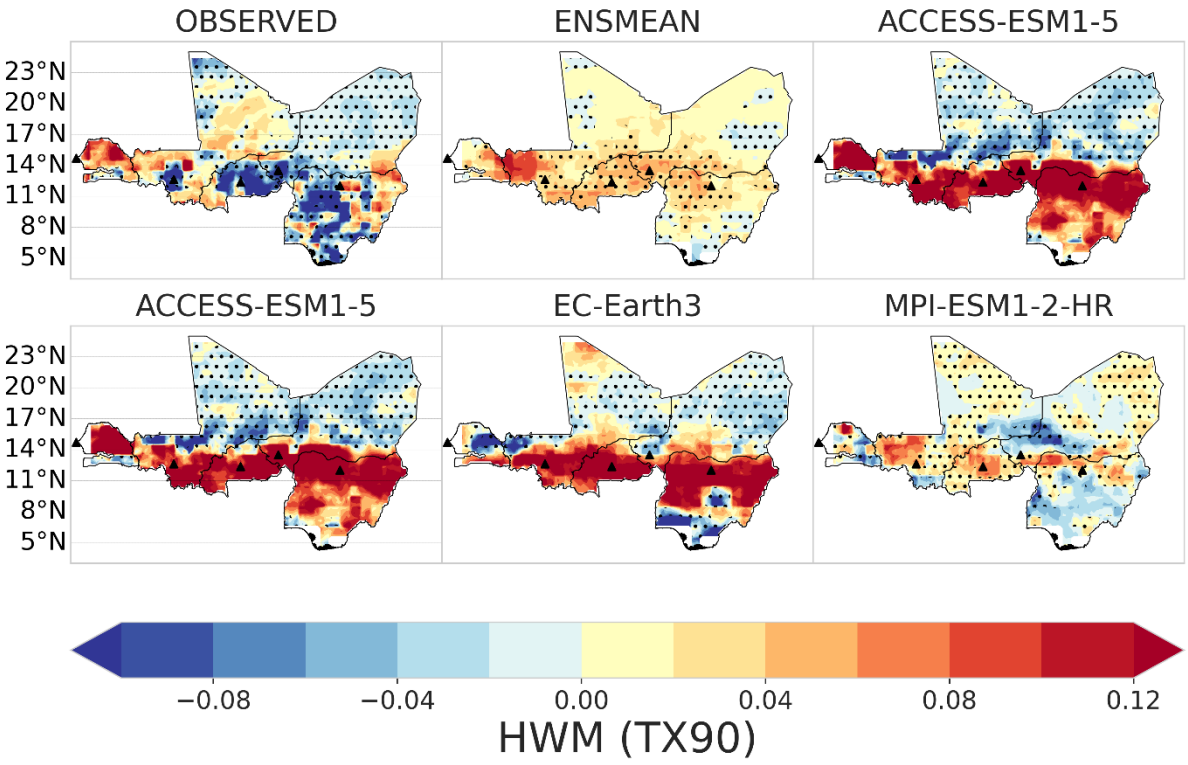

Figure 33 : Trend analysis of heatwaves for HWM (Heatwave Magnitude) for daytime (TX90th) from 1984 – 2014, days/decade. Black indicates statistical significance of trends at the 5%.

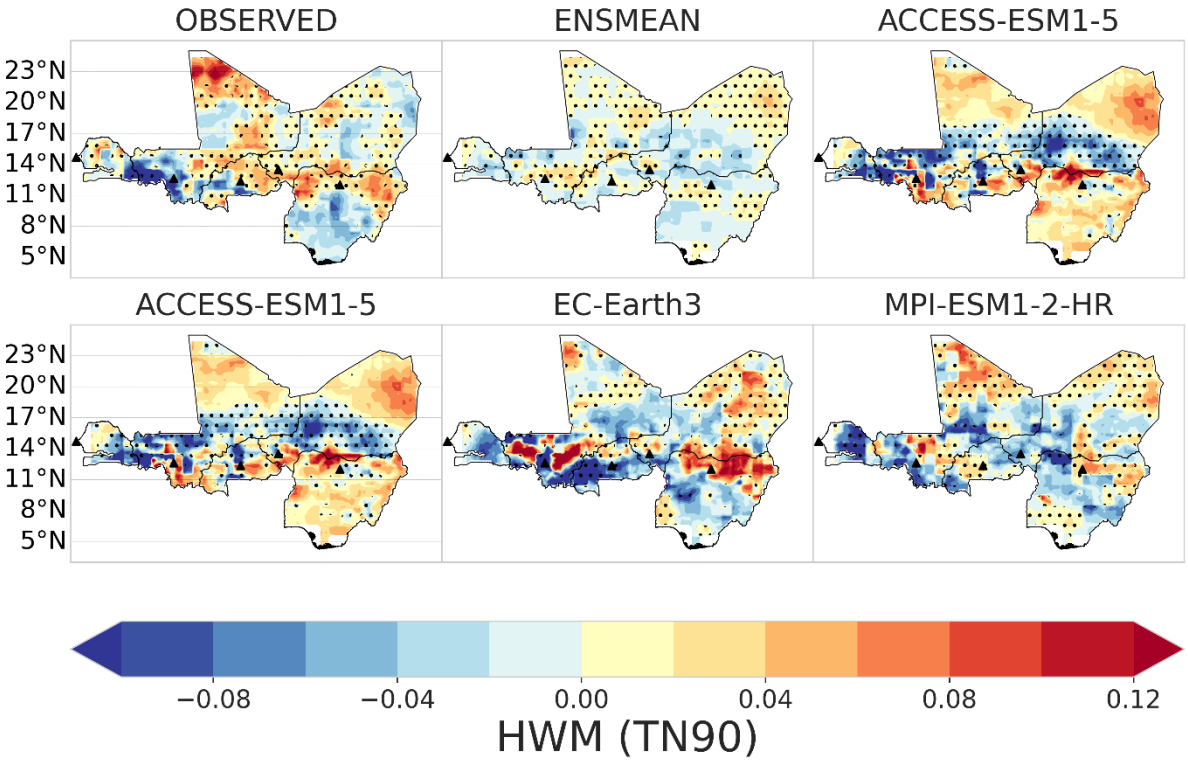

Figure 34 : Trend analysis of heatwaves for HWM (Heatwave Magnitude) for nighttime (TN90th) from 1984 – 2014, days/decade. Black indicates statistical significance of trends at the 5%.

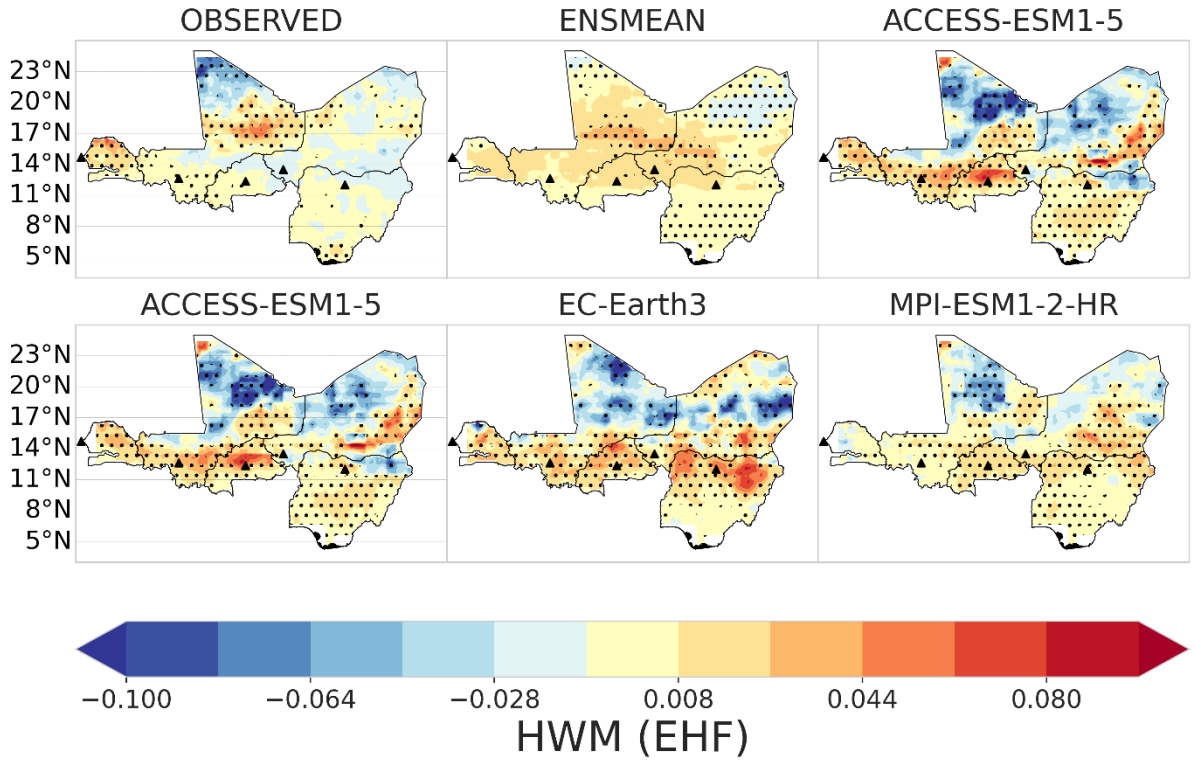

Figure 35 : Trend analysis of heatwaves for HWM (Heatwave Magnitude) for Excess Heat Factor (EHF) from 1984 – 2014, days/decade. Black indicates statistical significance of trends at the 5%.

3.5 Future Projection of Heatwave Characteristics

a. Heatwave Amplitude

The HWA_EHF projections (Figure 36) demonstrate minimal changes in the near future (2030-2060) under both SSP245 and SSP585 scenarios, with values remaining largely stable across the region. However, the far future (2061-2091) presents a stark contrast, particularly under SSP585, where the northern and central portions of the Sahel experience dramatic increases reaching 2.7°C. Under SSP245, the far future shows more moderate increases of 0.4°C to 1.2°C, primarily concentrated in the central regions. This pattern suggests that while SSP245 allows for gradual adaptation strategies, SSP585 would require immediate and comprehensive intervention measures to address the severe heat amplification.

The HWA_TN90 results (Figure 37) reveal a progressive intensification of nighttime heat extremes. The near future under SSP245 shows moderate warming (29-32°C) across the northern regions, while SSP585 exhibits minimal change. The far future projections indicate substantial warming under both scenarios, with SSP245 showing temperatures reaching 31-34°C in the northern areas, and SSP585 displaying extreme conditions with temperatures exceeding 35°C across extensive portions of the region. This nighttime warming pattern is particularly concerning as it eliminates the natural cooling relief that typically occurs after sunset, compounding health risks by preventing physiological recovery from daytime heat stress, consistent with findings by Oueslati *et al.* (2017) and Russo *et al*. (2014).

The HWA_TX90 projections (Figure 38) show the most dramatic changes, with the near future (2030-2060) under SSP245 exhibiting moderate increases in the northern regions (43-45°C), while SSP585 remains relatively stable. The far future (2061-2091) presents severe warming under both scenarios, with SSP245 showing temperatures reaching 45-47°C in the northern areas, and SSP585 demonstrating extreme conditions exceeding 49°C across significant portions of the region. The spatial distribution reveals a clear northward intensification gradient, with the most severe impacts concentrated in the northern Sahel.

The SSP245 scenario, while still challenging, offers more manageable increases that could accommodate phased adaptation approaches. The intensification of both daytime and nighttime temperatures under these scenarios poses significant risks to public health, agricultural productivity, and infrastructure resilience across the region, as noted in studies examining West African climate extremes by Odoulami *et al.* (2017).

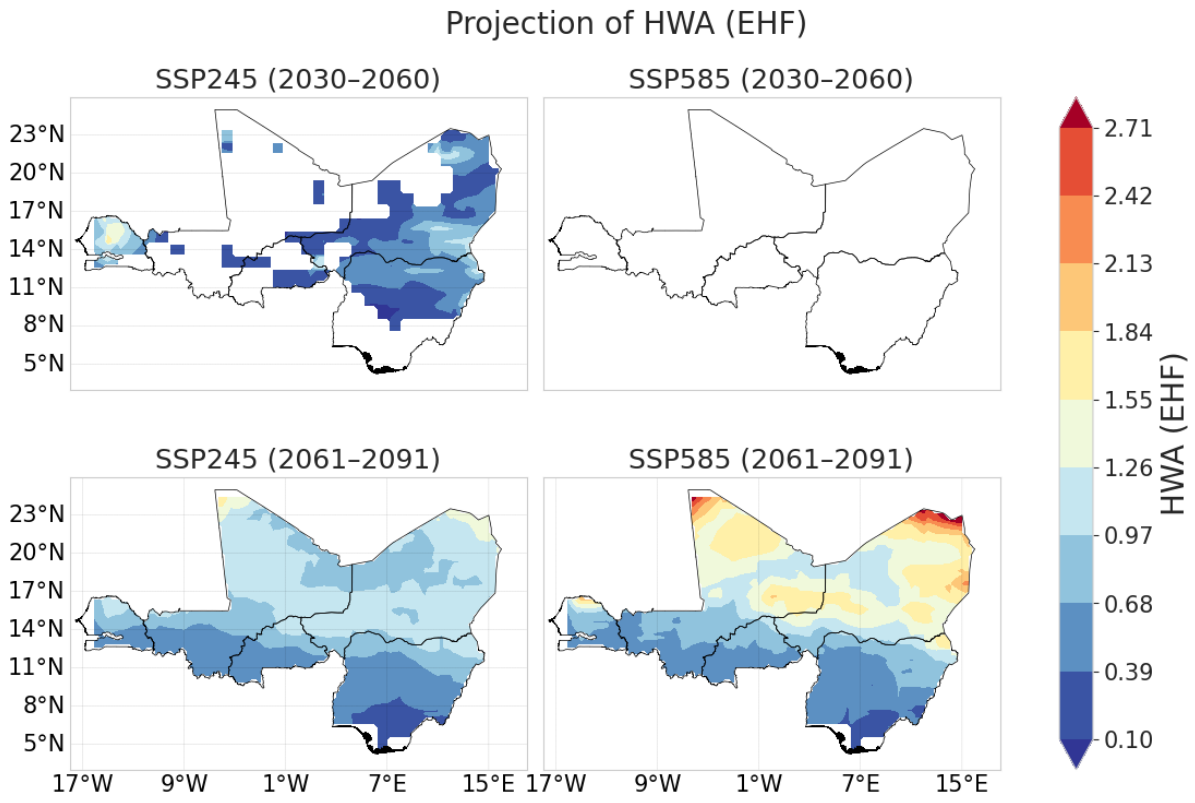

Figure 36 Projection of heatwaves over Sahel for HWA (Heat Wave Amplitude) °C for EHF for near future, 2030-2060, and far future, 2061 – 2091.

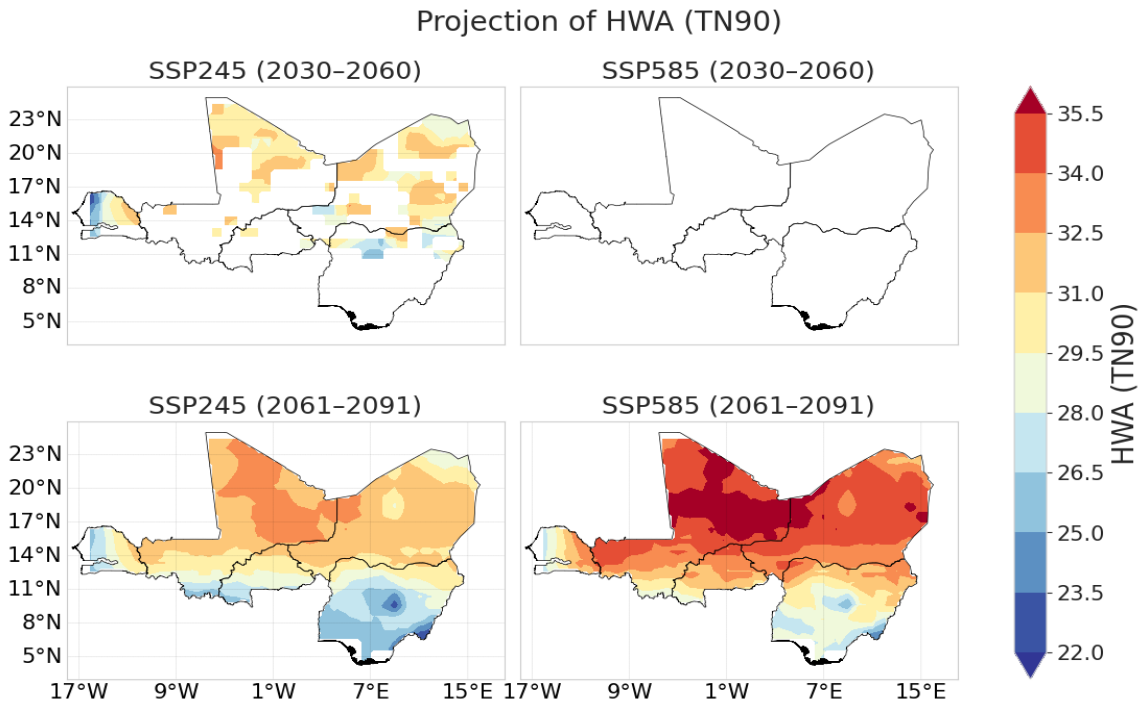

Figure 37 : Projection of heatwaves over Sahel for HWA (Heat Wave Amplitude) °C for TN90 for near future, 2030-2060, and far future, 2061 – 2091.

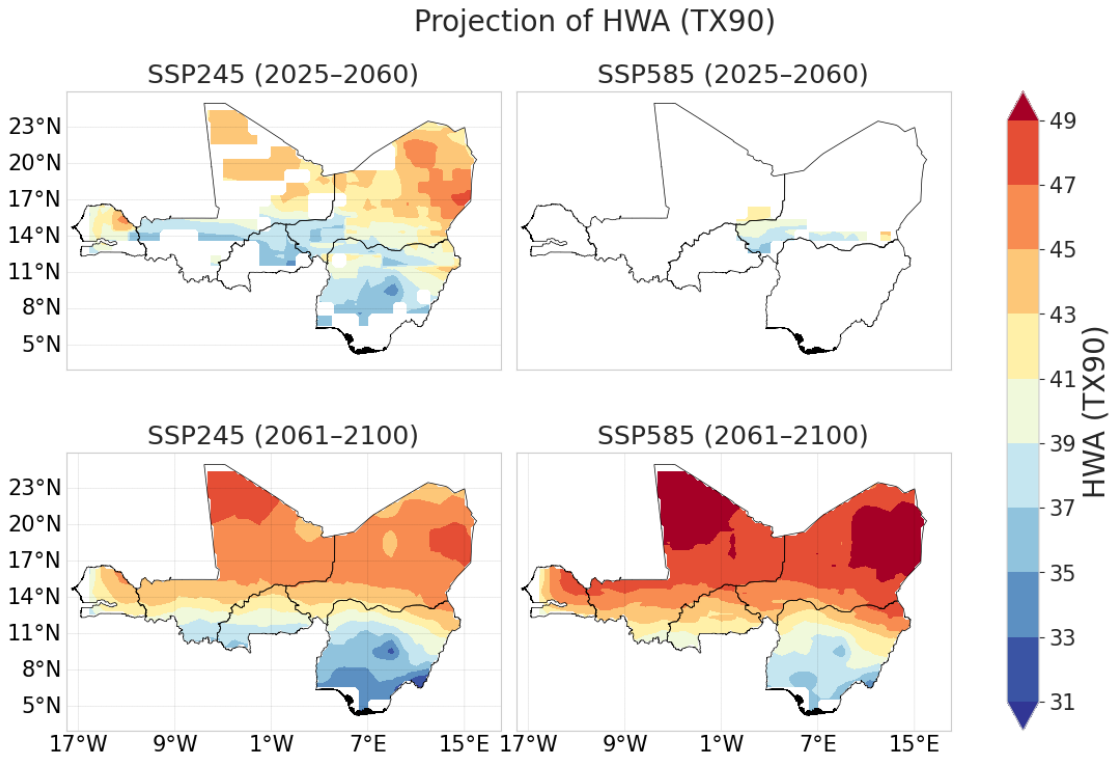

Figure 38 : Projection of heatwaves over Sahel for HWA (Heat Wave Amplitude) °C for TX90 for near future, 2030-2060, and far future, 2061 – 2091.

b. Heatwave Duration (HWD)

For HWD_EHF (Figure 39) the near future projections (2030-2060) show moderate increases under both SSP245 and SSP585 scenarios. Under SSP245, the northern regions exhibit values predominantly in the 6.0-7.4 day range, while SSP585 shows minimal projected changes with most areas remaining below 6.0 days. However, the far future projections (2061-2091) present a stark contrast. Under SSP245, HWD_EHF increases substantially across the region, with values reaching 9.5-12.3 days in the northern and eastern areas. The most dramatic changes occur under SSP585, where the entire region experiences significant increases, with central and southern areas reaching extreme levels of 10.9-12.3 days, indicating that the cumulative impact of high daytime and nighttime temperatures will be severe by the end of the century, as highlighted by Dimitriadou et al. (2021).

The HWD_TN90 (Figure 40) projections reveal a moderate rise in the near future under both scenarios, with SSP245 showing values of 5.0-6.0 days across most of the region, while SSP585 exhibits minimal change. In the far future, SSP245 projects increases to 6.0-7.0 days in northern areas, representing a still-manageable trend for adaptation. However, SSP585 shows more concerning projections, with southern and eastern regions experiencing increases to 8.0-9.5 days, creating conditions where heat stress would become critical due to sustained high nighttime temperatures. This higher nighttime HWD is particularly pressing as it suggests limited cooling opportunities, increasing mortality risks among vulnerable populations, consistent with findings by Guigma et al. (2020).

For HWD_TX90 (Figure 41), the near future projections under both scenarios show moderate increases, with SSP245 displaying values of 3.0-5.1 days and SSP585 showing minimal change across most areas. The far future projections under SSP245 indicate a gradual rise to 5.8-7.9 days, with northern regions showing slightly higher values. Under SSP585, the increases become more pronounced, with central and southern areas reaching 6.5-8.6 days, and some localized areas exceeding 9.0 days. These prolonged daytime heatwaves heighten agricultural and water demands, reduce crop yields, and increase the likelihood of droughts, echoing concerns raised by Boureima et al. (2017) on climate-induced drought risks in West African agriculture.

Each metric demonstrates a steeper increase in HWD by 2061-2091, highlighting the cumulative impacts of climate change on heatwaves over time. SSP585 consistently projects more intense and prolonged heatwave days than SSP245 across all three metrics, indicating that high-emission scenarios will lead to more extreme heat stress. The spatial patterns reveal that while northern regions generally show higher baseline values, the southern and central areas experience the most dramatic relative increases under the high-emission scenario, suggesting a regional shift in heat stress patterns that would require comprehensive adaptation strategies across the entire Sahel region.

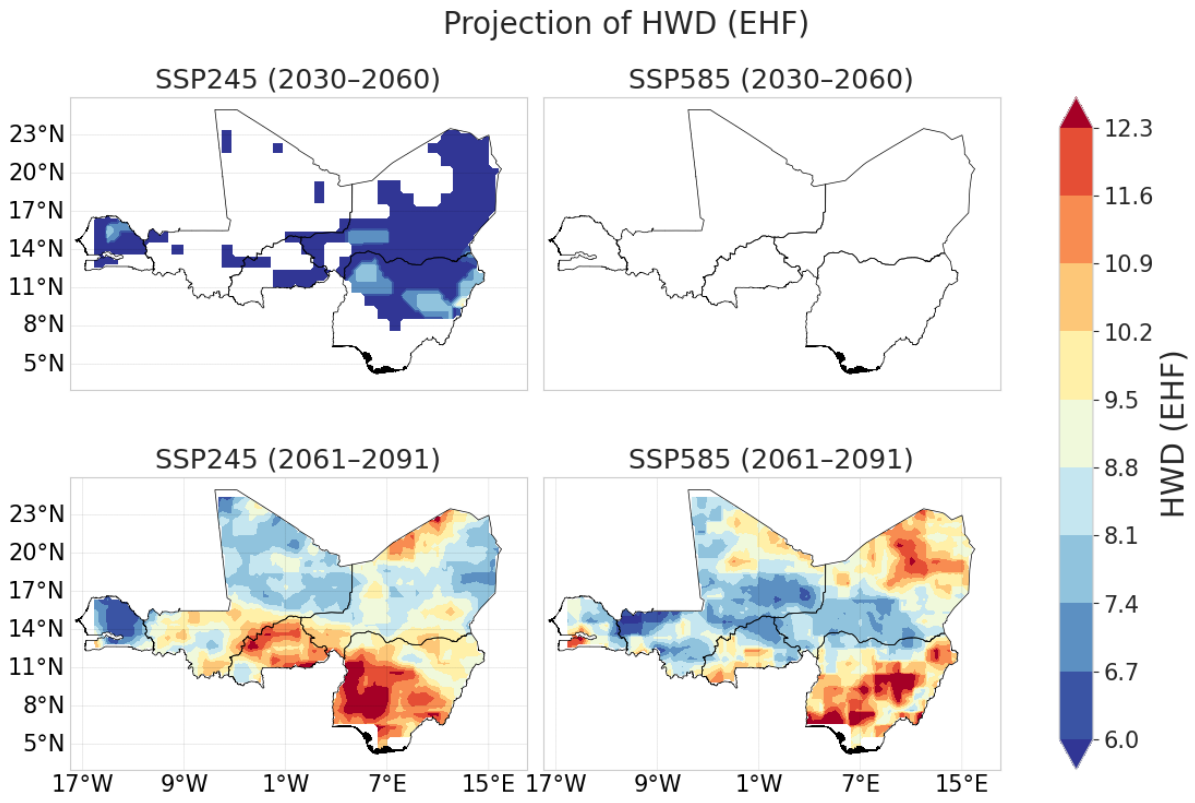

Figure 39 : Projection of heatwaves over Sahel for HWD (Heatwave Duration) °C for EHF for near future, 2030-2060, and far future, 2061 – 2091.

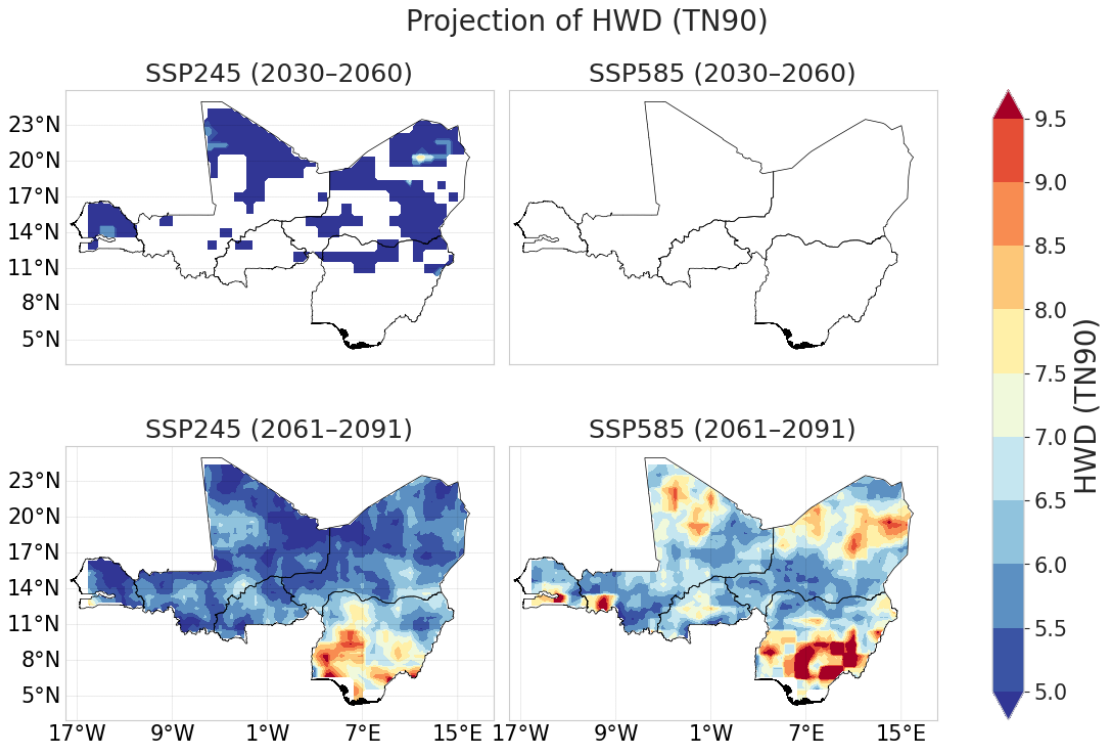

Figure 40 : Projection of heatwaves over Sahel for HWD (Heatwave Duration) °C for TN90 for near future, 2030-2060, and far future, 2061 – 2091.

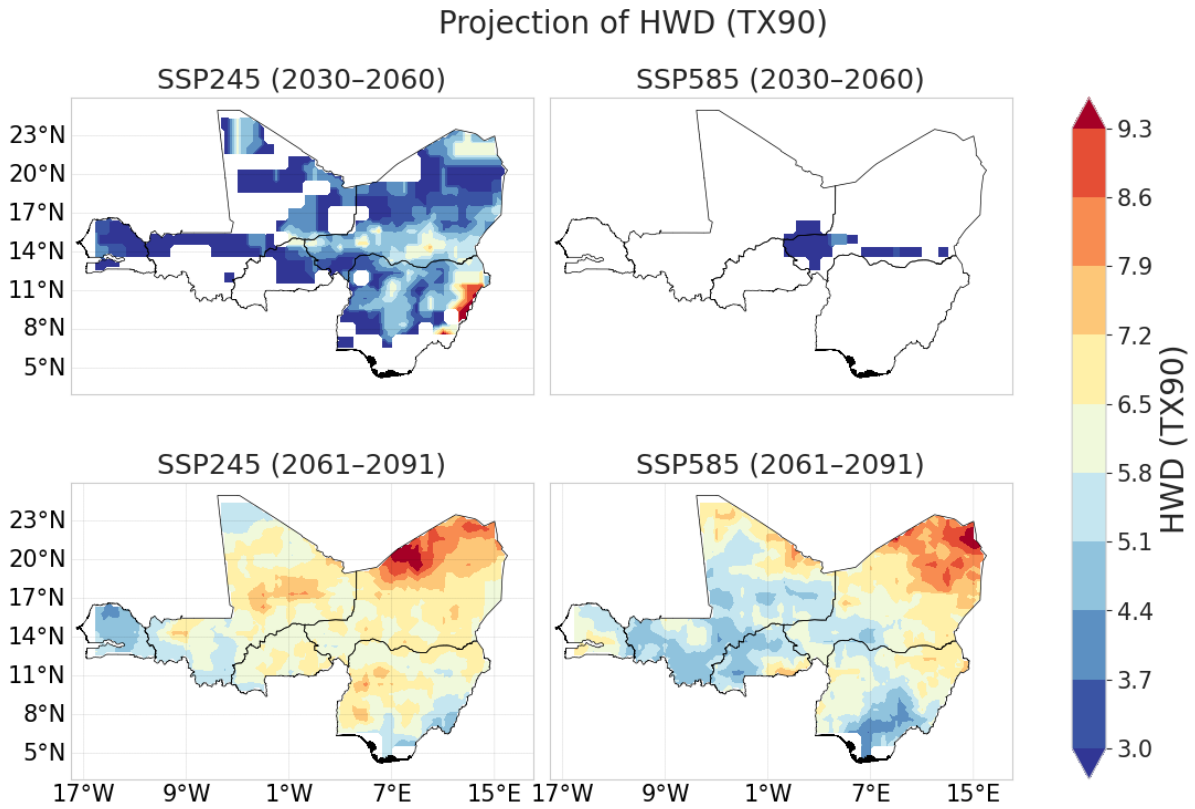

Figure 41 : Projection of heatwaves over Sahel for HWD (Heatwave Duration) °C for TX90 for near future, 2030-2060, and far future, 2061 – 2091.

c. Heatwave Frequency

Based on the spatial projection results for the Sahel region, the heatwave frequency (HWF) analysis reveals distinct patterns across different climate scenarios and temporal periods.

For the near future projections (2030-2060), the HWF_EHF analysis (Figure 42) shows remarkably similar patterns between SSP245 and SSP585 scenarios, with both displaying uniform low frequencies (approximately 5.0 days per year) across the entire Sahel region. This suggests minimal differentiation between moderate and high emission scenarios in the immediate decades ahead. However, the far future projections (2061-2091) reveal dramatic divergence between the two scenarios. Under SSP245, heatwave frequency increases substantially, particularly in the eastern regions where values reach 15-18.5 days per year, while western areas experience more moderate increases of 12-15 days per year. The SSP585 scenario presents a contrasting pattern with generally lower frequencies (6.5-11 days per year)

but more uniform distribution across the region, suggesting different heat accumulation mechanisms under extreme emission conditions.

The HWF_TN90 (Figure 43) projections demonstrate similar temporal patterns but with different magnitude scales. Near future projections under both scenarios remain consistently low (approximately 3.0 days per year) across the Sahel region. The far future projections show SSP245 developing a pronounced west-to-east gradient, with eastern regions experiencing the highest nighttime heatwave frequencies (11-13.8 days per year) while western areas maintain more moderate levels (7-9 days per year). Under SSP585, nighttime heatwave frequency remains more spatially uniform but at intermediate levels (5-7 days per year), indicating that extreme emission scenarios may lead to different atmospheric dynamics affecting nighttime temperature patterns.

The HWF_TX90 (Figure 44) analysis reveals the most pronounced scenario-dependent differences. Near future projections again show minimal variation between scenarios and across space. However, the far future projections under SSP245 exhibit a clear latitudinal gradient with northern regions experiencing the highest daytime heatwave frequencies (13-16.4 days per year) declining southward to approximately 8-10 days per year. The SSP585 scenario shows a more complex spatial pattern with moderate frequencies (6-8 days per year) but notable east-west variability, suggesting that extreme emission pathways may alter regional atmospheric circulation patterns, affecting daytime heat accumulation as noted by Engdaw *et al.* (2022), who documented increasing heat wave trends across Africa using observational data.

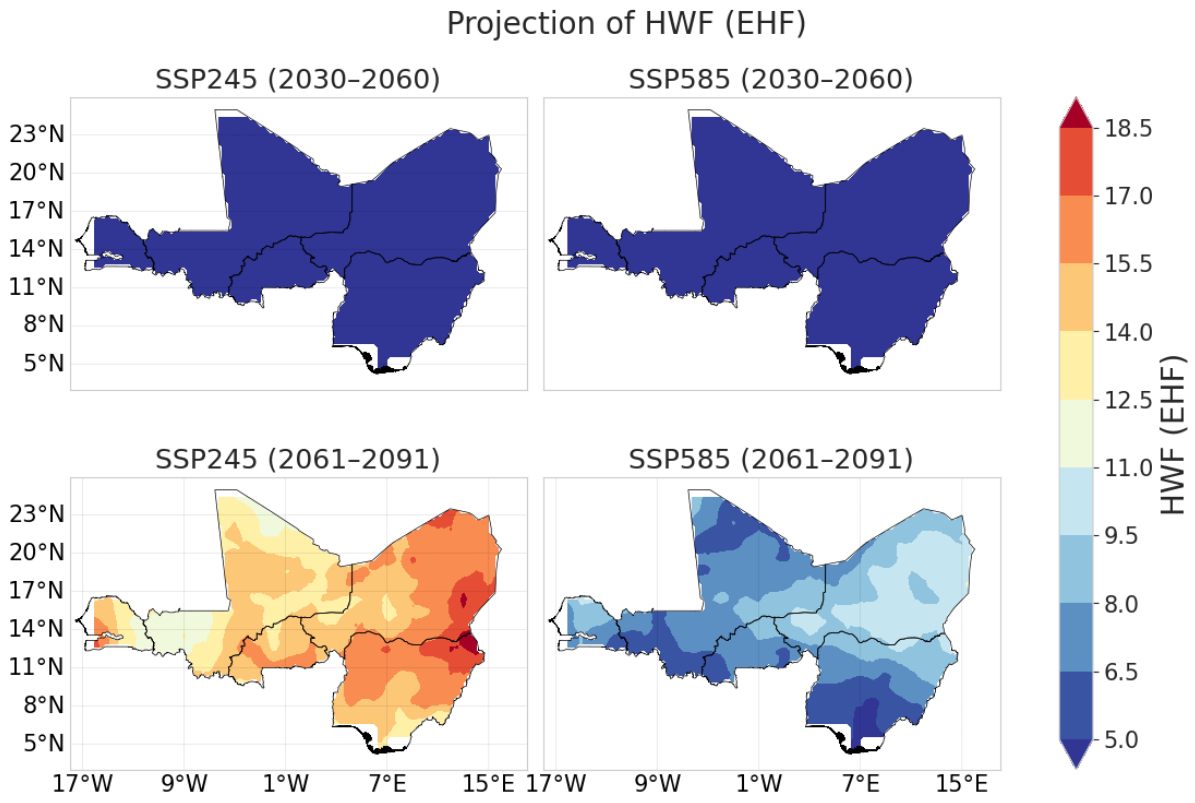

Figure 42 : Projection of heatwaves over Sahel for HWF (Heatwave Frequency) °C for EHF for near future, 2030-2060, and far future, 2061 – 2091.

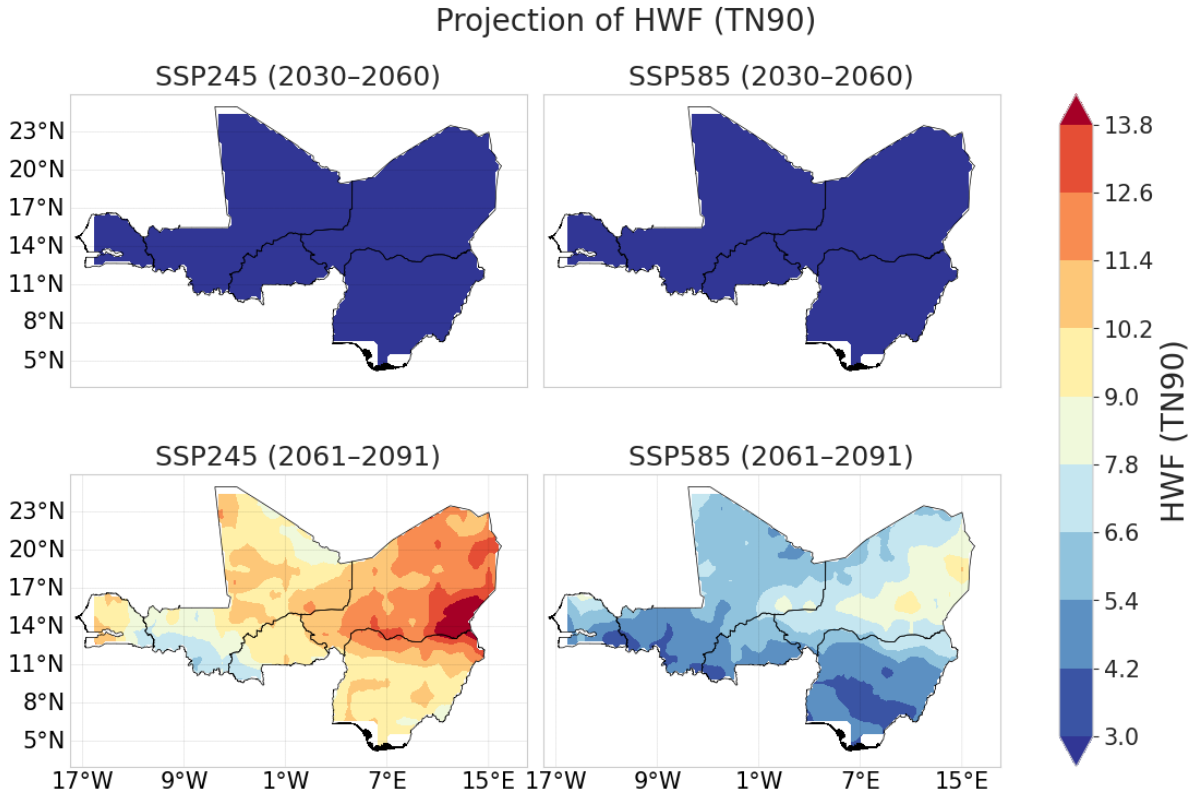

Figure 43 : Projection of heatwaves over Sahel for HWF (Heatwave Frequency) °C for TN90 for near future, 2030-2060, and far future, 2061 – 2091.

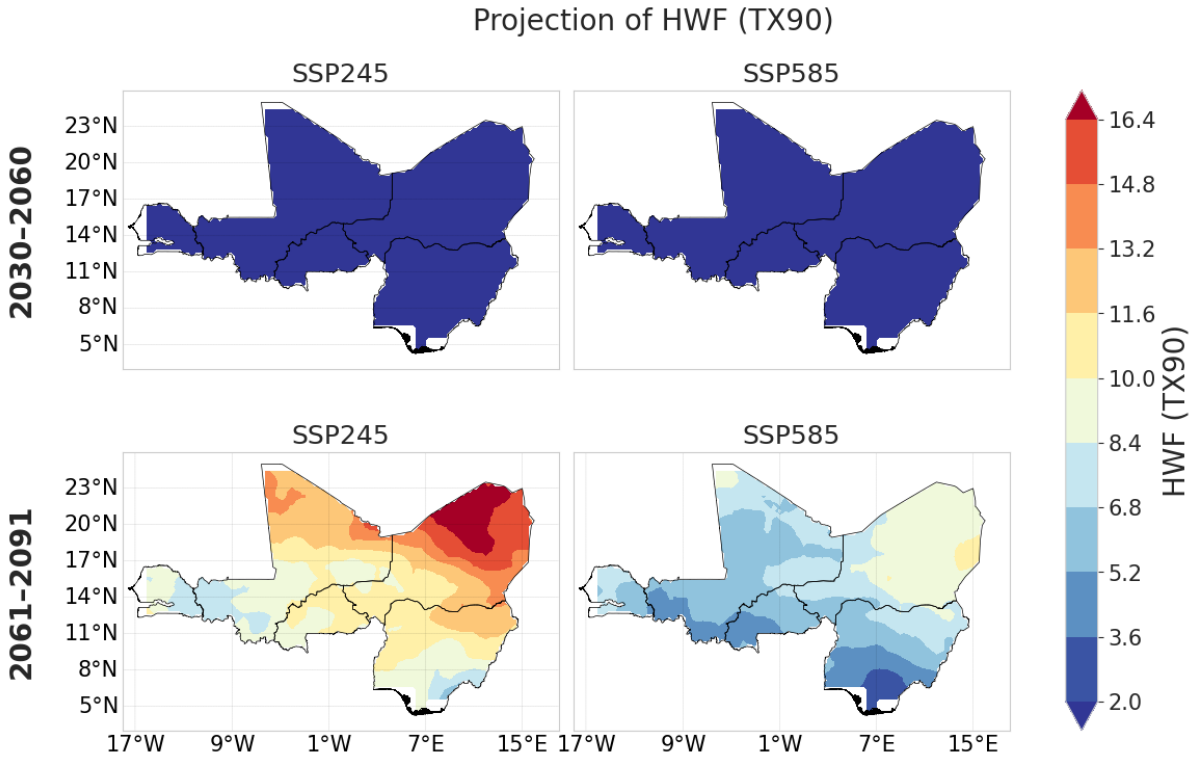

Figure 44 : Projection of heatwaves over Sahel for HWF (Heatwave Frequency) °C for TX90 for near future, 2030-2060, and far future, 2061 – 2091.

d. Heatwave Magnitude

The near future projection of HWM_EHF (Figure 45) showed relatively minimal increases across the Sahel under both SSP245 and SSP585 scenarios. Under SSP245, the region exhibits modest increases ranging from 0.1°C to 0.31°C, with slightly higher values concentrated in the western areas. The SSP585 scenario demonstrates even more subdued changes during this period, with most areas showing negligible increases in heatwave magnitude. The far future projections (2061-2091) reveal a dramatically different scenario, with substantial increases in HWM_EHF across the Sahel region. Under SSP245, the increase ranges from 0.17°C to 0.38°C, with a notable north-south gradient where northern areas experience higher magnitudes. The SSP585 scenario projects extreme increases, with values reaching 0.45°C to 0.73°C in the northern regions, representing a significant escalation in heatwave intensity compared to the moderate emission pathway.

The near-future projection of HWM_TN90 (Figure 46) showed that nighttime heatwave magnitudes remained relatively stable across the Sahel under both scenarios. SSP245 exhibits localized increases primarily in the western coastal areas, with values ranging from 30°C to 32°C, while most inland areas show minimal change. Under SSP585, the region demonstrates even more constrained increases during this period. The far future HWM_TN90 projections (2061-2091) indicate a pronounced intensification of nighttime heatwave conditions. Under SSP245, the Sahel experiences moderate increases, with values ranging from 28°C to 31°C, particularly pronounced in the northern and eastern regions. The SSP585 scenario projects extreme nighttime heatwave magnitudes, with temperatures reaching 32°C to 34°C across large portions of the region, suggesting that nighttime temperatures during heatwaves will provide minimal relief from thermal stress.

The projected HWM_TX90 (Figure 47) under SSP245 showed localized increases in daytime heatwave magnitude in the near future (2030-2060), with the northern Sahel experiencing the most bsignificant rise, reaching temperatures of 42°C to 44°C. The western and southern regions exhibit more moderate increases, ranging from 38°C to 40°C. Under SSP585, the near-future projections remained comparatively subdued across most of the region. The far future HWM_TX90 projections (2061-2091) demonstrate extreme increases in daytime heatwave magnitude across the Sahel. Under SSP245, temperatures range from 40°C to 44°C, with the northern regions showing the highest values. The SSP585 scenario projects unprecedented daytime heatwave magnitudes, with temperatures exceeding 46°C in northern areas and ranging from 44°C to 48°C across most of the region, representing a substantial escalation in extreme heat conditions.

The projected HWM across all three metrics (TN90, TX90, and EHF) indicates a consistent pattern of moderate increases in the near future, with more pronounced changes under SSP245 in certain areas compared to SSP585. However, the far future projections reveal a significant intensification of heatwave conditions across the Sahel, with the largest increases expected under SSP585 by the end of the century. These changes could severely impact human health, agricultural productivity, and water resources across the region. Perkins-Kirkpatrick and Lewis (2020) have demonstrated that under high-emission scenarios, heatwaves become increasingly severe, with cumulative thermal stress significantly affecting populations in vulnerable regions like the Sahel. The combined increase in both nighttime and daytime intensities suggests that

the region will face sustained extreme thermal conditions, making comprehensive adaptation strategies essential for maintaining livelihood security and ecosystem stability. Campbell et al. (2018) emphasize that such heightened heatwave magnitudes will substantially affect agricultural systems and human comfort, as sustained heat increases both crop stress and labor productivity challenges across the Sahel.

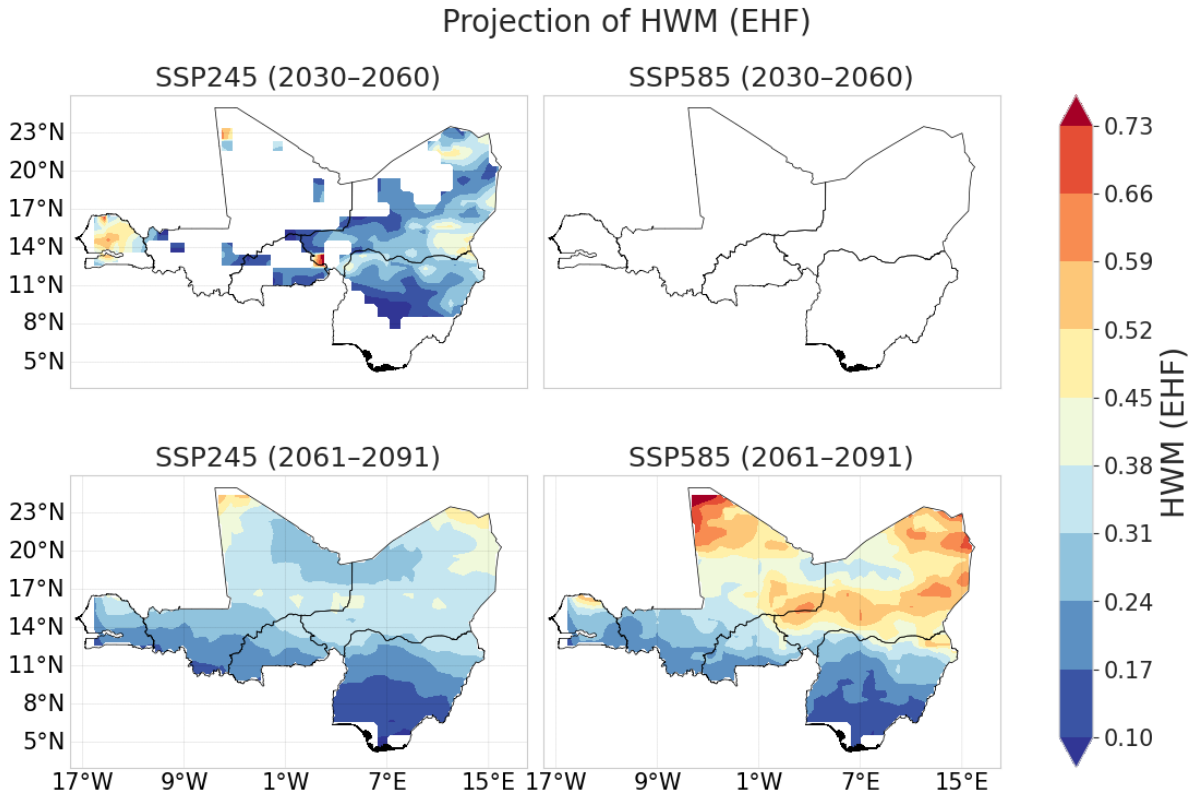

Figure 45 : Projection of heatwaves over Sahel for HWM (Heatwave Magnitude) °C for EHF from near future, 2030-2060, and far future, 2061 – 2091.

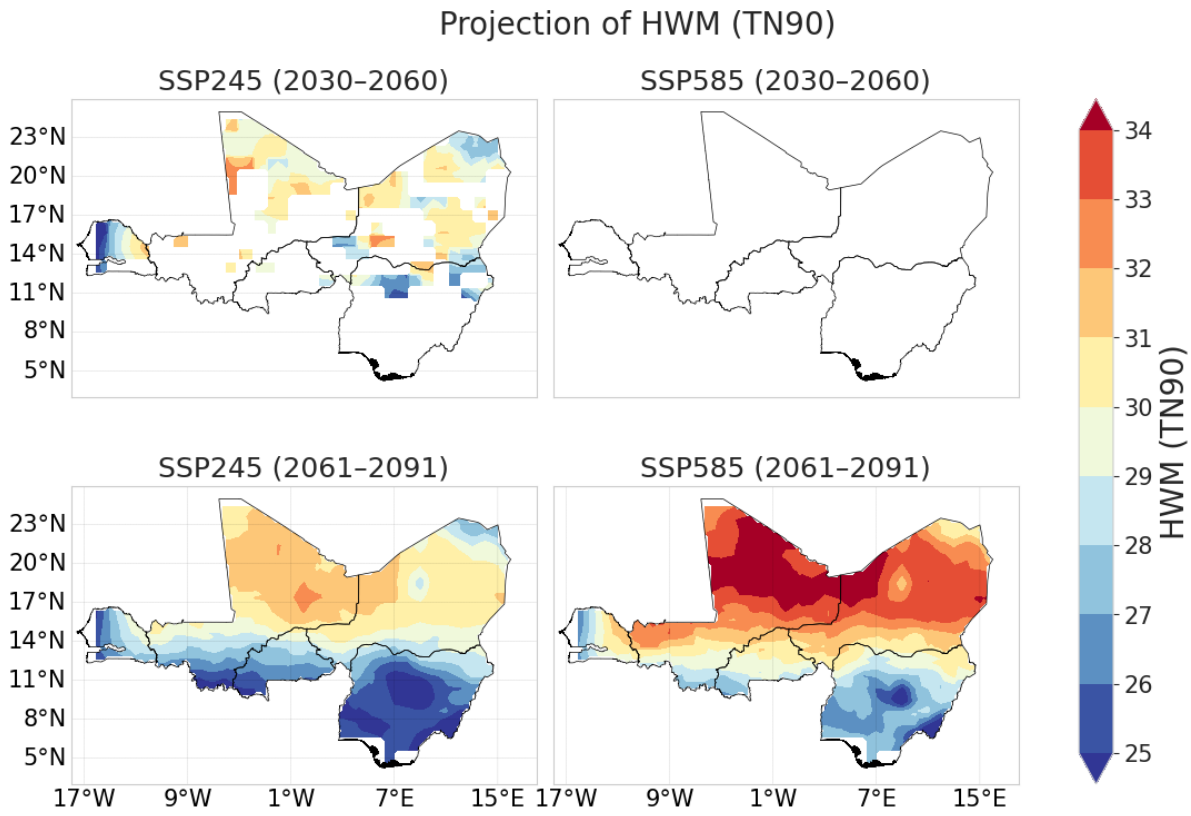

Figure 46 : Projection of heatwaves over Sahel for HWM (Heatwave Magnitude) °C for TN90 from near future, 2030-2060, and far future, 2061 – 2091.

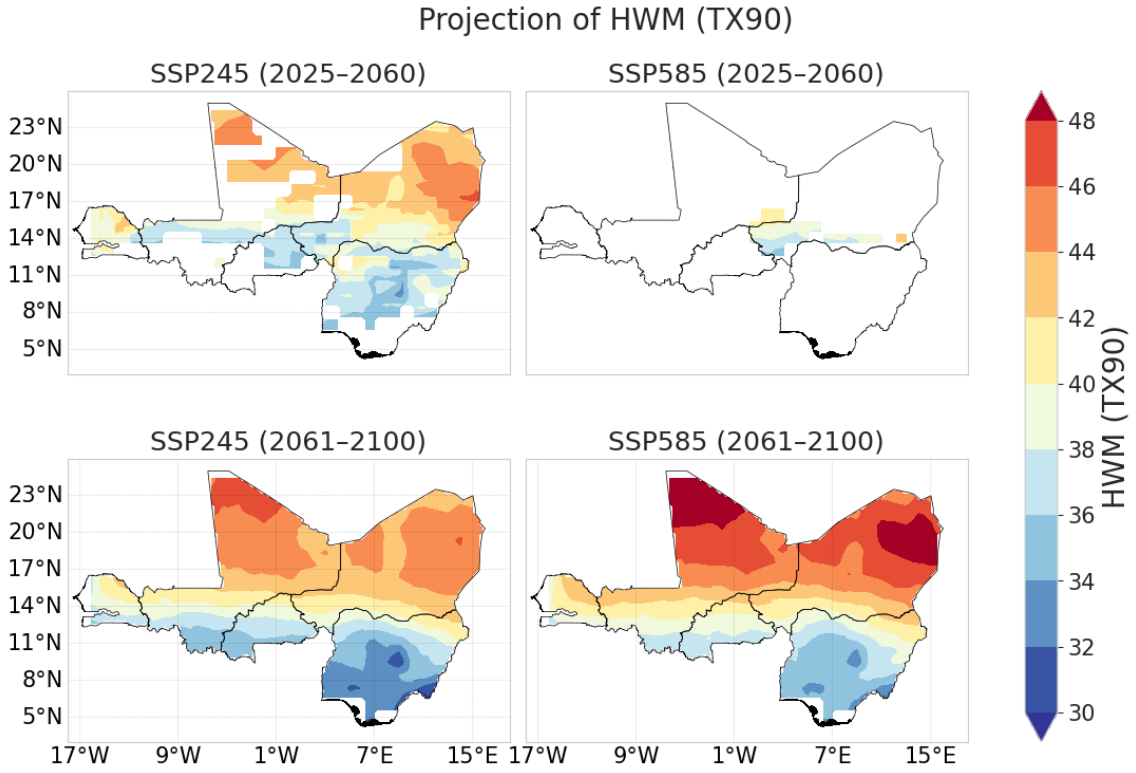

Figure 47: Projection of heatwaves over Sahel for HWM (Heatwave Magnitude) °C for TX90 from near future, 2030-2060, and far future, 2061 – 2091.

e. Heatwave Number

In the SSP245 scenario for the near future (2030-2060), the HWN_EHF (Figure 48) projections show relatively uniform low values across the Sahel region, with most areas displaying deep blue coloration indicating minimal heatwave frequency (approximately 0.60-0.89 events). This suggests that under moderate climate change scenarios, the region may experience limited increases in heatwave occurrence during the mid-century period. The SSP585 scenario for the same period shows a similar pattern, with comparable low values across the region, indicating that even under high emission scenarios, near-term heatwave frequency remains relatively stable. However, the far future projections (2061-2091) reveal a dramatically different scenario. Under SSP245, there is a marked increase in HWN_EHF across the entire Sahel region, with values ranging from 1.76 to 3.21 events per year. The spatial distribution shows a notable east-west gradient, with the eastern portions of the region experiencing the highest frequency of heatwave events (red and orange areas), while western areas show moderate increases (yellow and light orange coloration). This pattern suggests that the eastern Sahel may be particularly vulnerable to increased heatwave frequency under moderate climate change scenarios by the end of the century.

The SSP585 far future projections present an interesting contrast, showing generally lower heatwave frequencies compared to SSP245, with values predominantly in the blue to light blue range (0.89-1.47 events per year). This counterintuitive result, where the high emission scenario shows lower heatwave frequency than the moderate scenario, may reflect complex climate dynamics and regional precipitation patterns that influence the calculation of the Excess Heat Factor (EHF). Similarly, the HWA_TN90 projections (Figure 49) show the models' capacity to simulate nighttime temperature extremes across the region. The observed pattern again displays the characteristic north-south gradient, with northern areas experiencing higher minimum temperatures during heatwaves (red areas, 31-33°C) compared to southern regions (blue areas, 24-26°C). The climate models show reasonable agreement with observations, particularly in capturing the overall spatial distribution of temperature extremes.

The comparison between observed and modeled HWA_TX90 data (Figure 50) demonstrates the models' ability to capture the north-south temperature gradient characteristic of the Sahel region. The observed data shows higher values in the northern areas (red and orange, 44-48°C) transitioning to lower values in the southern regions (blue, 30-34°C). The various climate models (ENSMEAN, ACCESS-ESM1-5, EC-Earth3, MPI-ESM1-2-HR, and MRI-ESM2-0) generally reproduce this pattern, though with varying degrees of accuracy in magnitude and spatial distribution.

These projections have significant implications for the Sahel region's vulnerability to climate change impacts. The substantial increase in heatwave frequency projected for the far future under SSP245, particularly in the eastern portions of the region, could severely affect agricultural productivity, water resources, and human health. adaptation strategy development across this climatically sensitive region.

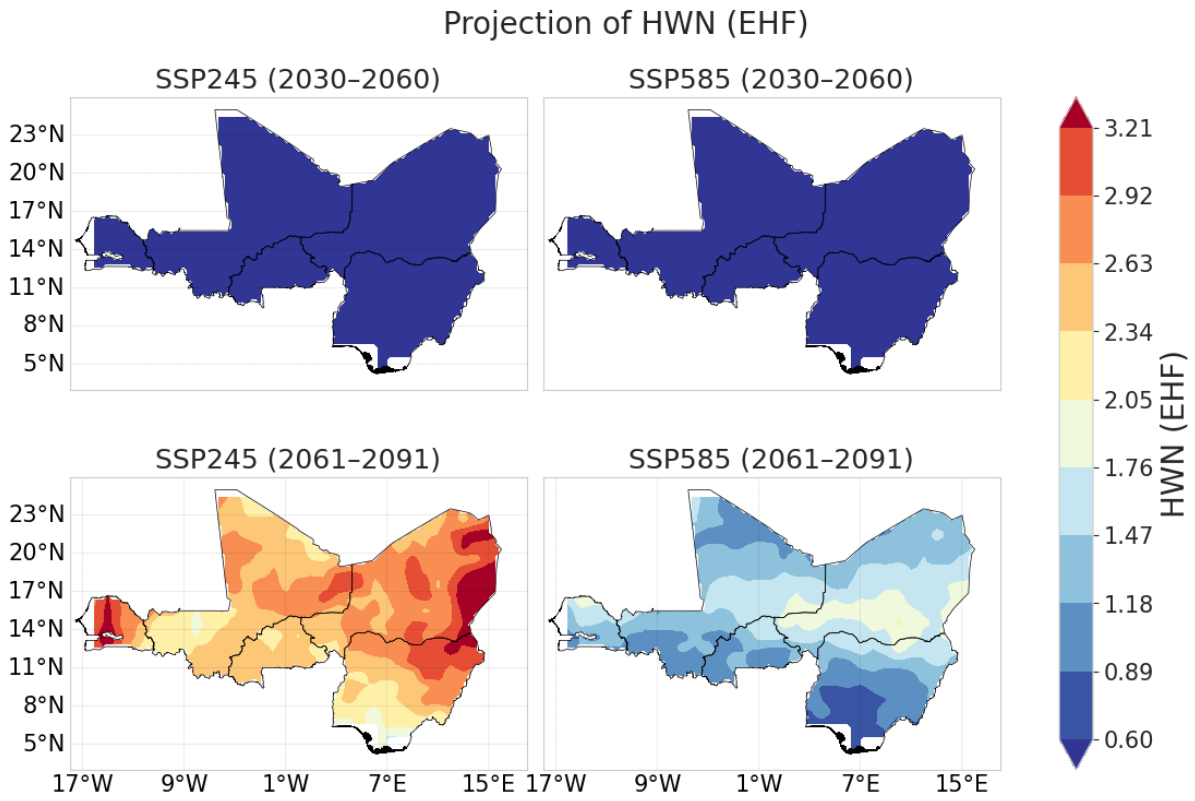

Figure 48 : Projection of heatwaves over Sahel for HWN (Heatwave Number) °C for EHF from near future, 2030-2060, and far future, 2061 – 2091.

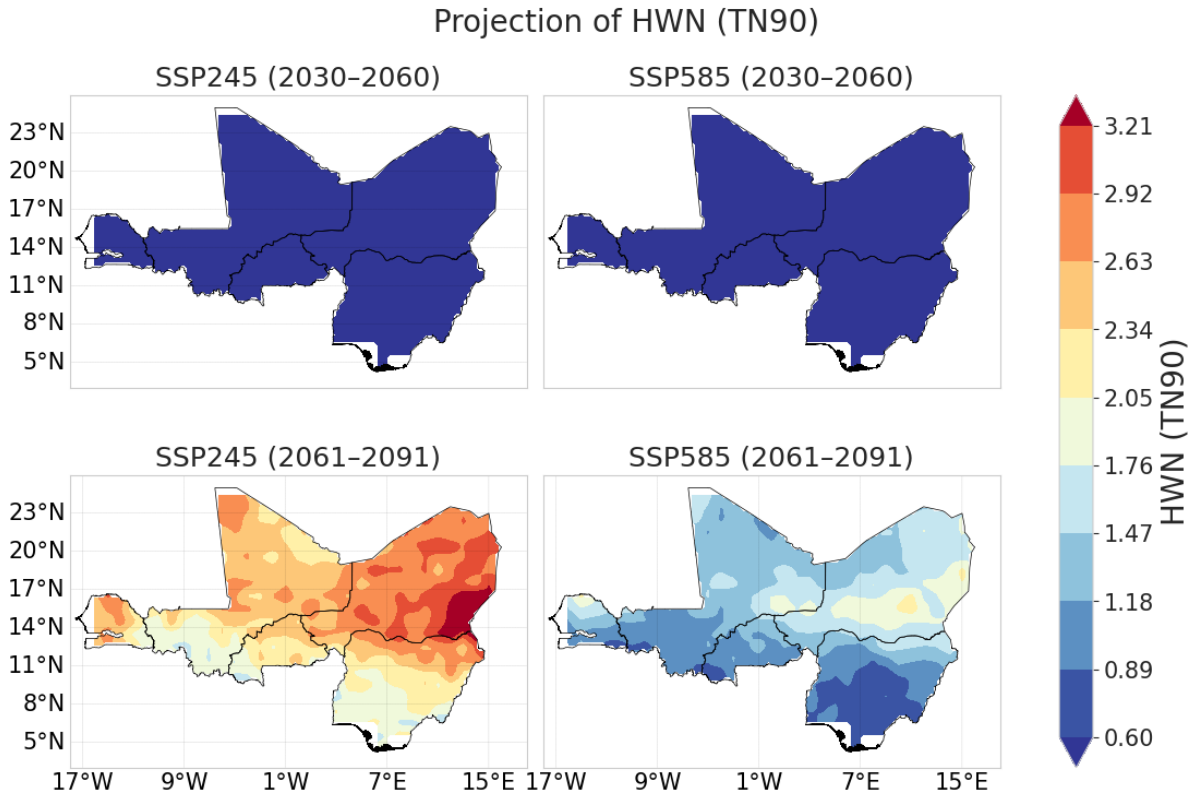

Figure 49 : Projection of heatwaves over Sahel for HWN (Heatwave Number) °C for TN90 from near future, 2030-2060, and far future, 2061 – 2091.

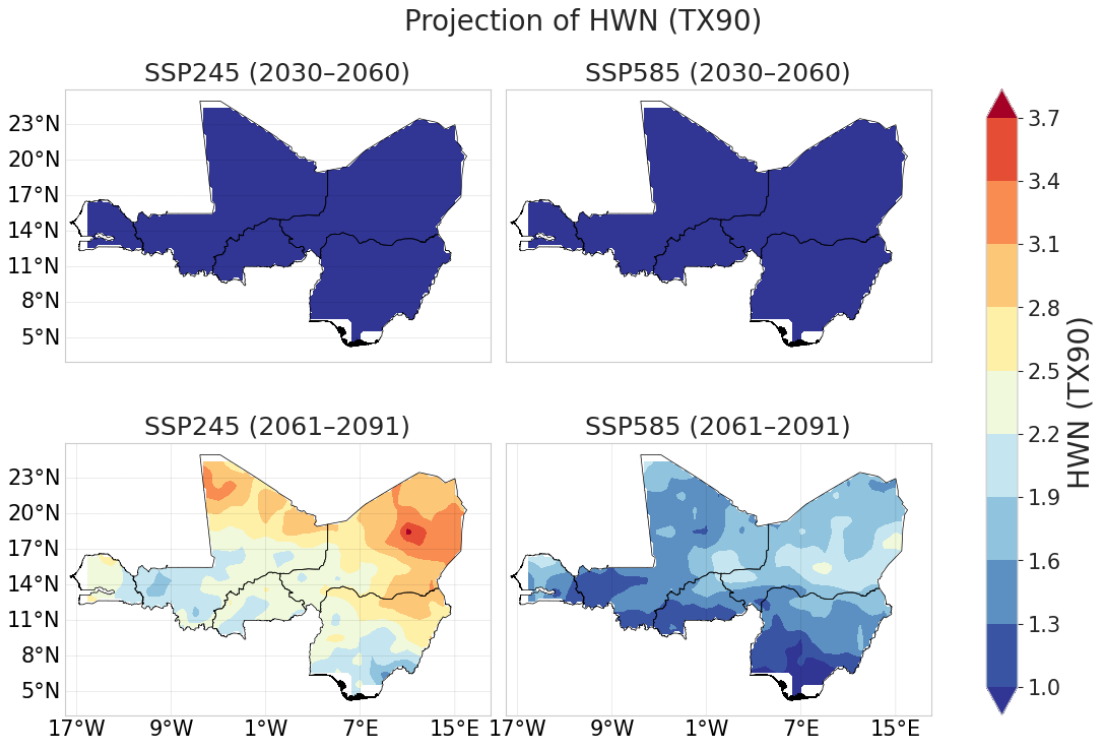

Figure 50 : Projection of heatwaves over Sahel for HWN (Heatwave Number) °C for TX90 from near future, 2030-2060, and far future, 2061 – 2091.

3.6 Future Heatwave Projection Trend Analysis

- **Heatwave Amplitude**

The near-future (2020-20300) projections for HWA across TX90 and EHF indices (Figures 51-52) revealed minimal spatial variation under both SSP245 and SSP585 scenarios. The absence of distinct color patterns suggests negligible trends in heatwave amplitude across the Sahel region during this period. However, far-future projections (2061-2091) indicate substantial regional differentiation. Under SSP245, mixed positive and negative trends emerge, with northern Sahel regions showing predominantly negative trends while southern areas exhibit positive increases. SSP585 projections demonstrate more pronounced positive trends, particularly in central and eastern Sahel regions, with amplitude increases reaching 0.19°C. This pattern aligns with Russo *et al.* (2014) findings on intensifying West African temperature extremes under high-emission scenarios.

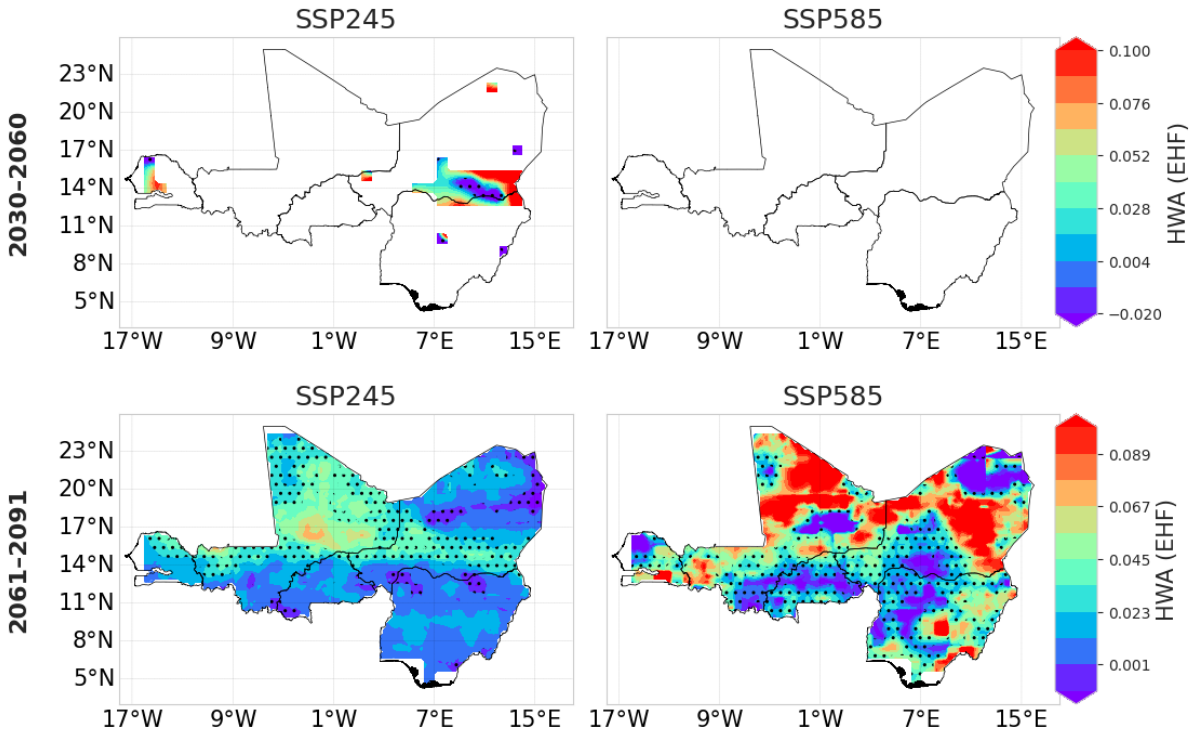

Figure 51 : Projected Trend analysis of heatwaves over Sahel for HWA (Heat Wave Amplitude) for Excess Heat Factor (EHF) from near future, 2030-2060, and far future, 2061 – 2091.

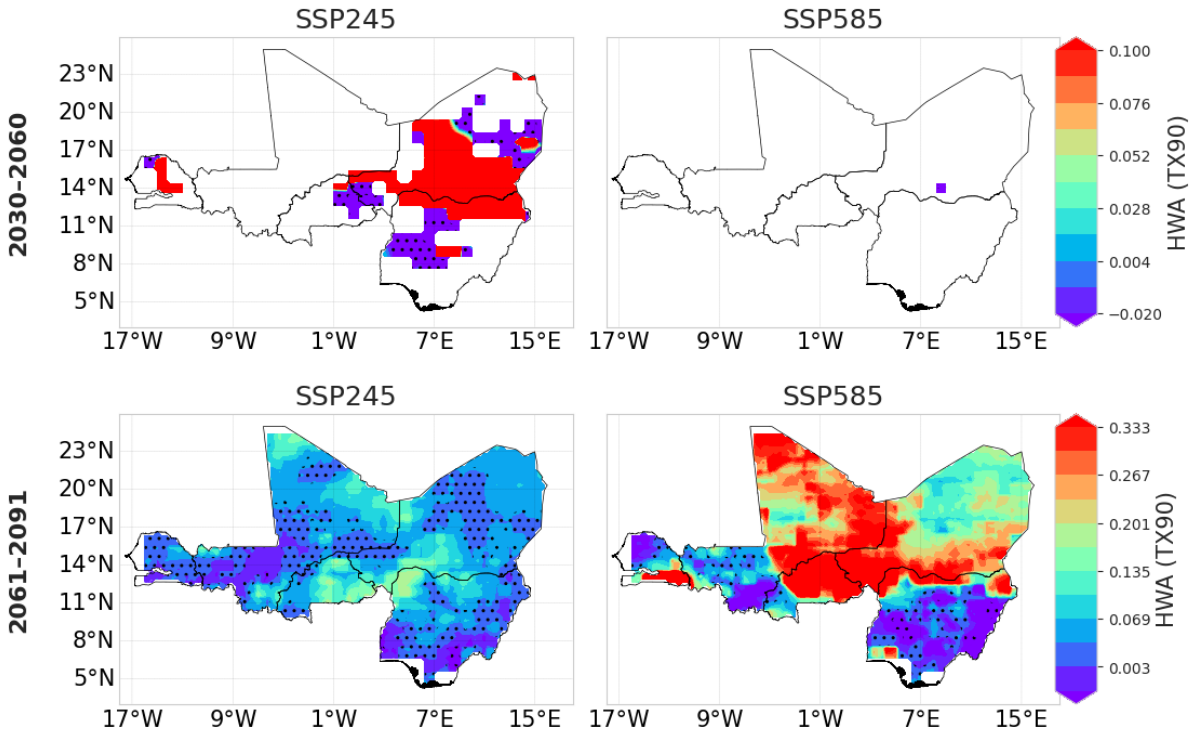

Figure 52 : Projected Trend analysis of heatwaves over Sahel for HWA (Heat Wave Amplitude) for TX90 from near future, 2030-2060, and far future, 2061 – 2091.

- **Heatwave Duration**

Near-future HWD projections (Figures 53- 55) across TN90, TX90, and EHF indices showed no discernible spatial patterns under either scenario, indicating stable heatwave duration trends through 2060. Far-future projections reveal contrasting scenarios: SSP245 demonstrates predominantly negative trends across the Sahel, suggesting shorter heatwave durations, while SSP585 projects positive trends, indicating prolonged heat events. The EHF-based projections show (Figure 53) statistically significant increases of 0.007 days under SSP245, though SSP585 trends lack statistical significance. These findings corroborate Vizy and Cook (2012) projections of extended heat events across the region, particularly emphasizing the vulnerability of Sahel populations to sustained heat exposure and associated health risks.

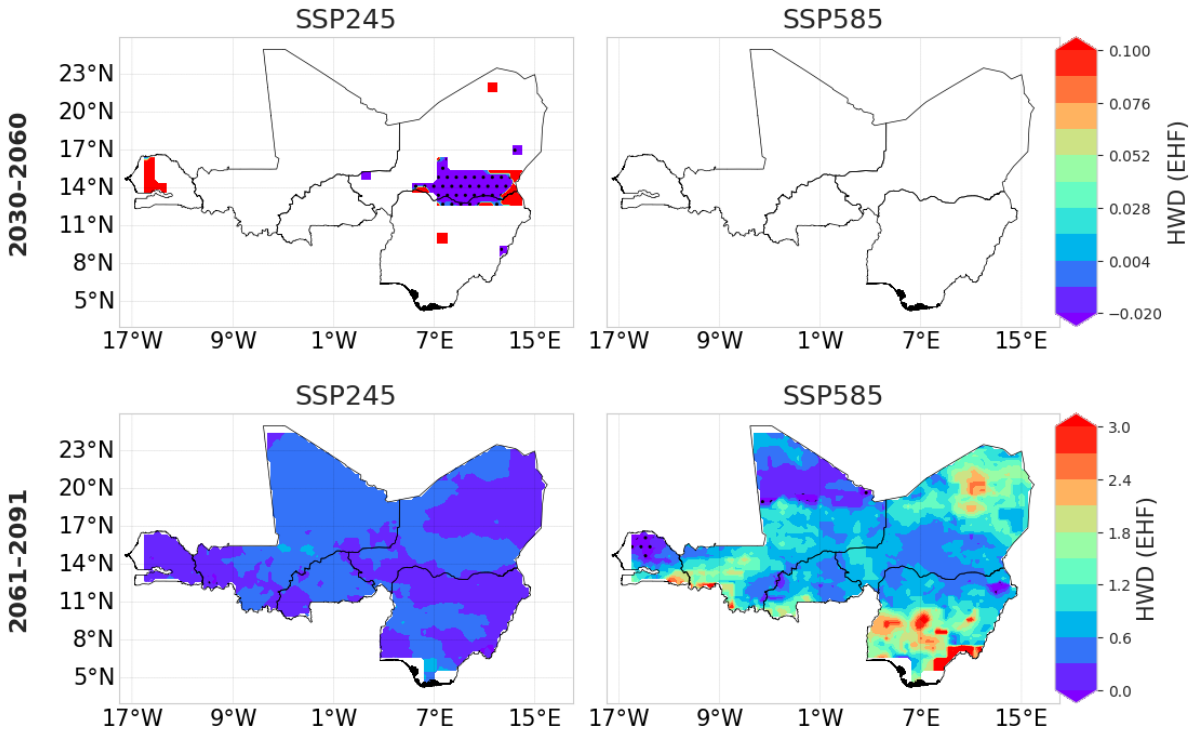

Figure 53 : Projected Trend analysis of heatwaves over Sahel for HWD (Heat Wave Duration) for Excess Heat Factor (EHF) from near future, 2030-2060, and far future, 2061 – 2091.

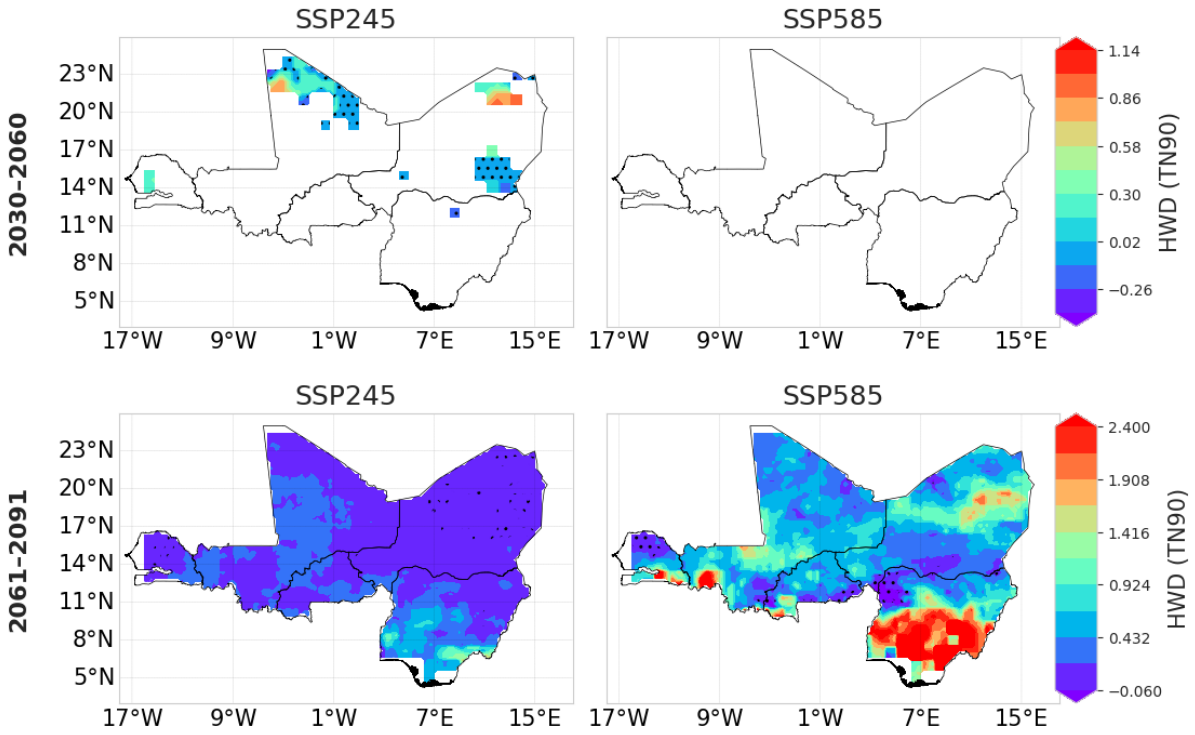

Figure 54 : Projected Trend analysis of heatwaves over Sahel for HWD (Heat Wave Duration) for nighttime (TN90) from near future, 2030-2060, and far future, 2061 – 2091.

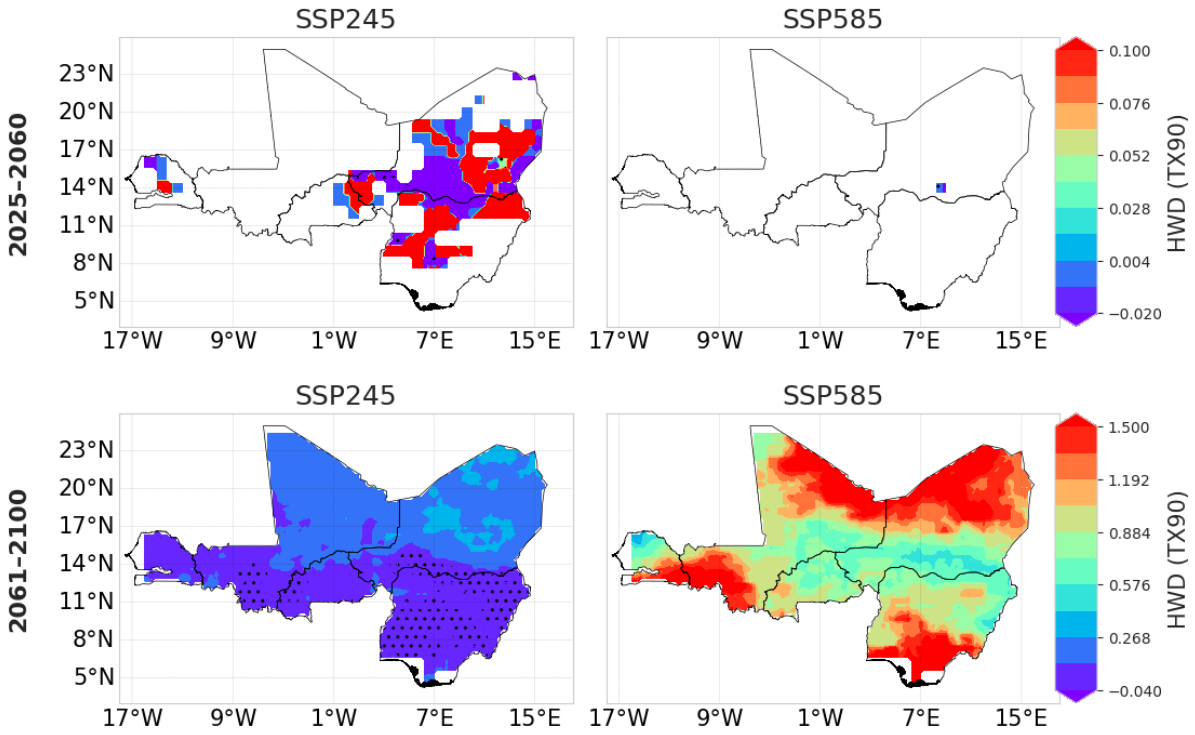

Figure 55 : Projected Trend analysis of heatwaves over Sahel for HWD (Heat Wave Duration) for daytime (TX90) from near future, 2030-2060, and far future, 2061 – 2091.

- **Heatwave Frequency**

The spatial analysis of HWF trends (Figures 56-58) reveals distinct temporal patterns across the Sahel region. Near-future projections indicate downward trends across all indices, though lacking statistical significance. Conversely, far-future projections demonstrate positive trends under both scenarios, with SSP245 showing broader statistical significance across southeastern regions and SSP585 exhibiting concentrated increases in northern areas. The EHF-based projections (Figure 56)indicate significant increasing trends toward northern Sahel regions under SSP585. These results align with Russo *et al.* (2014) and Nangombe *et al.* (2019) findings, suggesting the Sahel could experience weekly heatwave conditions during peak seasons by 2100, intensifying cumulative stress on healthcare systems and agricultural productivity.

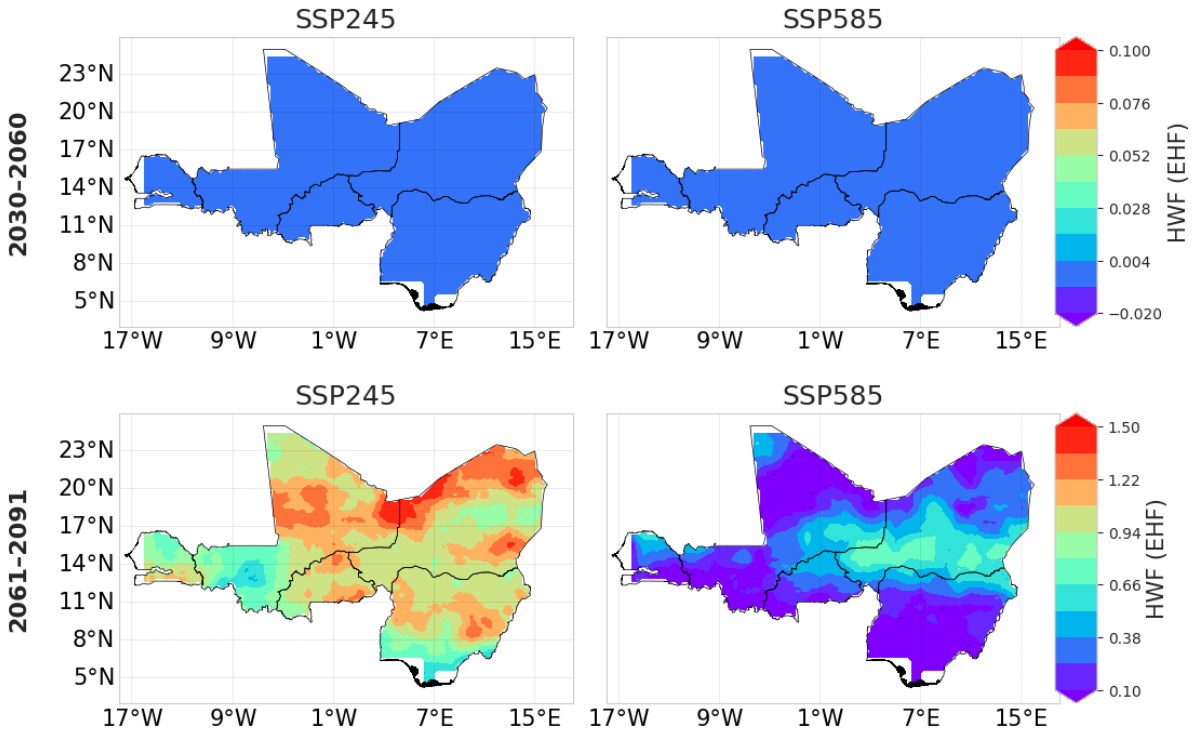

Figure 56 : Projected Trend analysis of heatwaves over Sahel for HWF (Heat Wave Frequency) for Excess Heat Factor (EHF) from near future, 2030-2060, and far future, 2061 – 2091.

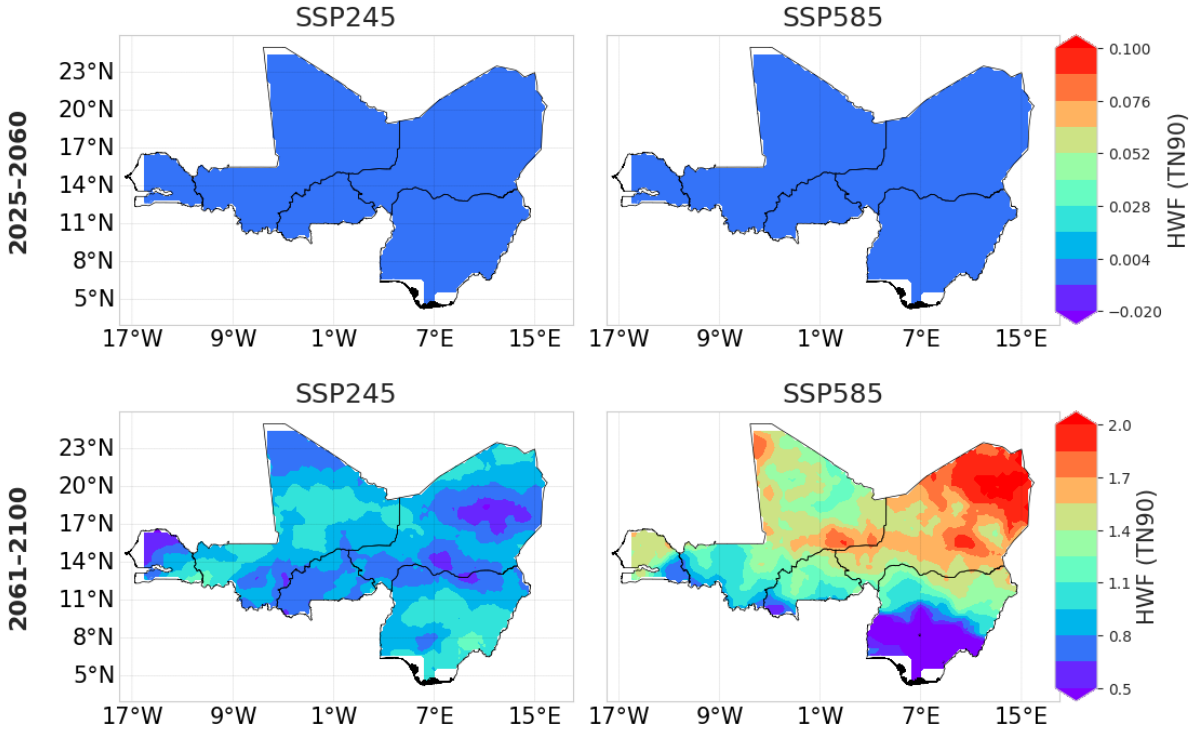

Figure 57 : Projected Trend analysis of heatwaves over Sahel for HWF (Heat Wave Frequency)

for nighttime (TN90) from near future, 2030-2060, and far future, 2061 – 2091.

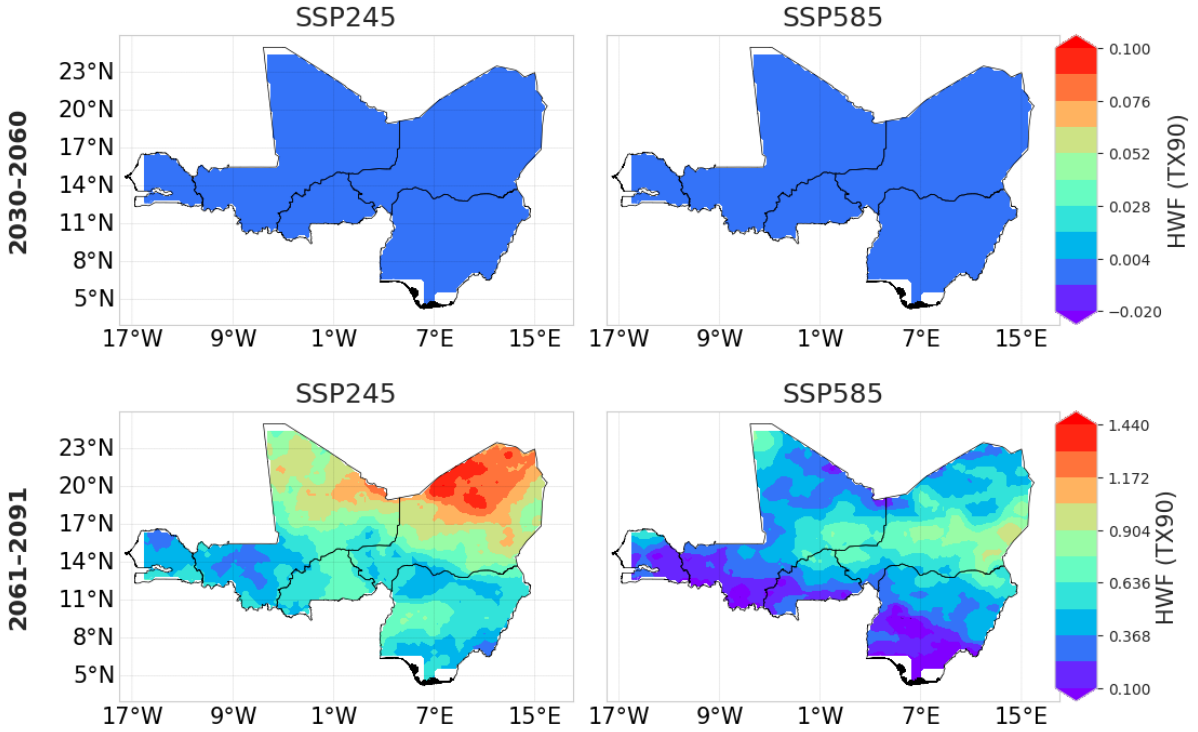

Figure 58 : Projected Trend analysis of heatwaves over Sahel for HWF (Heat Wave Frequency) for daytime (TX90) from near future, 2030-2060, and far future, 2061 – 2091.

- **Heatwave Magnitude**

Near-future HWM projections (Figures 59-61) across all indices showed minimal spatial variation, indicating stable magnitude trends through 2050. Far-future projections reveal complex regional patterns: TN90-based (Figure 60) projections under SSP245 display mixed trends with eastern Sahel regions showing significant increases while other areas demonstrate decreases. SSP585 projections indicate widespread decreasing trends. TX90-based projections (Figure 61) show northern regions experiencing positive trends while southeastern areas exhibit negative trends under both scenarios. EHF-based projections demonstrate contrasting patterns, with SSP245 showing negative trends and SSP585 displaying positive trends. These findings support Perkins and Alexander (2013) observations of intensifying heatwave events, emphasizing risks to public health, agriculture, and infrastructure across the Sahel region.

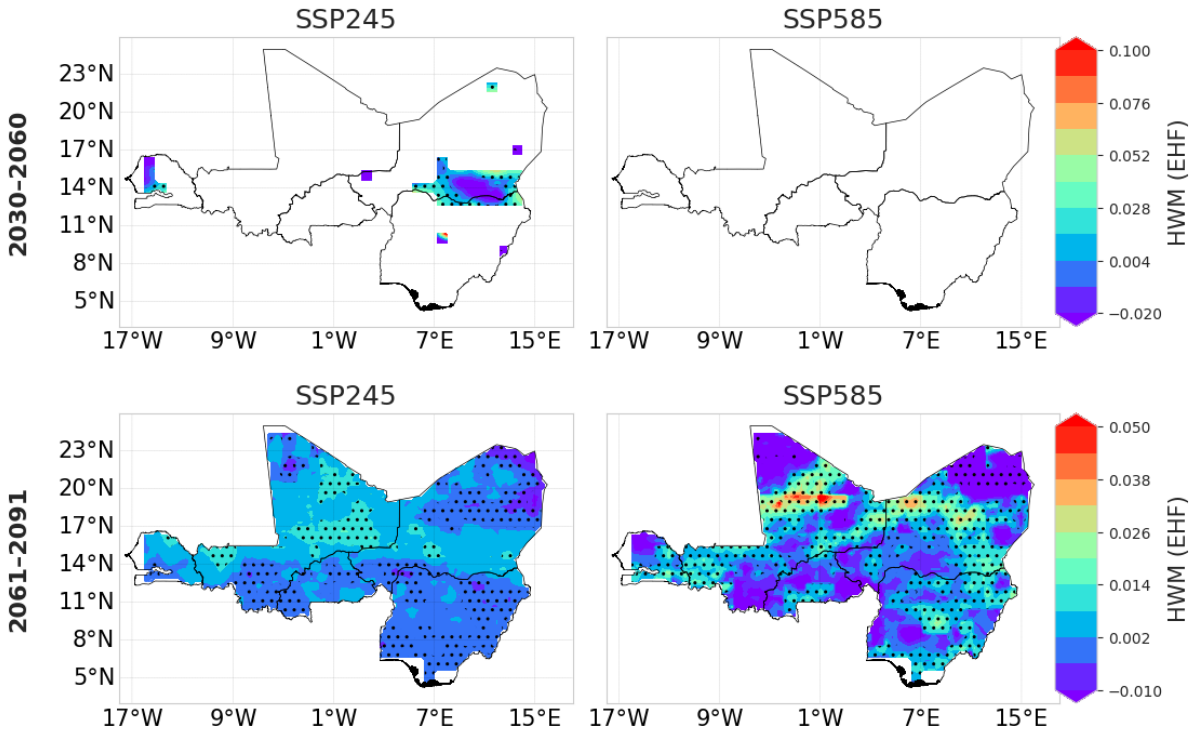

Figure 59 : Projected Trend analysis of heatwaves over Sahel for HWM (Heat Wave Magnitude) for Excess Heat Factor (EHF) from near future, 2030-2060, and far future, 2061 – 2091.

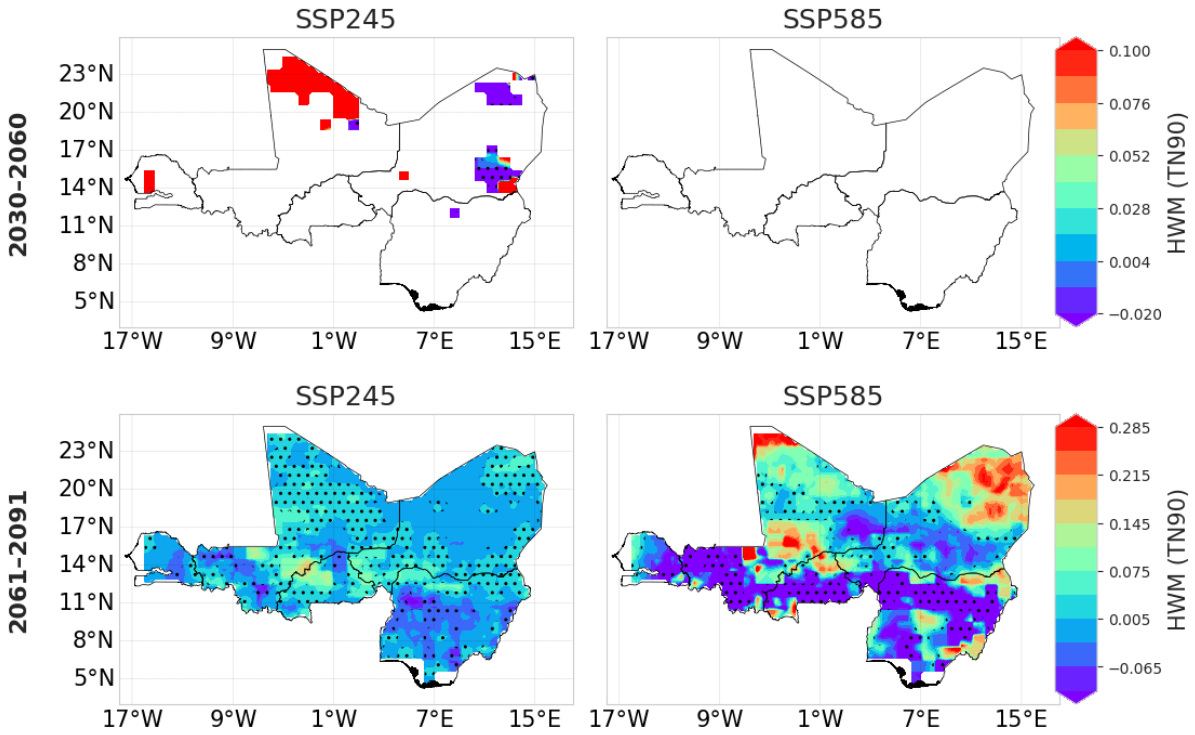

Figure 60 : Projected Trend analysis of heatwaves over Sahel for HWM (Heat Wave Magnitude) for nighttime (TN90) from near future, 2030-2060, and far future, 2061 – 2091.

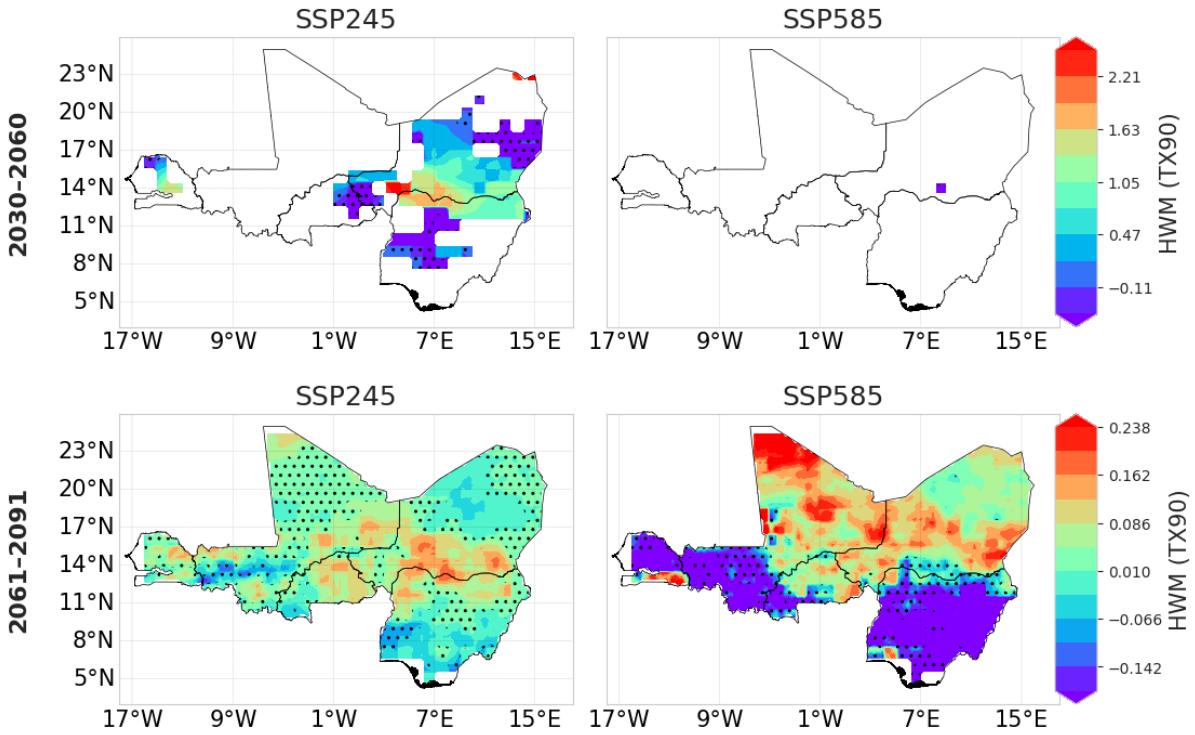

Figure 61 : Projected Trend analysis of heatwaves over Sahel for HWM (Heat Wave Magnitude) for daytime (TX90) from near future, 2030-2060, and far future, 2061 – 2091.

- **Heat wave Number**

The spatial projection analysis for HWN (Figures 62-64) indicates minimal near-future trends across all indices. Far-future projections reveal consistent positive trends across the Sahel region under both scenarios. . EHF-based projections (Figure 62) show positive trends under SSP245 with limited statistical significance, while SSP585 demonstrates concentrated increases in northern and southeastern regions.TN90-based projections (Figure 63) show statistically significant northward increases under SSP245, while SSP585 demonstrates less pronounced but positive trends. TX90-based projections (Figure 64) indicate substantial increases under both scenarios, with northern regions experiencing the highest values These results corroborate Russo et al. (2014) and Ceccherini et al. (2017) projections of 15 or more heatwave events by 2091, suggesting extreme heat may become a permanent climate feature across the Sahel region.

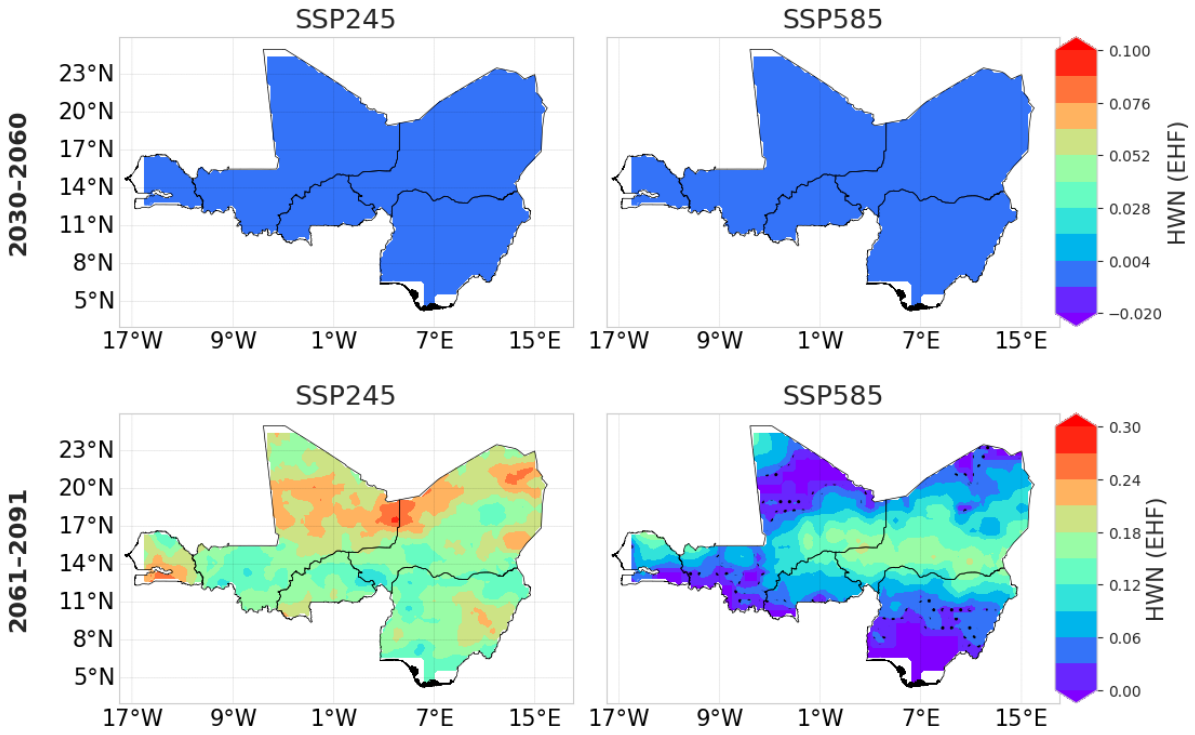

Figure 62 : Projected Trend analysis of heatwaves over Sahel for HWN (Heat Wave Number) for Excess Heat Factor (EHF) from near future, 2030-2060, and far future, 2061 – 2091.

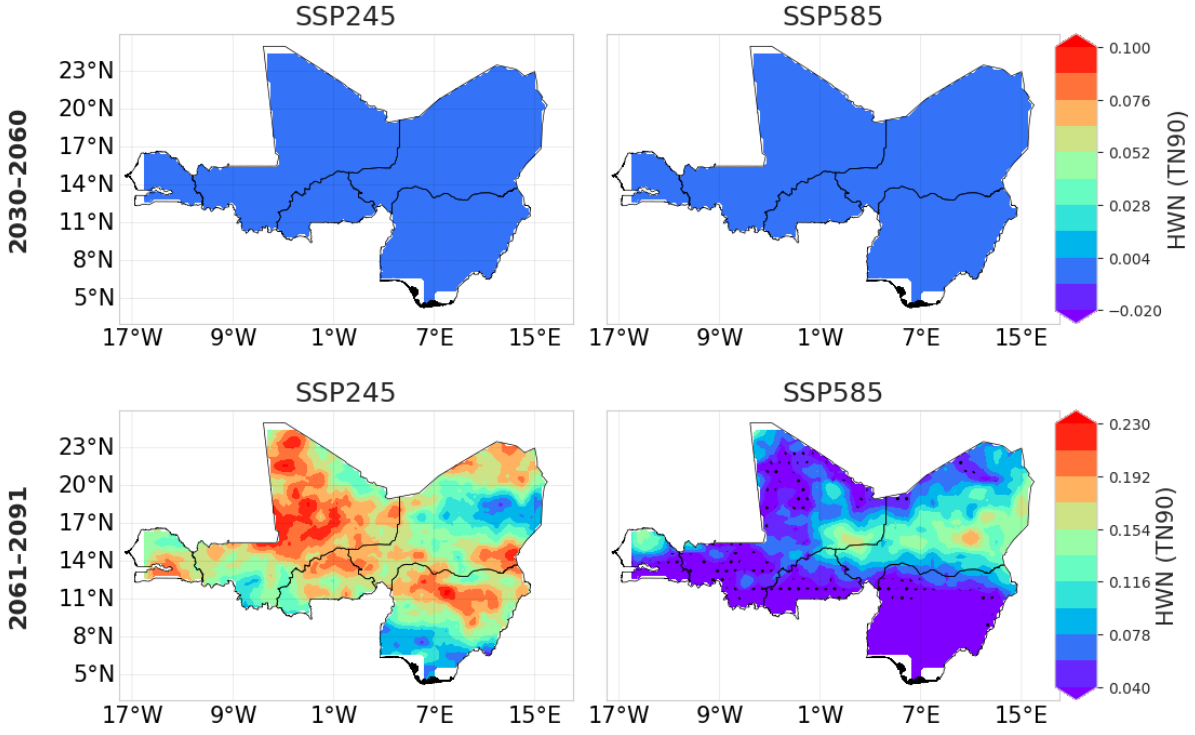

Figure 63 : Projected Trend analysis of heatwaves over Sahel for HWN (Heat Wave Number)

for nighttime (TN90) from near future, 2030-2060, and far future, 2061 – 2091.

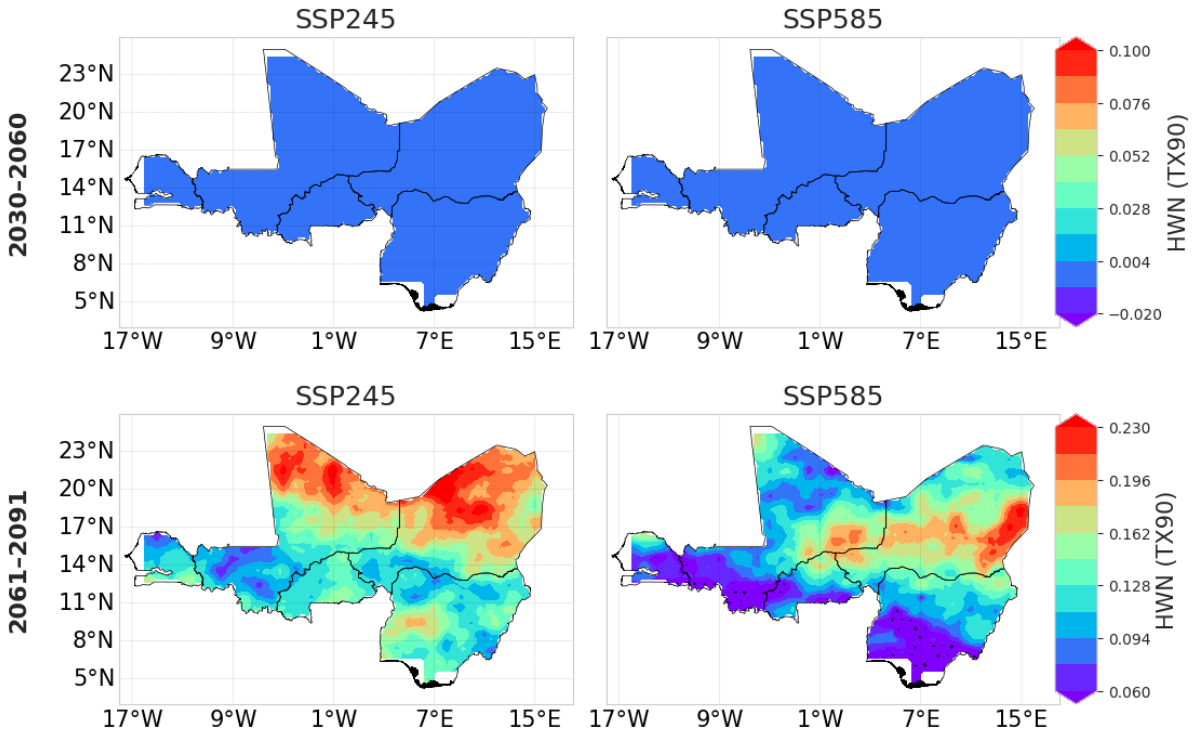

Figure 64 : Projected Trend analysis of heatwaves over Sahel for HWN (Heat Wave Number) for Daytime (TX90) from near future, 2030-2060, and far future, 2061 – 2091.

3.7 Discussion

The future projections of heatwaves over the Sahel underscore an alarming trajectory: more **frequent**, **longer-lasting**, **intense**, and **numerous** heatwave events. The consistency across all heatwave indices TX90, TN90, and EHF, adds robustness to the projection trends, validating similar findings from Sylla *et al.* (2018) and Dajuma *et al.* (2024). This convergence suggests that climate models, despite uncertainties, offer a reliable forecast of heat-related hazards in the Sahel. The sharp rise in **heatwave amplitude** and **duration**—especially under the EHF metric—highlights the dual burden of intensity and persistence, which directly affects human health and productivity (Sherwood and Huber, 2010; Kunda *et al.*, 2024). The inability of nighttime temperatures to cool sufficiently reflected in the TN90 trendsadds to cumulative heatwave, particularly in urban and densely populated areas (Ceccherini *et al*., 2017).

Moreover, the increasing **number** and **frequency** of events may transform the regional climate into a "heatwave-prone regime," as noted by Engdaw *et al*. (2022) and Fotso-Nguemo *et al*. (2023). These changes not only affect physical systems but also undermine **agricultural**

resilience, **infrastructure planning**, and **public health systems** (Sultan and Gaetani, 2016; Barbier *et al.,* 2018). The broader implications of these findings suggest the urgent need for anticipatory adaptation measures, particularly early-warning systems and localized heat adaptation policies (Deglon *et al.,* 2025; USAID, 2024). The projected future heatwave trends across the Sahel region of West Africa reflect an alarming escalation in thermal extremes, with widespread and intensifying impacts anticipated under both moderate (SSP245) and high-emissions (SSP585) scenarios. The analysis of heatwave characteristics including amplitude, duration, frequency, magnitude, and number, indicates that the region is on a trajectory towards more frequent, intense, and longer-lasting heatwave events, especially during the far-future period (2061–2091). In the near-future projections (2030–2060), minimal changes are detected across most indices and scenarios. However, by the end of the 21st century, the situation drastically intensifies, particularly under SSP585. For example, daytime heatwave amplitude (HWA_TX90) is projected to rise significantly, with northern Sahel regions expected to face extreme temperatures exceeding 49°C, surpassing the physiological heat tolerance of many crops and humans alike. Similarly, nighttime heatwave amplitude (HWA_TN90) under SSP585 is projected to exceed 35°C in northern areas—temperatures that eliminate the typical nocturnal cooling vital for human health and agricultural recovery. These patterns are consistent with the findings of Russo et al. (2014), who emphasized the intensification of heat extremes under high-emission scenarios across West Africa.Heatwave duration (HWD) follows a similarly troubling trend. Under SSP585, both daytime (TX90) and nighttime (TN90) durations increase dramatically in the far-future, with values surpassing 9 days in many regions. The most significant increases are observed in Excess Heat Factor (EHF)-based metrics, where prolonged exposure to both elevated daytime and nighttime temperatures exacerbates cumulative thermal stress. These findings are aligned with the work of Dimitriadou et al. (2021), which highlighted the increasing prevalence and duration of compound heat extremes in semi-arid climates.

The frequency of heatwaves (HWF) also shows significant upward trends, particularly under SSP245 in the eastern Sahel, where projections estimate up to 18.5 heatwave days annually by 2091. Although SSP585 shows somewhat lower but more spatially uniform frequencies, the combined thermal stress is still likely to overwhelm adaptive capacity. Increased nighttime heatwave frequency is particularly critical, as it prevents the physiological and environmental

reset that typically occurs overnight, compounding stress on vulnerable populations. These projections resonate with observations by Guigma et al. (2020), who identified minimum temperature-based heatwaves as especially threatening due to limited relief and prolonged exposure.

Heatwave magnitude (HWM) shows pronounced increases under SSP585, with projected values for daytime heatwaves (TX90) exceeding 48°C in the northern Sahel and nighttime values (TN90) rising to 34°C. These extremes represent unprecedented stress levels, particularly in areas with limited access to healthcare, water, or cooling infrastructure. As noted by Perkins-Kirkpatrick and Lewis (2020), such high-magnitude heat events can result in widespread mortality and reduced labor productivity, especially in agrarian societies.

The number of heatwave events (HWN) is expected to rise across all metrics, with SSP245 projecting more events in eastern Sahel compared to SSP585—a counterintuitive result possibly driven by nonlinear interactions in precipitation and land-atmosphere feedbacks. Nevertheless, the general trend points toward heatwaves becoming a near-permanent climate feature, consistent with findings by Ceccherini et al. (2017). These findings have dire implications. Public health systems will face mounting stress due to prolonged exposure to heat without nocturnal relief. Agricultural yields will decline as crops suffer from thermal thresholds being surpassed more frequently. Infrastructure, particularly in rural and semi-urban areas, is ill-equipped to withstand repeated extreme heat events. Water resources will be strained due to increased evapotranspiration, exacerbating existing drought conditions. Socially, heat-induced displacement and competition over diminishing resources could trigger conflict and large-scale migration, posing additional governance and humanitarian challenges. Therefore, these projections demand urgent and context-specific adaptation strategies. Under SSP245, there remains a window for phased adaptation through sustainable agricultural practices, early warning systems, and improved urban planning. However, the catastrophic projections under SSP585 highlight the need for aggressive mitigation efforts at both regional and global scales. Effective responses must integrate climate-smart infrastructure, community-based adaptation, and international support to address what may soon become irreversible changes in the Sahel's climate system.

CONCLUSION AND PERSPECTIVE

This study set out to investigate the historical and projected dynamics of heatwaves across the Sahel region of West Africa, driven by the hypothesis that heatwaves in the region are intensifying in frequency, duration, and magnitude, and are projected to accelerate under future climate scenarios. The analysis confirmed this hypothesis through a detailed assessment of heatwave indices derived from ERA5 reanalysis data and CMIP6-based downscaled projections.

The historical characterization revealed that daytime heatwaves (TX90) occur at frequencies between 1.0 and 1.9 events/year, with amplitudes exceeding 46°C in the northern Sahel. Nighttime events (TN90) were less frequent (0.5–1.6 events/year), but showed the strongest upward trends, especially in the northern and eastern subregions. The Excess Heat Factor (EHF) further highlighted regions at risk due to compounding heat intensity and duration. The Mann-Kendall trend analysis confirmed statistically significant increases, particularly in HWN and HWF under TN90 and EHF metrics, validating the hypothesis of intensifying heatwave dynamics.

Future projections under SSP2-4.5 and SSP5-8.5 scenarios indicate alarming increases. By the far-future period (2061–2091), the Sahel is expected to experience HWF values exceeding 25 days/year under EHF and HWA amplitudes surpassing 50°C. These projected changes imply that large portions of the Sahel will face physiologically intolerable heat conditions without intervention. The disparity between model outputs, particularly ACCESS-ESM1-5's tendency to overestimate and MPI-ESM1-2-HR's conservative trends, emphasizes the necessity of ensemble approaches for robust decision-making.

The results validate both specific and main hypotheses, underscoring that the Sahel is a critical hotspot for heatwave escalation. These insights should inform urgent climate adaptation strategies, early warning systems, and equitable resource allocation to protect vulnerable populations across this increasingly heat-stressed region.

For perspectives on broadening this work, future research could look into a more localized impact assessment by downscaling climate model outputs to finer spatial resolutions, potentially incorporating urban heat island effects more explicitly. Exploring the socio-economic vulnerabilities and adaptive capacities of specific communities in conjunction with these climate projections would provide a more complete picture for policy formulation.

BIBLIOGRAPHY/ REFERENCES

Adeniyi, M.O., (2017). 'Modeling the impact of changes in Atlantic sea surface temperature on the climate of West Africa'. *Meteorology and Atmospheric Physics*, *129*, pp.187-210.

Aderotoye, D., Zaitchik, B. and Asare, S. (2024) 'Heat Waves Trends and Patterns in West Africa: Definitions and Drivers', *104th AMS Annual Meeting*. Available at: https://ams.confex.com/ams/104ANNUAL/mediafile/Handout/Paper431278/Aderotoye_et%20al._heatwaves.pdf (Accessed: 15 May 2025).

Alexander, L. and Herold, N. (2016) *ClimPACT2: Indices and software*. Available at: https://github.com/ARCCSSextremes/climpact2 (Accessed: 10 March 2025).

Alliance Sahel (2024) *The Sahel and the Challenges of Climate Change*. Available at: https://www.alliance-sahel.org/en/news/sahel-climate-change-challenges/ (Accessed: 23 May 2025).

Arowolo, A.V. and Oluleye, A. (2022) 'Assessing the influence of intertropical discontinuity on total column ozone variation over West Africa', *Environmental Science and Pollution Research*, 29(44), pp. 66689-66704.

Arowolo, A.V., Odunmorayo, M.T., Okeyode, I.A., Raji, I.A., Ibukun, B. and Tella, I.A. (2025) 'Exploring Added Value of NASA NEX-GDDP High Resolution Model in Simulating West Africa Present and Future Climate', *Earth Systems and Environment*, pp. 1-24.

Barbier, J., Guichard, F., Bouniol, D., Couvreux, F. and Roehrig, R. (2018) 'Detection of intraseasonal large-scale heat waves: characteristics and historical trends during the Sahelian spring', *Journal of Climate*, 31(1), pp. 61-80.

Bi, D., Dix, M., Marsland, S., O'Farrell, S., Sullivan, A., Bodman, R., et al. (2020) 'Configuration and spin-up of ACCESS-CM2, the new generation Australian community climate and earth system simulator coupled model', *Journal of Southern Hemisphere Earth Systems Science*, 70(1), pp. 225-251.

Boucher, O., Servonnat, J., Albright, A.L., Aumont, O., Balkanski, Y., Bastrikov, V., Bekki, S., Bonnet, R., Bony, S., Bopp, L. and Braconnot, P. (2020) 'Presentation and evaluation of the IPSL-CM6A-LR climate model', *Journal of Advances in Modeling Earth Systems*, 12(7), p. e2019MS002010.

Busby, J.W., Cook, K.H., Vizy, E.K., Smith, T.G. and Bekalo, M., (2014). Identifying hot spots of security vulnerability associated with climate change in Africa. *Climatic change*, *124*, pp.717-731.

Ceccherini, G., Russo, S., Ameztoy, I., Marchese, A.F. and Carmona-Moreno, C. (2017) 'Heat waves in Africa 1981–2015, observations and reanalysis', *Natural Hazards and Earth System Sciences*, 17(1), pp. 115-125.

Copernicus (2024) *Heatwaves – a brief introduction*. Available at: https://climate.copernicus.eu/heatwaves-brief-introduction (Accessed: 15 May 2025).

Dajuma, A., Sylla, M.B., Tall, M., Almazroui, M., Afiesimama, E., Dosio, A., Moufouma-Okia, W., Diedhiou, A. and Giorgi, F. (2024) 'Projected intensification and expansion of heat stress and related population exposure over Africa under future climates', *Earth's Future*, 12(12), p. e2024EF004646.

Deglon, M., Africa, C., Soepnel, L.M., Kapwata, T., Aikins, A.D.G., Bedu-Addo, K., Howard, G., Lambert, E.V., Rae, D.E., Sibanda, M. and Gordon, C. (2025) 'Heat Adaptation Benefits for Vulnerable groups In Africa (HABVIA): a study protocol for a controlled clinical heat adaptation trial', *BMC Public Health*, 25(1), pp. 1-15.

Döscher, R., Acosta, M., Alessandri, A., Anthoni, P., Arsouze, T., Bergman, T., et al. (2022) 'The EC-Earth3 Earth system model for the Coupled Model Intercomparison Project 6', *Geoscientific Model Development*, 15, pp. 2973-3020.

Eberle, C., Higuera Roa, O. and Sparkes, E. (2022) *Technical Report: British Columbia heatwave*.

EC-Earth Consortium (EC-Earth) (2020) *EC-Earth-Consortium EC-Earth3-Veg-LR model output prepared for CMIP6 ScenarioMIP ssp119*. Version YYYYMMDD[1]. Earth System Grid Federation.

Engdaw, M.M., Ballinger, A.P., Hegerl, G.C. and Steiner, A.K. (2022) 'Changes in temperature and heat waves over Africa using observational and reanalysis data sets', *International Journal of Climatology*, 42(2), pp. 1165-1180.

Fotso-Nguemo, T.C., Weber, T., Diedhiou, A., Chouto, S., Vondou, A.D., Rechid, D. and Jacob, D. (2023) 'Projected impact of increased global warming on heat stress and exposed population over Africa', *Authorea Preprints*.

Giannini, A., Biasutti, M. and Verstraete, M.M. (2008) 'A climate model-based review of drought in the Sahel: Desertification, the re-greening and climate change', *Global and Planetary Change*, 64(3-4), pp. 119-128.

Gleckler, P.J., Taylor, K.E. and Doutriaux, C. (2008) 'Performance metrics for climate models', *Journal of Geophysical Research: Atmospheres*, 113(D6).

Gleixner, S., Demissie, T. and Diro, G.T. (2020) 'Did ERA5 improve temperature and precipitation reanalysis over East Africa?', *Atmosphere*, 11(9), p. 996.

Guigma, K.H. (2021) *Heat waves in the West African Sahel: nature, drivers and predictability*. Doctoral dissertation, University of Sussex.

Guigma, K.H., Guichard, F., Todd, M., Peyrille, P. and Wang, Y., (2021) 'Atmospheric tropical modes are important drivers of Sahelian springtime heatwaves'. *Climate Dynamics, 56,* pp.1967-1987.

Guigma, K.H., Todd, M. and Wang, Y. (2020) 'Characteristics and thermodynamics of Sahelian heatwaves analysed using various thermal indices', *Climate Dynamics*, 55, pp. 3151-3175.

Havenith, G. (2001) 'Individualized model of human thermoregulation for the simulation of heat stress response', *Journal of Applied Physiology*, 90(5), pp. 1943-1954.

Hersbach, H., Bell, B., Berrisford, P., Hirahara, S., Horányi, A., Muñoz-Sabater, J., Nicolas, J., Peubey, C., Radu, R., Schepers, D., Simmons, A., Soci, C., Abdalla, S., Abellan, X., Balsamo, G., Bechtold, P., Biavati, G., Bidlot, J., Bonavita, M., De Chiara, G., Dahlgren, P., Dee, D., Diamantakis, M., Dragani, R., Flemming, J., Forbes, R., Fuentes, M., Geer, A., Haimberger, L., Healy, S., Hogan, R.J., Hólm, E., Janisková, M., Keeley, S., Laloyaux, P., Lopez, P., Lupu, C., Radnoti, G., de Rosnay, P., Rozum, I., Vamborg, F., Villaume, S. and Thépaut, J.N. (2020) 'The ERA5 global reanalysis', *Quarterly Journal of the Royal Meteorological Society*, 146(730), pp. 1999-2049.

Ilori, O.W. and Ajayi, V.O. (2020) 'Change detection and trend analysis of future temperature and rainfall over west Africa', *Earth Systems and Environment*, 4(3), pp. 493-512.

Jones, B. and O'Neill, B.C. (2016) 'Spatially explicit global population scenarios consistent with the Shared Socioeconomic Pathways', *Environmental Research Letters*, 11(8), p. 084003.

Kendall, M.G. (1975) *Rank correlation methods*. 4th edn. London: Charles Griffin.

Knutti, R., Abramowitz, G., Collins, M., Eyring, V., Gleckler, P.J., Hewitson, B. and Mearns, L. (2010) 'Good practice guidance paper on assessing and combining multi-model climate projections', in *IPCC Expert Meeting on Assessing and Combining Multi-Model Climate Projections*. Bern: IPCC Working Group I Technical Support Unit.

Kunda, J.J., Gosling, S.N. and Foody, G.M. (2024) 'The effects of extreme heat on human health in tropical Africa', *International Journal of Biometeorology*, 68(6), pp. 1015-1033.

Lee, W.L., Wang, Y.C., Shiu, C.J., Tsai, I.C., Tu, C.Y., Lan, Y.Y., Chen, J.P., Pan, H.L. and Hsu, H.H. (2020) 'Taiwan Earth System Model Version 1: description and evaluation of mean state', *Geoscientific Model Development*, 13(9), pp. 3887-3904.

Lovato, T., Peano, D., Butenschön, M., Materia, S., Iovino, D., Scoccimarro, E., Fogli, P.G., Cherchi, A., Bellucci, A., Gualdi, S., Masina, S. and Navarra, A. (2022) 'CMIP6 simulations with the CMCC earth system model (CMCC-ESM2)', *Journal of Advances in Modeling Earth Systems*, 14(3), p. e2021MS002814.

Mann, H.B. (1945) 'Nonparametric tests against trend', *Econometrica*, 13, pp. 245-259.

Mauritsen, T., Bader, J., Becker, T., Behrens, J., Bittner, M., Brokopf, R., et al. (2019) 'Developments in the MPI-M Earth System Model version 1.2 (MPI-ESM1.2) and its response to increasing CO2', *Journal of Advances in Modeling Earth Systems*, 11(4), pp. 998-1038.

Meque, A., Pinto, I., Maúre, G. and Beleza, A. (2022) 'Understanding the variability of heatwave characteristics in southern Africa', *Weather and Climate Extremes*, 38, p. 100498.

Mondal, A., Kundu, S. and Mukhopadhyay, A. (2012) 'Rainfall trend analysis by Mann-Kendall test: a case study of north-eastern part of Cuttack district, Orissa', *International Journal of Geology, Earth and Environmental Sciences*, 2(1), pp. 70-78.

Morton, J.F. (2007) 'The impact of climate change on smallholder and subsistence agriculture', *Proceedings of the National Academy of Sciences*, 104(50), pp. 19680-19685.

Müller, W.A., Jungclaus, J.H., Mauritsen, T., Baehr, J., Bittner, M., Budich, R., et al. (2018) 'A higher-resolution version of the max planck Institute earth system model (MPI-ESM1.2-HR)', *Journal of Advances in Modeling Earth Systems*, 10(7), pp. 1383-1413.

Muzenda, M. (2025) *How is Africa Responding to the Climate and Health Nexus?*

N'gobi, G.M.L., Danani, K. and Soulé, M., (2022) 'Climate change and biodiversity in West Africa Sahel: a review'. *Restoration Ecology*, *4*, pp.20-29.

Nairn, J.R. and Fawcett, R.J. (2015) 'The excess heat factor: a metric for heatwave intensity and its use in classifying heatwave severity', *International Journal of Environmental Research and Public Health*, 12(1), pp. 227-253.

Nangombe, S.S., Zhou, T., Zhang, W., Zou, L. and Li, D. (2019) 'High-temperature extreme events over Africa under 1.5 and 2°C of global warming', *Journal of Geophysical Research: Atmospheres*, 124(8), pp. 4413-4428.

Ngoungue Langue, C.G., Lavaysse, C. and Flamant, C. (2025) 'Subseasonal forecasts of heat waves in West African cities', *Natural Hazards and Earth System Sciences*, 25(1), pp. 147-168.

Ngoungue Langue, C.G., Lavaysse, C., Vrac, M. and Flamant, C. (2023) 'Heat wave monitoring over West African cities: uncertainties, characterization and recent trends', *Natural Hazards and Earth System Sciences*, 23(4), pp. 1313-1333.

Odoulami, R.C., Abiodun, B.J., Ajayi, A.E., Diasso, U.J. and Saley, M.M. (2017) 'Potential impacts of forestation on heatwaves over West Africa in the future', *Ecological Engineering*, 102, pp. 546-556.

Omotosho, J.B. and Abiodun, B.J. (2007) 'A numerical study of moisture build-up and rainfall over West Africa', *Meteorological Applications*, 14(3), pp. 209-225.

Ouédraogo, M., Dembélé, Y. and Somé, L. (2010) 'Perceptions et stratégies d'adaptation aux changements des précipitations: cas des paysans du Burkina Faso', *Science et changements planétaires/Sécheresse*, 21(2), pp. 87-96.

Oueslati, B., Pohl, B., Moron, V., Rome, S. and Janicot, S. (2017) 'Characterization of heat waves in the Sahel and associated physical mechanisms', *Journal of Climate*, 30(9), pp. 3095-3115.

Parkes, B., Buzan, J.R. and Huber, M. (2022) 'Heat stress in Africa under high intensity climate change', *International Journal of Biometeorology*, 66(8), pp. 1531-1545.

Perkins, S.E. and Alexander, L.V. (2013) 'On the measurement of heat waves', *Journal of Climate*, 26(13), pp. 4500-4517.

Poynting, M. and Stallard, E. (2024) *How climate change worsens heatwaves, droughts, wildfires and floods*. Available at: https://www.bbc.com/news/science-environment-58073295 (Accessed: 15 May 2024).

Ragatoa, D.S., Amekudzi, L.K., Fink, A.H., Maranan, M., Klutse, N.A.B., Edjame, K.S. and Ogunjobi, K.O. (2024) 'Droughts and heatwaves in the West African monsoon system', *International Journal of Climatology*, 44(11), pp. 3681-3705.

Sambou, M.J.G., Pohl, B., Janicot, S., Landry Famien, A.M., Roucou, P., Badiane, D. and Gaye, A.T. (2021) 'Heat waves in spring from Senegal to Sahel: evolution under climate change', *International Journal of Climatology*, 41(14), pp. 6238-6253.

Sherwood, S.C. and Huber, M. (2010) 'An adaptability limit to climate change due to heat stress', *Proceedings of the National Academy of Sciences*, 107(21), pp. 9552-9555.

Slayi, M., Zhou, L. and Jaja, I.F. (2024) 'Strategies, challenges, and outcomes of heat stress resilience in sub-Saharan African community-based cattle feedlots: a systematic review', *Frontiers in Veterinary Science*, 11, p. 1455917.

Sow, M. and Gaye, D., (2024). Categorization and multi-criteria analysis of heat wave vulnerability in Senegal. *Journal of Water and Climate Change*, *15*(11), pp.5382-5396.

Sultan, B. and Gaetani, M. (2016) 'Agriculture in West Africa in the twenty-first century: climate change and impacts scenarios, and potential for adaptation', *Frontiers in Plant Science*, 7, p. 1262.

Sylla, M.B., Faye, A., Giorgi, F., Diedhiou, A. and Kunstmann, H. (2018) 'Projected heat stress under 1.5°C and 2°C global warming scenarios creates unprecedented discomfort for humans in West Africa', *Earth's Future*, 6(7), pp. 1029-1044.

Tambol, T., Vodounou, G.M.B. and Moussa, S. (2023) 'Impacts of mining on the environment in West African Sahel: A review', *Environmental Protection Research*, pp. 263-277.

Tatebe, H., Ogura, T., Nitta, T., Komuro, Y., Ogochi, K., Takemura, T., et al. (2019) 'Description and basic evaluation of simulated mean state, internal variability, and climate sensitivity in MIROC6', *Geoscientific Model Development*, 12(7), pp. 2727-2765.

Taylor, K.E. (2001) 'Summarizing multiple aspects of model performance in a single diagram', *Journal of Geophysical Research: Atmospheres*, 106(D7), pp. 7183-7192.

Tesfaye, B. (2022) *Climate change and conflict in the Sahel*. New York: Council on Foreign Relations.

USAID (2024) *CASE STUDY: CLIMATE INFORMATION SERVICES FOR HEALTH SYSTEMS STRENGTHENING A Health Early Warning System to Reduce Extreme Heat Impacts in Senegal*. USAID Climate Adaptation Support Activity.

Wane, D., Coëtlogon, G.D., Lazar, A., Wade, M. and Gaye, A.T., (2024). Atmospheric response to seasonal changes in sea surface temperature during the boreal summer in the Tropical Atlantic. *Climate Dynamics*, *62*(3), pp.1597-1612.

Wang, W., Yi, Z. and Chen, D. (2021) 'Mann-kendall mutation analysis of temporal variation of apparent stress in Qinba mountains and its adjacent areas', in *IOP Conference Series: Earth and Environmental Science*, 660(1). IOP Publishing, p. 012112.

World Weather Attribution (2025) *Extreme Sahel heatwave that hit highly vulnerable population at the end of Ramadan would not have occurred without climate change*. Available at: https://www.worldweatherattribution.org/extreme-sahel-heatwave-that-hit-highly-vulnerable-population-at-the-end-of-ramadan-would-not-have-occurred-without-climate-change/ (Accessed: 15 May 2025).

Wu, Y., Miao, C., Duan, Q., Shen, C. and Fan, X. (2020) 'Evaluation and projection of daily maximum and minimum temperatures over China using the high-resolution NEX-GDDP dataset', *Climate Dynamics*, 55, pp. 2615-2629.

Wu, S., Luo, M., Zhao, R., Li, J., Sun, P., Liu, Z., Wang, X., Wang, P. and Zhang, H. (2023) 'Local mechanisms for global daytime, nighttime, and compound heatwaves', *npj Climate and Atmospheric Science*, 6(1), p. 36.

Yan, Y., Wang, H., Li, G., Xia, J., Ge, F., Zeng, Q. and Tan, L. (2022) 'Projection of future extreme precipitation in China based on the CMIP6 from a machine learning perspective', *Remote Sensing*, 14(16), p. 4033.

Yukimoto, S., Kawai, H., Koshiro, T., Oshima, N., Yoshida, K., Urakawa, S., et al. (2019) 'The meteorological Research Institute Earth System Model Version 2.0, MRI-ESM2.0:

Description and basic evaluation of the physical component', *Journal of the Meteorological Society of Japan*, 97(5), pp. 931-965.

Ziehn, T., Chamberlain, M.A., Law, R.M., Lenton, A., Bodman, R.W., Dix, M., et al. (2020) 'The Australian Earth System Model: ACCESS-ESM1.5', *Journal of Southern Hemisphere Earth Systems Science*, 70(1), pp. 193-214.

APPENDIX

Appendix A: Taylor Diagrams

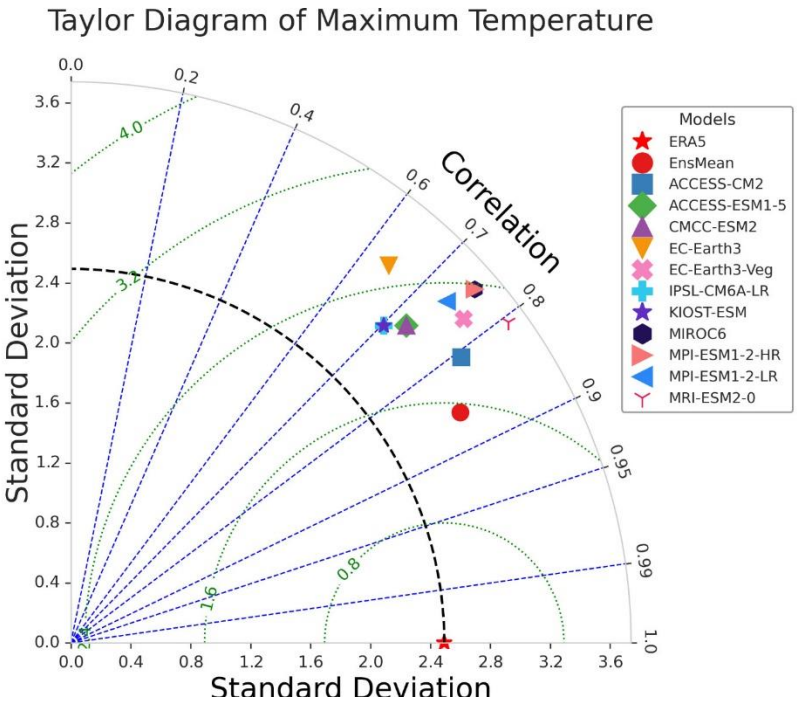

Figure 65 : Maximum Temperature For Taylor Diagram

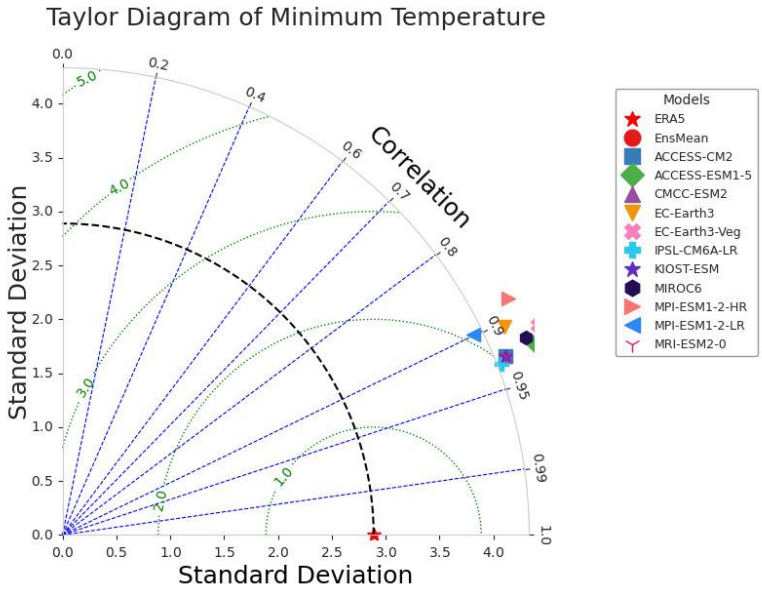

Figure 66 : Minimum Temperature for Taylor Diagram